EVALUATION OF GEOTECHNICS, SEISMICITY AND TECTONIC PROCESSES TO CHARACTERIZE POSSIBLE GEOHAZARDS IN MENENGAI GEOTHERMAL PROJECT FIELD.

By:

CONVINE OMONDI NYAMWEYA

I56/61004/2010

A dissertation submitted in partial fulfillment of the requirements for the degree of Master of Science in Engineering Geology, Department of Geology, School of Physical Sciences, University of Nairobi

NOVEMBER, 2016

DECLARATION

I declare that this thesis is my original work and has not been submitted elsewhere for examination, award of a degree or publication. Where other people's work or my own work has been used, this has properly been acknowledged and referenced in accordance with the University of Nairobi's requirement.

Signature_____ Date: _____

This dissertation/thesis has been submitted for examination with our approval as the supervisor;

	Signature	**Date**
Dr. Edwin Dindi Department of Geology, School of Physical Sciences, University of Nairobi		
Prof. Nobert Opiyo-Aketch Department of Geology, School of Physical Sciences, University of Nairobi		
Dr. Josphat K. Mulwa Department of Geology, School of Physical Sciences, University of Nairobi		

DECLARATION OF ORIGINALITY

Name of Student:	Convine Omondi Nyamweya
Registration Number:	I56/61004/2010
College:	College of Biological Physical Sciences
School:	School of Physical Sciences
Department:	Department of Geology
Course Name:	Master of Science in Engineering Geology
Title of the Work:	**EVALUATION OF GEOTECHNICS, SEISMICITY AND TECTONIC PROCESSES TO CHARACTERIZE POSSIBLE GEOHAZARDS IN MENENGAI GEOTHERMAL PROJECT FIELD.**

1. I understand what Plagiarism is and I am aware of the University's policy in this regard.
2. I declare that this thesis is my original work and has not been submitted elsewhere for examination, award of a degree or publication. Where other people's work or my own work has been used, this has properly been acknowledged and referenced in accordance with the University of Nairobi's requirements.
3. I have not sought or used the services of any professional agencies to produce this work.
4. I have not allowed, and shall not allow anyone to copy my work with the intention of passing it off as his/her own work.
5. I understand that any false claim in respect of this work shall result in disciplinary action, in accordance with University Plagiarism Policy.

Signature _____

Date _____

DEDICATION

My Late Parents, Family and fellow Engineering Geologists

ACKNOWLEDGEMENT

I express my heartfelt gratitude to my supervisors; Dr. Edwin Dindi, Prof. Nobert Opiyo-Aketch and Dr. Josphat K. Mulwa for their invaluable encouragements, suggestions, comments and advice given towards the realization of this project. I am also indebted to Independent Power Producers; Sosian Energy for availing to me rock-cores, insitu field test results, laboratory test results from the sampled rocks and disturbed and undisturbed soils and SRT and MASW Seismic results. Further, appreciate colleagues in Geothermal Development Company for the consent, support, discussions and data collections that made this project a success. I want to particularly thank the entire lecturing fraternity of Geology Department, University of Nairobi for tirelessly guiding me through to this postgraduate level all the way from my undergraduate. I attribute my current professional acumen from a strong geological foundation acquired from the department of Geology, University of Nairobi. Finally, I want to thank my family and friends for their love, patience, support and encouragement.

ABSTRACT

Menengai geothermal project area is situated within a closed volcanic system of a relatively young caldera which seems that can still be tectonically activated by agents associated with geotechnics and seismicity. Topography of caldera floor is highly rugged following intensive lava flows from post caldera eruptions. Over thirty (30) geothermal wells have already been drilled on floor caldera within an approximate surface area of 4 km^2 largely at the central area of the caldera. Even though the near surface is observed to be geotechnically suitable for foundations of constructions and infrastructure, deep-seated processes are bound to destabilize and affect the geothermal development program. Probable geohazards are observed to affect geothermal reservoir within the caldera, productivity of drilled wells, and stability of caldera floor to hold buildings, steam gathering system and infrastructures. This study has observed that caldera floor can be subdivided into five (5) main caldera compartments; SE, SW, NE, NW and NNW formed by sub-sequential subsidence due to tectono-volcanic induced processes with down-throws influenced by either Molo or Solai TVA related structures within the caldera. The compartments are defined by major fault-scarps (N-S and E-W) which appear to be main conduits of cold in-flows to the geothermal wells and reservoir. Geothermal wells are concentrated within a tectonically less stable NW Compartment; this may enhance further landmass movements at depth following increased seismicity from a combination of frictional forces being exerted by steam-jets from discharging wells at one-go during geothermal production stage. Geothermal development plan and layout on surface constructions and infrastructure dominate slopes within NW Compartment thus categorized as high risk going by the amount of investment being put in place. Possible geohazards in Menengai Geothermal Project are observed to be as a result of integrated failures related to geotechnics, seismicity and tectonic processes due to occur within the caldera.

TABLE OF CONTENTS

LIST OF TABLES

LIST OF FIGURES

CHAPTER ONE

1.0 GENERAL INTRODUCTION

1.1 Overview

Geothermal development is an expensive venture that requires real security of investment being put in place for maximum yield in output. This study analyses, evaluates geotechnical properties/parameters acquired from site investigation at the proposed Sosian Energy Power plant site in correlation with regional and local seismicity, geology, tectonic settings and topographic slope analysis to characterize possible geohazards that may affect geothermal development within Menengai caldera.

1.2 Statement of the problem

The proposed project is located within a closed caldera floor of a composite volcanic complex. The caldera floor is covered by relatively young lava flows of syn and post-caldera times. Over thirty (30) geothermal wells have been drilled within the caldera at the time this study and these would easily exert a lot of pressures onto the sub-surface trachytic strata triggering dip landmass movements along buried structures thus enhancing seismicity which may cause some insitu landmass movements. Critical look at temperature and pressure profiles for both vertical and directional discharging wells indicate a lot of crisscrossing deep intra-caldera structures that may pose great geotechnical risk within the caldera. Topographic slopes' analysis of caldera floor surface and risk- matrix shows possibility of unstable land surface within the entire caldera and along numerous crisscrossing presumed rims of mini-calderas and fault scarps. Power plants' construction is an intensive operation that requires thorough assessment of the site to ascertain foundation stability of structural design. Prior identification of possible geohazards during and after construction works is very important in establishing proper mitigation measures in advance.

1.3 Aim and Objectives

1.3.1 Main Aim

The main aim is to characterize possible geohazards that will hamper geothermal development program within the Menengai caldera through evaluation of geotechnical parameters acquired at proposed power plant site, local and regional seismicity, structural and tectonic evolution and local topography.

1.3.2 Specific Objective

1. To descriptively analyze and correlate geotechnical insitu field tests and laboratory results.
2. To analyze seismic engineering parameters of near surface layers at power plants site and regional seismicity.
3. To analyze geological, structural and tectonic settings within caldera and establish volcano-tectonic chronology that resulted to the current set-up of the larger Menengai caldera.
4. To undertake topographic analysis to help construct risk matrix from hazardous slopes using 2-m contour map and evaluate degree of the possible landmass movements.
5. To identify and characterize likely geohazards that could hamper geothermal development within Menengai Caldera.

1.4 Justification and Significance of Research

The study area is within an enclosed young compositic caldera volcano of which pre-, syn- and post caldera trachytic lava flows are unconformably separated by thick volcanic ash layers. Over thirty (30) geothermal wells have already been drilled on floor caldera concentrated within an approximate surface area of 4 km^2 in the central area of caldera. This

number of wells may create a lot of compressional and tensional stresses during the production stage due to vibrations from discharging wells which are characteristically associated with high pressure steam jets emanating from deep-seated feed zones. The hot steam passes through larger part of well column thereby exerting outward pressures to the walls of the well as frictional forces. This scenario is worse off in cases within wellbore where steam-jets penetrated through compositic geological layers of competent and loose/incompetent formations. Zones of incompetent formation normally do not exert equal opposite reactional and compressive forces to that being exerted with the on-motion steam-jet flowing upwards within the wellbore. A combination of differential reactional forces along sections of well columns poses great threat to the stability of the wellbore and thus create seismic wave that can results to movement/displacement along underneath faults and overlying landmass hence affecting built structures on the floor at surface. Most wells penetrate through unconformable succession of pre-caldera, syn-caldera and post-caldera lava flows.

This study will significantly help to identify and characterize imminent geohazard and risks following eminent seismic events within the reservoir that are not foreseen during geothermal production.

1.5 The Study Area

1.5.1 General information of the area

Menengai caldera volcano is located on the floor of the Kenya rift valley (Figure 1-1). It is one of seven late Quaternary caldera volcanoes in the inner trough of the Kenya rift valley, which are asssociated with a high thermal gradient as a result of shallow intrusions. Other volcanoes within the rift, from north to south include Barrier, Emuruangogolak, Silali, Paka, Korosi, Longonot and Suswa; all of which are associated with geothermal activity.

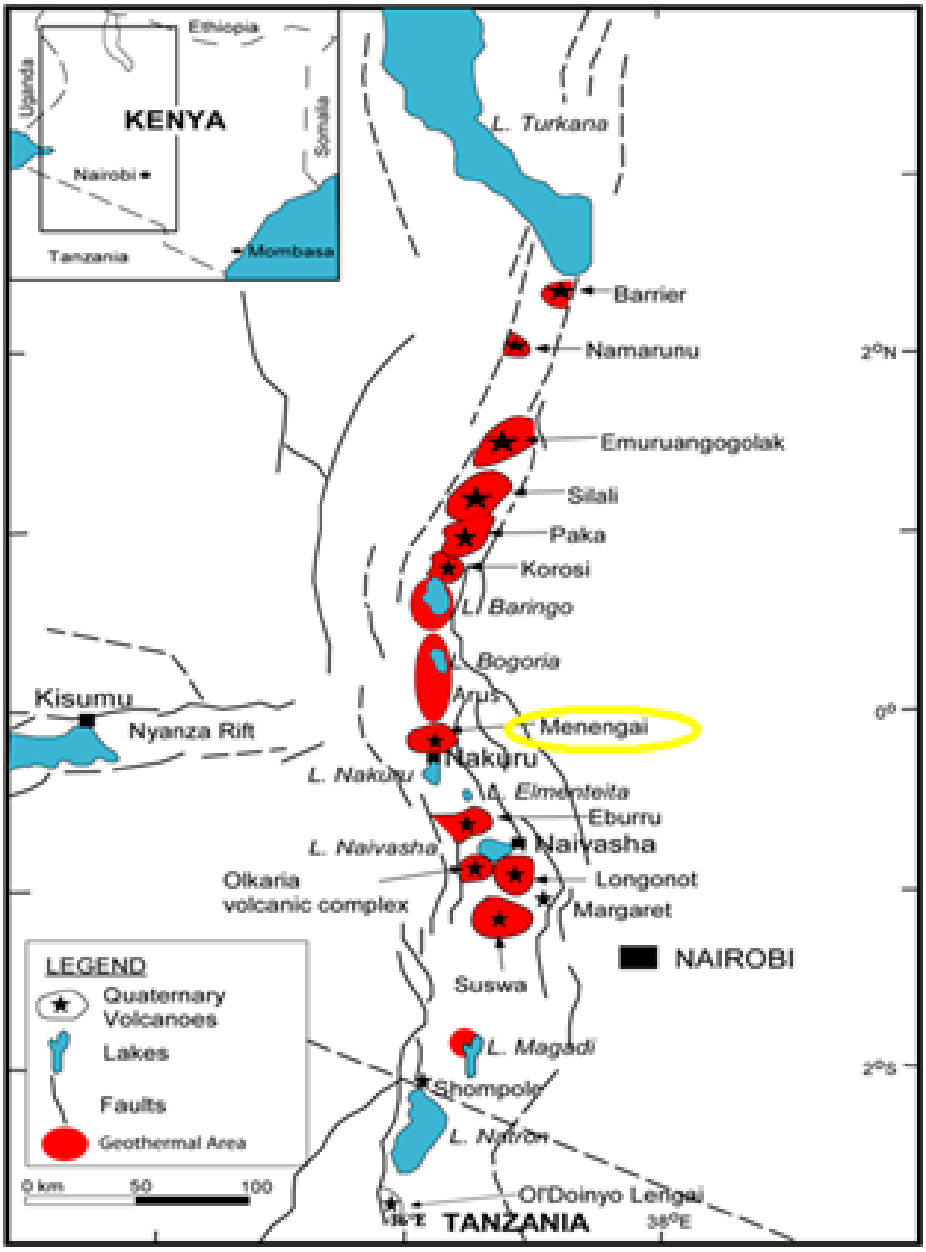

Figure 1-1: Location of Menengai geothermal prospect and other prospects along the Kenya Rift Valley (GDC, 2010)

1.5.2 Location and Description

The Menengai Caldera Geothermal Prospect is bound by the UTM co-ordinates 157000 E to 185000 E and 9966000 N to 0 (Equator) (Figure 1-2). The area encompasses Menengai volcano, Ol'Rongai volcanic field, the Olbanita plains and parts of the Solai graben. The prospect area measures 870 km^2 and extends from the immediate north of Nakuru Town in

the south to Kisanana in the north. The site can be accessed via Wanyororo route off Bahati-Solai road and Mr. Barclay's farm off Nakuru-Kabarak road in the northeastern and western planks of caldera respectively. The caldera has been grazing ground for the herders from surrounding areas in the past. Currently, there exist a lot of drilling activities, all-weather road networks, camps and engineering workshop yards for GDC's operations. The caldera has been in-habitable except for the northeastern section of caldera which has minimal settlement.

The caldera is a prominent geographical feature on the rift floor and its presence was noted as early as 1894 by travelers but first studied in details by McCall (1967). The caldera is partially filled by young rugged lava flows. Nakuru area lies at elevations between 1560 m and 2260 m above sea level and is characterized by rather flat topography, as a result of filling of the rift by volcanic rocks, and flattening topography by ignimbrites and other pyroclastic deposits locally covering faulting and differential uplift (e.g. Leat, 1991). The eastern shoulder of the inner trough rises some 600 m higher and forms the Bahati platform and the western shoulder forms the Mau plateau.

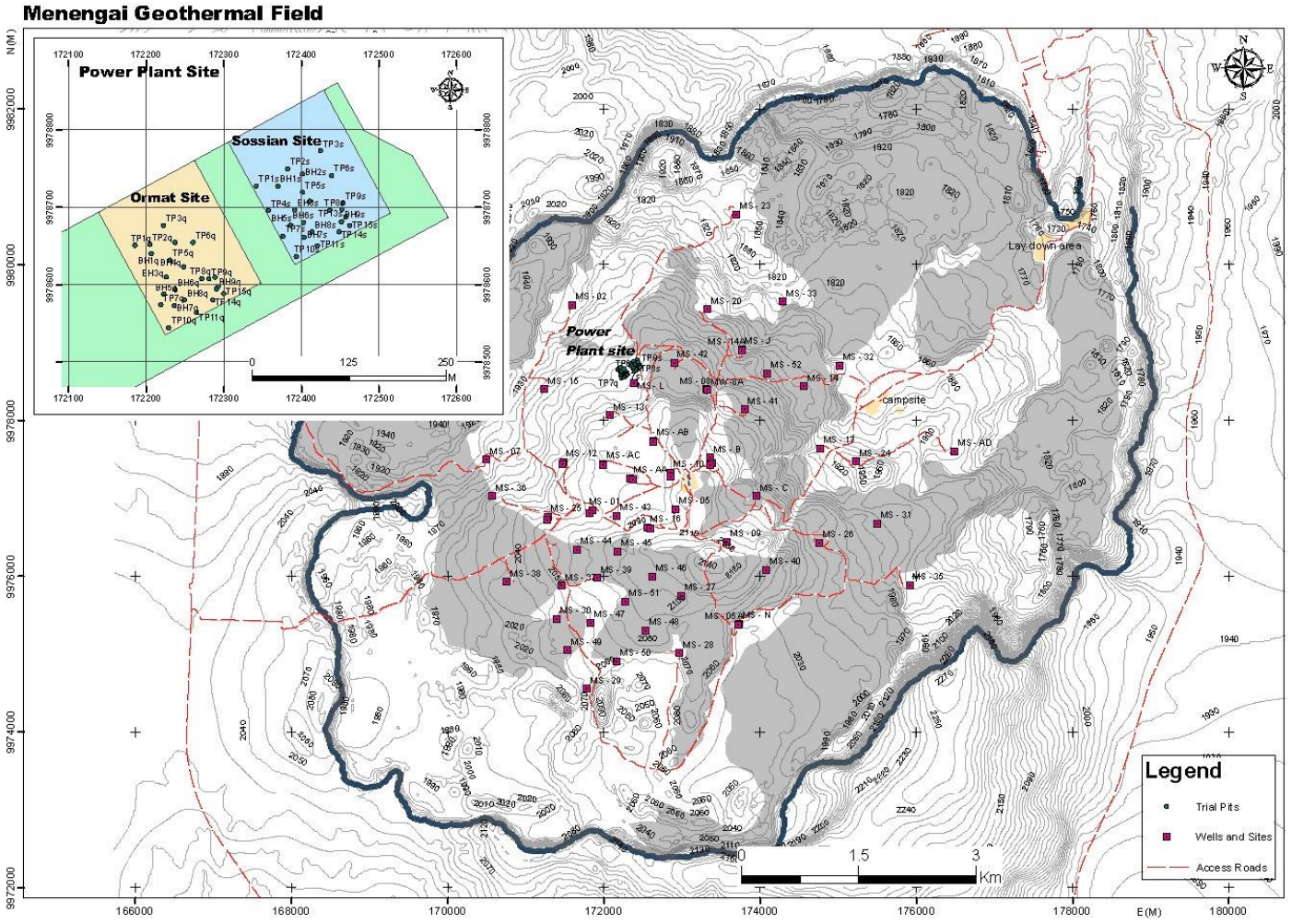

Figure 1-2: Map of the Menengai Caldera showing power plant location.

1.5.3 Menengai Geothermal Power plants

Three Independent Power Producers (IPPs) have been selected by Geothermal Development Company (GDC) (Figure 1-3). The IPPs will be required to put up 35MWe flash power plants in Menengai totaling to 105 MWe for the first 105MW phase of the 400MW project.

The IPPs are required to pay for the construction of the project in return for an equity stake and a share of the proceeds from the sale of power under an agreement that lasts in excess of 20 years. (GDC Strategic plan, 2013).

Figure 1-3: Layout of the power plants (Sosian sites 3) (GDC Strategic plan, 2013)

Power plant components include; steam separators, flashers, turbines, condensers, hot-well pumps, cooling towers, gas removal systems, generators, transformer systems and switchyard.

1.5.4 Climate

Rainfall in the prospect area is seasonal and fairly variable. The long rains start at the end of March through July with maximum in May, while short rains start at the end of September through November with the maximum rains in October. Minimum rainfall is experienced in January. Mean monthly maximum temperatures range from 22.8^0 C to 29.3^0 C. The seasonal variations show lowest temperatures in June–July period while highest temperatures are recorded in February-March period. Wind flow in generally characterized by south-easterly and easterly winds.

1.5.5 Vegetation

The vegetation of the area within and outside Menengai Caldera rim can be classified to bushed woodland, mixed bushland, bushed grassland, open grassland, and forest.

1.5.6 Land Use and Land Resources

Land ownership is mainly freehold with individuals owning land parcels with title deeds around Menengai. The Government of Kenya owns parts of Menengai and Bahati Forests and Lake Nakuru National Park.

Large-scale sisal farming and livestock (cattle, goats and sheep) keeping characterize the northern sector of the prospect particularly around Mogotio, Ol'Banita and Kisanana areas. Livestock keeping by pastoral communities is also practiced inside the caldera particularly in accessible areas. The Northeastern part of the prospect including Solai and Bahati areas is mainly characterized with large-scale coffee and dairy farming.

1.5.7 Physiography and Drainage

The location of Menengai is on the rift floor where the hydrogeological regime comprises of recharge from the higher rift scarps and the intense rift floor fracture/faulting resulting from extensional tectonics of continental rifting thus providing a good structural set-up that allows water from the rift scarps to penetrate deep into the crust. The water then flows towards the hot magmatic intrusives under the rift floor and the normal faults provide the conduits for the hot fluids to percolate to depth into possible geothermal reservoirs at shallower depths. (GDC, 2010). The regional tectono-volcanic axes; Solai and Molo TVAs may be such an important conduit of deep fluids thus an important geothermal controlling feature in the area.

Intra-caldera lake sediments of well bedded pumiceous sands with rounded pebbles in the north-eastern part of the caldera floor (Figure 1-4) indicates the existence of a palaeo-lake believed to be the result of overflow from the 'Gamblian' lake into the caldera through the SE graben and partly through underground channels, along joints and through tephra and soil horizons (Leat, 1984). The intra-caldera lake indicates a massive shallow groundwater body being recharged from eastern flank of the rift valley and Laikipia ranges. The ground water body could have great contribution to the aquifers being tapped by boreholes at the eastern foot of caldera for drilling water.

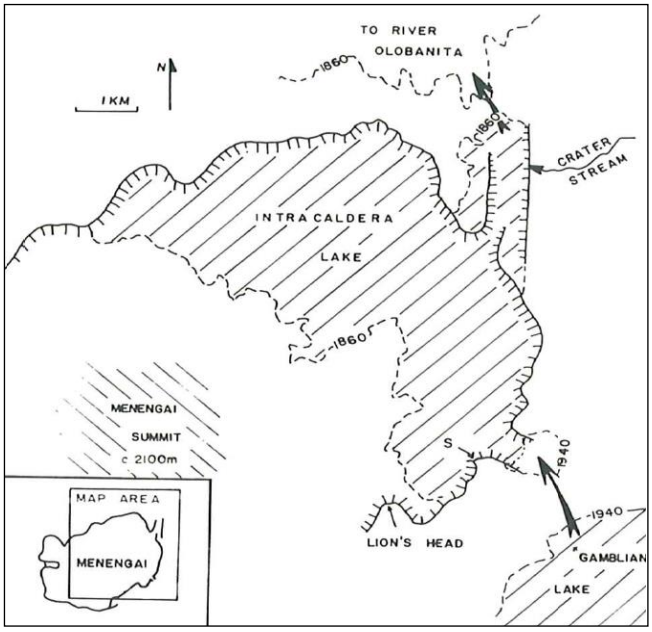

Figure 1-4: Intra-Caldera lake sediments (diagonal crosses). Arrows indicate probable water flow directions into and out of the caldera. (Leat, 1984).

CHAPTER TWO

2.0 LITERATURE REVIEW

2.1 Previous Geotechnical work within Menengai Caldera

The first ever geotechnical investigations in the study area was done by Independent Power Producers (IPPs) between the period of September to December 2014. The site investigation was restricted only to their respective proposed power plant sites at northwestern section of the caldera floor. The scope of geotechnical works for each IPP involved coring nine (9) boreholes of depths between 20 m – 30 m and digging fifteen (15) Trial pits to depths of 3 m each (figure 2-1).(Gibbs, 2015).

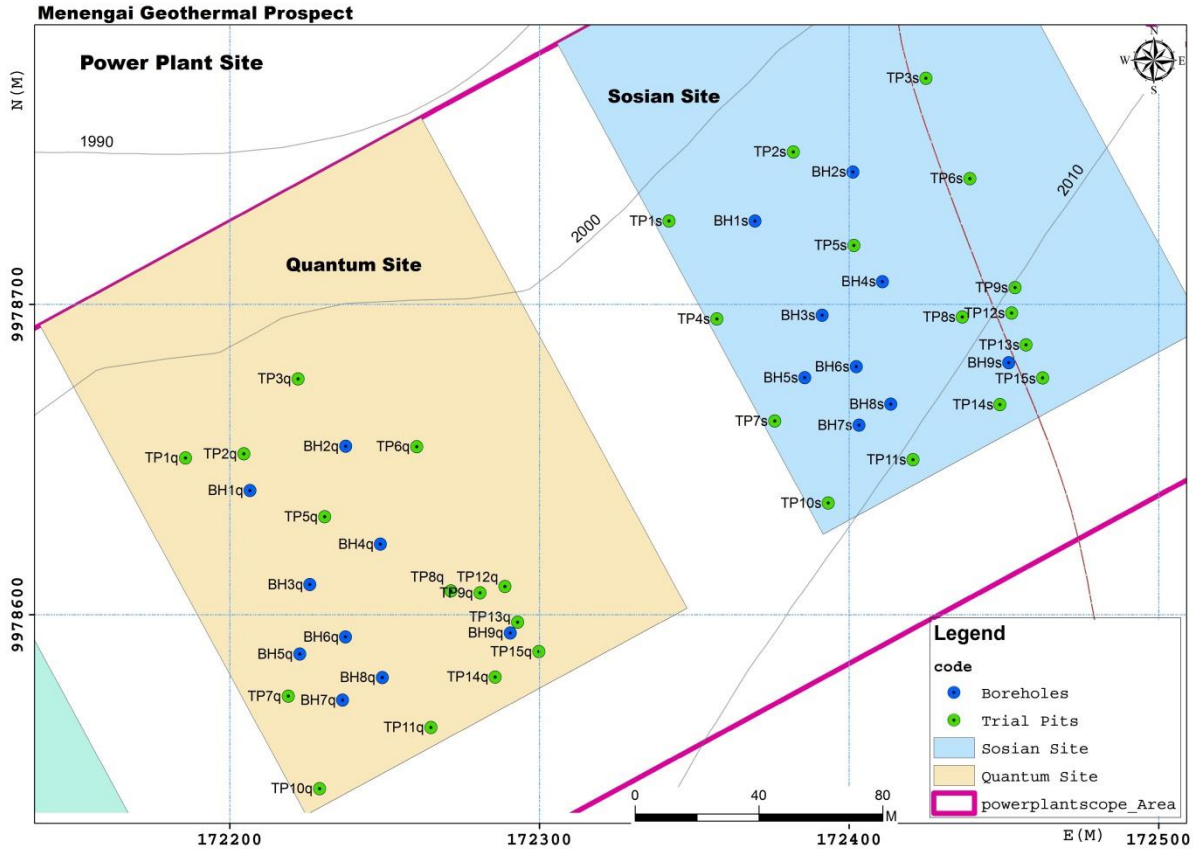

Figure 2-1: Site layout showing Sosian site (blue shade) for cored boreholes (BH) and Trial pits (TP). (Modified from Gibbs, 2015)

Core boring indicated quite homogeneous subsoils with top soils composed of a thin sandy gravel of extremely weathered trachytic lava/ rock fragments and pyroclastic material which are poorly sorted and angular mixed with volcanic glass to semi-pumiceous ash material (Gibbs, 2015). Below 2.0 m, the formation showed fine grained grayish and slightly weathered to fresh trachyte rock (Annex I). No groundwater was however encountered in during core drilling of 30 m meaning groundwater table is deeper than 30 m however there was lot of loss of circulation during core drilling implying highly fractured subsurface layers (Gibbs, 2015).

Atterberg Limit, Triaxial Tests (i.e. Unconsolidated Undrained Triaxial and Quick Test), Consolidation Test and Unconfined Compression Tests (UCS) could not be achieved since the rock and soil samples are non-plastic and granular (Gibbs, 2015). Standard proctor test and California Bearing Ratio (CBR) was conducted to check the compactibility of the soils. Compaction test (Standard Proctor test) was done to determine the relationship between the moisture content and the dry density of the soil for a specified compactive effort (Gibbs, 2015).

Actual soil Bulk Density could not be tested since there were no undisturbed samples recovered on site due to granular nature of the soils; consequently no field density tests were performed on site. However, soil bulk density estimated (Table 2-1) from compaction test done on disturbed bag samples obtained was from the boreholes. Samples from each borehole were subjected to laboratory CBR tests with the aim of proposing a pavement structure under estimated suitability of the material on site after testing (Table 2-1). It was assumed that the functions of the pavement will be under different loading of light capacity to those of heavy capacity (Gibbs, 2015). (Table 2-1).

Table 2-1: CBR results summary (Gibbs, 2015)

BH	**DEPTH** (m)	**OMC** (%)	**MDD** (Kg/m^3)	Estimated Bulk Density (Kg/m^3)	CBR (%)	Swell (%)
1B	0.0-1.4	29.0	1055	1408	24.0	0
2B	0.0-1.0	25.2	1205	1659	58.0	0
3B	0.0-1.2	28.5	1004	1525	39.0	0
4B	0.0-0.7	34.0	1006	1315	41.0	0
5B	0.0-0.8	30.5	1030	1364	31.0	0
6B	0.0-1.0	32.5	1018	1442	88.0	0
7B	0.0-1.5	35.8	1085	1523	41.0	0
8B	0.0-1.5	18.2	1192	1558	33.0	0
9B	0.0-1.5	34.5	1315	1671	67.0	0

Gibbs (2015) noted Standard Proctor test in soils to have low density following high degree of fracturing on the near surface subsoils and should be given more attention during the design phase, failure to that can result to over settlement under heavy loading leading to the collapse of the structures. Compaction test indicated the rocks are suitable for use in the construction as fill material mixed with imported clay (binder) materials. Standard Proctor test and California Bearing Ration (CBR) showed that pumiceous silty sand has the requisite compacted strength for use as sub-base material for the service loading on the site and adequate enough to receive the pavement structure (Gibbs, 2015). One dimensional Swell test determined from California Bearing Ratio test indicated that soils have no swelling potential (Gibbs, 2015).

Point load Test on core samples were done from cores selected from various depths (Table 2-2 and 2-3). Rock specimens were selected in areas where rock core could not satisfy UCS specimen requirements. Point load and Uniaxial Compression (UCS) tests on rock cores showed that the trachytic rock layers are largely weak to moderately strong due to high degree of fracturing and pumiceous in nature and can easily fracture upon slightest blow or impact (Gibbs, 2015).

Table 2-2: Rock specimen tested for point load (Gibbs, 2015).

BORE HOLE	DEPTH (m) From - To	IS P/H^2 KN/m^2	IS(50) KN/m^2	TERM	WEATHERING GRADE
1B	2.85-3.00	2.602	3.251	Strong	II
2B	1.50-1.70	2.334	2.750	Strong	II
3B	3.30-3.50	3.510	4.136	Strong	II
4B	2.20-2.40	2.932	3.454	Strong	III
5B	3.20-3.40	2.007	2.508	Strong	II
6B	2.75-2.95	1.859	2.322	Strong	II
7B	2.50-2.80	1.115	1.393	Weak	III
8B	3.00-3.50	1.933	2.415	Strong	III
9B	3.65-3.80	3.375	3.977	Strong	III

Table 2-3: Rock specimen tested for UCS (Gibbs, 2015).

BOREHOLE	DEPTH (m) From - To	Density kg/m^3	STRENGTH ACHIEVED (MPa)	TERM	WEATHERING GRADE
1B	3.70-3.90	1359	6.761	Weak	II
	6.00-6.20	2013	23.578	Moderately strong	II
2B	4.20-4.50	2379	24.560	Moderately strong	I
	5.80-6.00	2013	20.139	Weak	I
3B	4.70-5.00	1902	17.192	Weak	I
	5.70-6.00	2132	12.236	Weak	II
4B	3.60-3.90	1723	8.596	Weak	II
	6.00-6.30	1987	18.175	Weak	I
5B	2.50-2.80	1849	14.225	Weak	II
	6.55-6.80	2119	17.420	Weak	I
6B	2.25-2.70	1905	14.181	Weak	II
	5.00-5.25	2129	20.607	Moderately strong	I
7B	5.25-5.50	1893	6.877	Weak	II
	7.60-7.80	1746	6.118	Weak	I
8B	5.20-5.50	2030	18.175	Weak	II
	7.00-7.20	1574	19.319	Weak	I
9B	4.60-4.80	2149	27.017	Moderately strong	III
	6.00-6.40	2047	14.736	Weak	III

The formation showed less cohesion with increased angle of shear (Table 2-4). Since no undisturbed sample was recovered due to granular nature of soils, there was no density test at site. However cohesion and angle of shear were extracted from laboratory as shown below;

Table 2-4: Cohesion and Angle of shear (Shear box) test. (Gibbs, 2015)

BH	DEPTH (m)	Cohesion (kPa)	Angle of shear (^{0})
1B	0.0-1.4	20.0	31
2B	0.0-1.0	10.0	37
3B	0.0-1.2	21.0	30
4B	0.0-0.7	21.0	26
5B	0.0-0.8	12.0	29
6B	0.0-1.0	18.0	29
7B	0.0-1.5	13.0	37
8B	0.0-1.5	22.0	32
9B	0.0-1.5	12.0	28

The soil was cohesion-less (frictional soil) for U100 sampling. Standard Penetration Test (SPT) could not be achieved on soil to assist in determining allowable Soil Bearing Capacity (Gibbs, 2015). However, allowable Load Bearing Capacity values was computed using Meyerhof's theory from values obtained from Direct Shear tests, Uniaxial Compression Shear tests of rock cores, Point Load tests, and SPT's N-value of rock core from borehole BH-9B between 1.50 m to 1.95 m depth. The allowable load capacity (Qa) was obtained by dividing the ultimate load capacity by a minimum safety factor of 3.

Substituting the corresponding values and employing security factor of 3, the allowable load bearing capacity values of the soil are presented in Tables 2-5 to 2-8. Differential settlement is estimated to be less than 25 mm (Gibbs, 2015).

Table 2-5: Obtained allowable load bearing capacity values from direct shear test (Gibbs, 2015).

BH	DEPTH (m)	Angle of shear (^{0})	Cohesion (kPa)	BREATH B (m)*(assumed)*	DEPTH D (m)*(assumed)*	Allowable Bearing capacity (KN/m^2)
1B	0.0-1.4	31.0	20.0	1.5	1.5	804
2B	0.0-1.0	37.0	10.0	1.5	1.5	1440
3B	0.0-1.2	30.0	21.0	1.5	1.5	759
4B	0.0-0.7	26.0	21.0	1.5	1.5	462
5B	0.0-0.8	29.0	12.0	1.5	1.5	472
6B	0.0-1.0	29.0	18.0	1.5	1.5	603
7B	0.0-1.5	37.0	13.0	1.5	1.5	1501
8B	0.0-1.5	32.0	22.0	1.5	1.5	1001
9B	0.0-1.5	28.0	12.0	1.5	1.5	466

Table 2-6: Obtained allowable load bearing capacity values from uniaxial compression shear tests of rock cores (Gibbs, 2015)

BOREHOLE	DEPTH (m) From - To	Density kg/m^3	STRENGTH ACHIEVED (MPa)	TERM	Allowable bearing capacity (kPa)
1B	3.70-3.90	1359	6.761	Weak	1,126.83
	6.00-6.20	2013	23.578	Moderately strong	3,929.67
2B	4.20-4.50	2379	24.560	Moderately strong	4,093.33
	5.80-6.00	2013	20.139	Weak	3,356.50
3B	4.70-5.00	1902	17.192	Weak	2,865.33
	5.70-6.00	2132	12.236	Weak	2,039.33
4B	3.60-3.90	1723	8.596	Weak	1,432.67
	6.00-6.30	1987	18.175	Weak	3,029.17
5B	2.50-2.80	1849	14.225	Weak	2,370.83
	6.55-6.80	2119	17.420	Weak	2,903.33
6B	2.25-2.70	1905	14.181	Weak	2,363.50
	5.00-5.25	2129	20.607	Moderately strong	3,434.50
7B	5.25-5.50	1893	6.877	Weak	1,146.17
	7.60-7.80	1746	6.118	Weak	1,019.67

8B	5.20-5.50	2030	18.175	Weak	3,029.17
	7.00-7.20	1574	19.319	Weak	3,219.83
9B	4.60-4.80	2149	27.017	Moderately strong	4,502.83
	6.00-6.40	2047	14.736	Weak	2,456.00

Table 2-7: Obtained allowable load bearing capacity values from point load tests of rock cores (Gibbs, 2015)

BORE HOLE	DEPTH (m) From - To	IS P/H^2 KN/m^2	IS(50) KN/m^2	TERM	Allowable bearing capacity (kPa)
1B	2.85-3.00	2.602	3.251	Strong	541.83
2B	1.50-1.70	2.334	2.750	Strong	458.33
3B	3.30-3.50	3.510	4.136	Strong	689.33
4B	2.20-2.40	2.932	3.454	Strong	575.67
5B	3.20-3.40	2.007	2.508	Strong	418.00
6B	2.75-2.95	1.859	2.322	Strong	387.00
7B	2.50-2.80	1.115	1.393	Weak	232.17
8B	3.00-3.50	1.933	2.415	Strong	402.50
9B	3.65-3.80	3.375	3.977	Strong	662.83

Table 2-8: Obtained allowable load bearing capacity values from SPT N-Values of rock cores (Gibbs, 2015)

BORE HOLE	DEPTH (m)		N-VALUES (No)	N'60 -VALUES	BREATH B (m)	DEPTH D (m)	D/B	k	Allowable Bearing capacity (KN/m^2)
BH 9B	1.50	1.95	47	37.6	1.5	1.5	1.00	1.33	300

To allow for variations in the rock, Gibbs, 2015 recommended that the design strength be taken as the lowest measured strength divided by a factor of 10 due rock fractures. In this way the very weak trachyte layer will have a design strength of 6.877/10 = 0.6877MPa.

The minimum design strength recorded from the unconfined compressive strength was 0.6877MPa in BH 7B at a depth of 5.5 m. On a pad footing of $1.5m^2$, placed 3 m below ground level the allowable bearing pressure rock with this strength was in excess of 1000 kPa on a strip or pad foundation. This bearing pressure was calculated to be five times the unconfined compressive strength divided by a factor of safety (Gibbs, 2015). According to the type of soil detected; the type of settlements that are expected will take place during the construction period, however, no settlement is expected to take place where foundations are taken to a rock formation (Gibbs, 2015).

The rocks showed slight to moderate weathering with coefficient of permeability through laboratory permeability test/falling head on remolded soil samples depths of 0-0.5 m (Table 2-9) showing excellent permeability with coefficients of sand and gravel (Gibbs, 2015).

Table 2-9: Coefficient of Permeability (Gibbs, 2015).

TEST LOCATION	DEPTH (m) From - To	Coefficient of permeability, k (mm/sec)
1B	1.0-2.0	0.022
2B	0.0-1.0	0.023
3B	1.0-4.0	0.026
4B	0.0-1.0	0.008
5B	0.0-0.5	0.009
6B	0.0-1.0	0.008
7B	0.0-0.5	0.007
8B	0.0-1.5	0.028
9B	0.0-1.5	0.006

Soil chemical studies for sulphates and chlorides were done to determine the subsoil content of salts that could affect the concrete foundation. pH values were obtained in order to quantify the state of alkalinity and acidity in the soil (Table 2-10). Sulphates and chlorides contents of soils showed concentration range from moderate to severe in terms of aggressiveness to concrete and slight alkalinity (Gibbs, 2015).

Table 2-10: Summary of Chemical Tests (Gibbs, 2015).

Test Location	Depth (m)	PH Value	Chloride content (%) m/m	Sulphate content SO_3 (%) m/m
BH 4B	0.0-0.7	7.92		
BH 5B	0.0-0.8		0.056	
BH 6B	0.0-1.0			0.043
BH 8B	0.0-1.5		0.043	
BH 9B	0.0-2.0			0.021

Natural Moisture Content and Specific Gravity were generally low due to dried post-caldera lava which is largely covering the surface (Gibbs, 2015).

2.2 Seismic Refraction Tomography (SRT) and Multi-Channel Analysis of Surface Wave (MASW) Seismic Survey

Seismic imagery by Gibbs, 2015 identified three sub-layers at power plant site through Seismic Refraction Tomography and Engineering parameters results; The first Layer

characterized by low Concentration Index (Ci) and high Stress Ratio (Si) which reflects weak incompetent soil /rock, Second layer characterized by relative low Concentration Index (Ci) and less Stress Ratio (Si) which reflected fairly competent soil and Third layer characterized by relative high Concentration Index (Ci) and low Stress Ratio (Si) which reflected moderate competent soil. Material Index (v) values for 1st layer reflected incompetent to slightly competent soil, 2nd layer reflected fairly to moderate competent soil while for the 3rd layer reflects moderate competent to competent soil/rock. Calculated Density Gradient (Di) for the 1st layer is characterized by relative high Density Gradient whereas 3rd layer reveals values characterized by relative low Density Gradient. Both Seismic Refraction Tomography (SRT) (Figure 2-1) and Multi-Channel Analysis of Surface Waves (MASW) (Figure 4-2) techniques were employed in seismic survey.

SRT Profile (S-N)

The profile 1 oriented SW-NE, comprised of three spreads of 72 m giving a total length of 216 m. The seismic section along Profile 1 depicted a probe within the upper 30 metres below the ground level revealing a total of three layers (Figure 2-2).

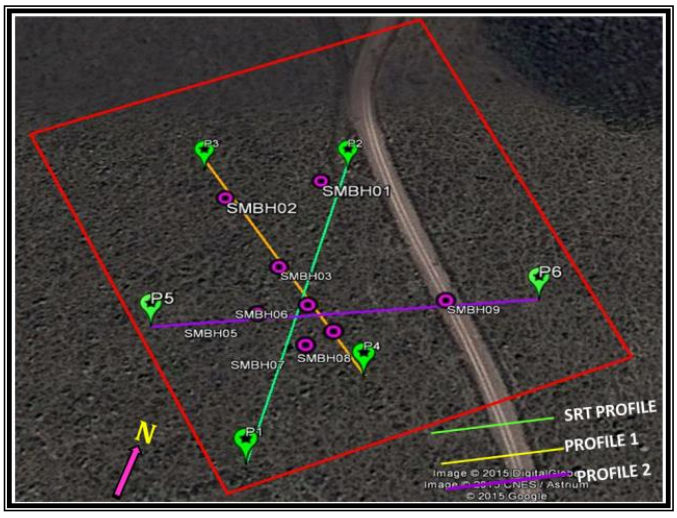

Figure 2-2: SRT Seismic profiles layout. (Gibbs, 2015).

The seismic model represent three distinct layers that stretch from the earth surface to a depth of between 28 metres and 30 metres (Figure 2-2) below the ground level and the profile was oriented in S-N direction. The results of each layer are described below:

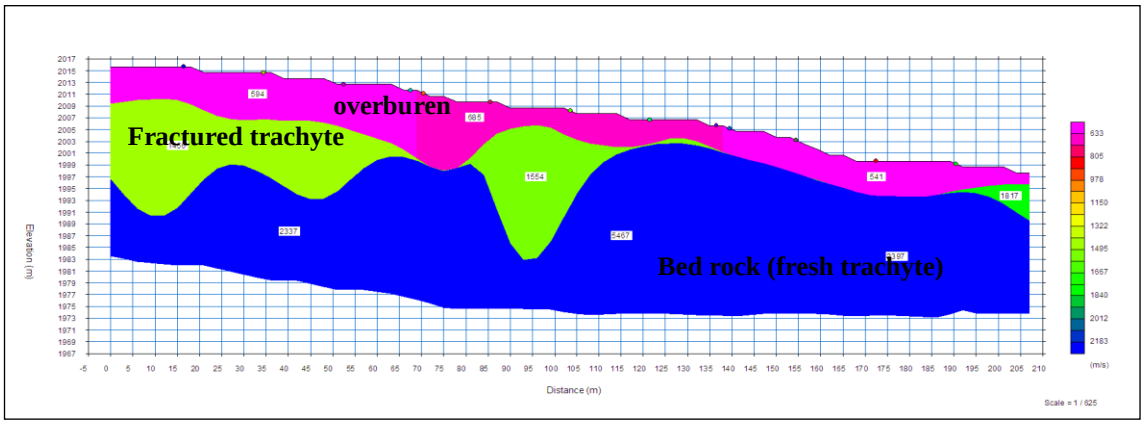

Figure 2-3: Geo-Velocity Model (Seismogram) for Profile 1(P3-P4) (Gibbs, 2015).

Layer 1 (Designated by pink colour)

The upper layer (pink) recorded variable layer thickness ranging between 2 m and 8 m below the ground level and velocity values from 541 m/s to 685 m/s with an average velocity value of 607 m/s. This velocity of 607 m/s represented very thick loose to compact dark brown to yellowish gravelly clayey sandy soil which represents the overburden material. The layer thickens gradually varying considerably from S towards N, with section between 0 m mark and 80 m mark has recorded the thickest overburden material with an average layer thickness of 7 m. The overburden layer thickness between 80 m mark 207 m mark varies between 2 m and 4 m with an average stratum thickness of 4 m. Generally, the overburden material across the seismogram is interpreted to be composed of loose gravelly silty sand with rumbles and stones of pumitic materials as observed during the fieldwork (Gibbs, 2015).

Layer 2 (Designated by light green colour)

Layer two is characterized by a geo-velocity values ranging from 1817 m/s to 1554 m/s with varying layer thickness and forms a stomach-shaped geological structure between 0 m mark and 75 m mark on the model with layer thickness decreases towards north. The maximum layer thickness achieved is 19 m between depths ranging from 6 m to 25 m below the ground

level at 10 m mark. The geo-velocity section represented between 80 m mark and 110 m mark for this layer has a thickness of 23 m with depth ranging between 2 m and 25 m and characterized by estimated lateral extent of 30 m. The geo-structural features at 10 m mark and 95 m mark are inferred as faulted zones within the project area. Layer two is interpreted as composed of marginally fractured and partially rock mass material (possibly pumitic trachytes and is easily rippable using Cat D9/R (Gibbs, 2015).

Layer 3 (Designated by blue colour)

Layer three marks the basal layer of the model with an average velocity of 3400 m/s which represents bedrock of Menengai Trachyte. The formation represents fresh and intact basal layer whose thickness is more than 25 metres from the model except at the faulted zones of the model where deep fracturing and weathering is witnessed. The velocity of the bedrock varies from 2337 m/s to 5467 m/s. The rock-head of the basal layer is characterized by irregular bedrock relief especially to the south which is a clear indication of fractured basement.

Multi-Channel Analysis of Surface Wave (MASW) measured shear-wave velocities within the project site. It showed that the soils are stiff from the surface to 8 m depth (Vs ~ 240–325 m/s), followed by partially weathered and marginally fractured rocks to a varying depth of 18 m (velocity ranging from 325 to 764 m/s) (Gibbs, 2015).

In most of the study areas of power plant sites, Vs30 falls in the range 350 m/s-708 m/s, except the northern parts of the site which has velocity of 213-325 m/s (Gibbs, 2015). Based on Vs30 of the soils, a major portion of the study area is predominantly classified as C-type (350–708 m/s) in accordance with the 1997 NEHRP provision. Sites located in the southern part of the area have Vs30 values larger than 360 m/s, thereby qualifying the soils as NEHRP class C-type (360–760 m/s). Based on the V_S30 value, Sosian site has been put into one

seismic zone (Vs30 >350m/s) which has been classified as class C (Gibbs, 2015).

In most of the study areas of power plant site, $Vs30$ falls in the range 350 m/s-708 m/s, except the northern parts of the site which has velocity of 213 - 325 m/s. Based on *Vs*30 of the soils, a major portion of the study area is predominantly classified as C-type (350–708 m/s) in accordance with the 1997 NEHRP provision. Sites located in the southern part of the area have V_{s30} values larger than 360 m/s, thereby qualifying the soils as NEHRP class C-type (360–760 m/s) (Gibbs, 2015).

In Gibbs report, data was analyzed using SeisImager/SW software and two dimensional shear wave velocity models at every 5 m depth from ground surface was developed. Also, the average shear wave velocity up to 30m (V_{S30}) was measured which is used for site characterization. Based on the V_{S30} value, Sosian site has been put into one seismic zone (V_{S30} >350m/s) which has been classified as class C (Figure 2-4).

MASW Classification

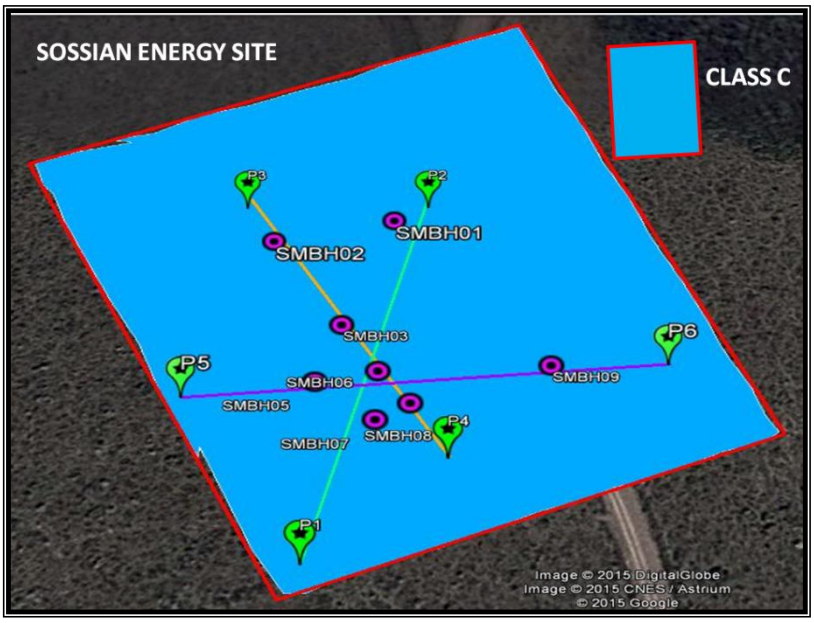

Figure 2-4: Seismic lines layout and classification of zones at Sosian site (Gibbs, 2015).

Profile 1

Profile 1 comprised of three seismic spreads in each spread of both 1D and 2D seismic surveys (Gibbs, 2015). For profile 1 the values of V_{S30} ranged from 213 to 708 m/s with average value of 450 m/s (Class C).

Profile 2

Profile 2 comprised of three seismic spreads which are combined into one single seismic profile. Both 1D and 2D seismic surveys were conducted. The V_{S30} for all the test sites are calculated. The values of V_{S30} are ranging from 325 to 562 m/s with an average of 435 m/s (Class C) (Gibbs, 2015).

Profile NW-SE

Seismic profile 1 was conducted in NW-SE direction covering a spatial horizontal distance of 120 m for both 1D and 2D active MASW. The results of seismic data indicated that the site has three distinct major layers whose geo-velocity values range from 280m/s to 800m/s (Gibbs, 2015). The S-wave velocity values between 280 m/s and 325 m/s typical of an overburden material which is interpreted as compact pyroclastic sediments (gravelly silty sand with cobbles and boulders). The velocity values ranging from 325 m/s to 480 m/s represent the upper layer of partially fractured and marginally weathered rock which is interpreted as pumitic trachyte (Gibbs, 2015). Velocity values between 480m/s to 800m/s is considered to represent very hard competent basement rocks basically trachyte (Gibbs, 2015). From the 1D active MASW analyses, the Vs30 value ranged from 298m/s to 682m/s with an average value across the site calculated as 435m/s. Seismic characterization, evidently classified as class C (Gibbs, 2015). Figure 2-5 below shows dispersion curve, field S-wave raw data, 1D shear wave velocity and 2D shear wave velocity model along Profile NW-SE.

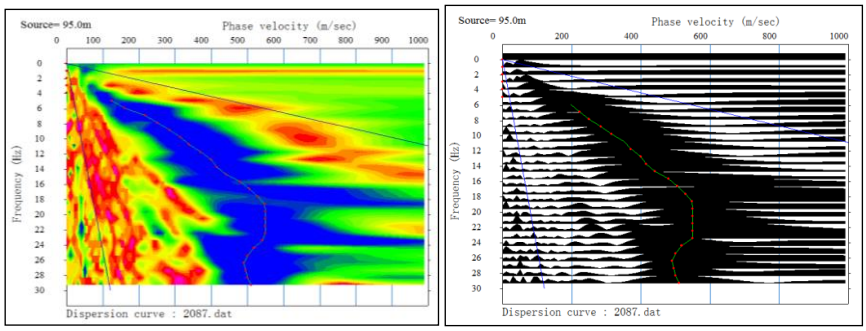

a) Dispersion Curves

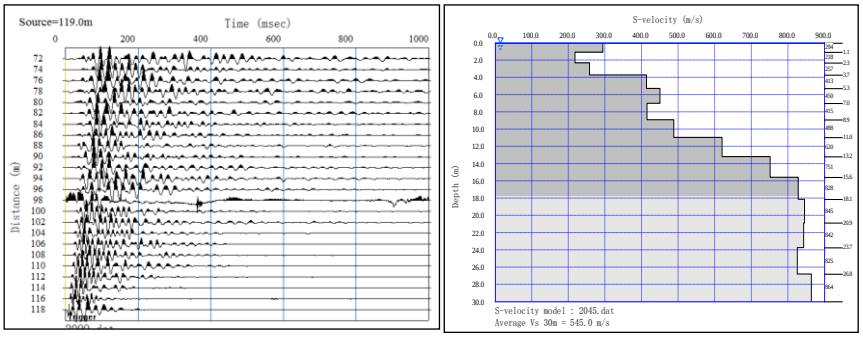

b) *Field S-Wave raw data* c) *1D shear wave velocity*

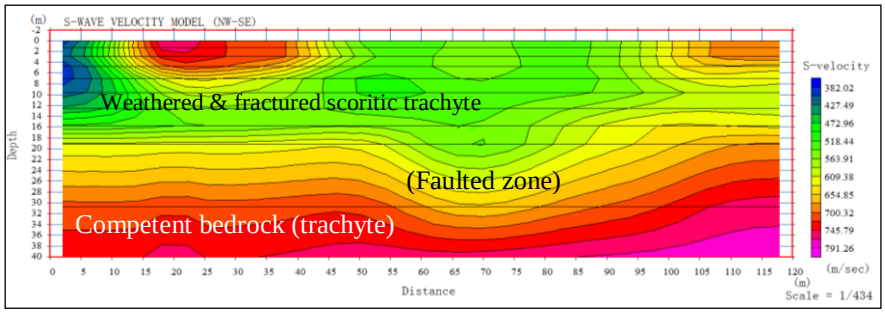

c) The 2D shear wave velocity model

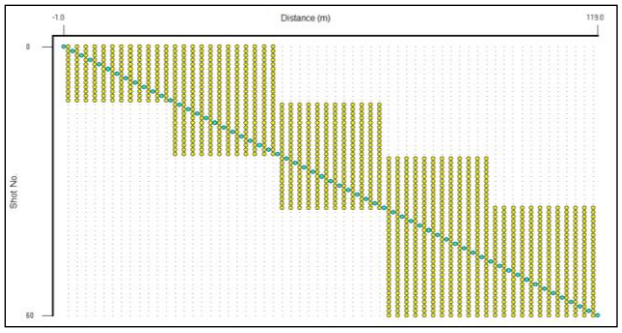

d) *2D MASW continuous fixed receiver geometry method for profile 1 (blue dots are shot locations while dot are receivers)*

Figure 2-5: Profile (NW-SE);- a) Dispersion Curve, b) Field S-wave raw data, c) 1D shear wave velocity and d) 2D shear wave velocity model (Gibbs, 2015).

2.3 Seismicity of Menengai and East African Rift System

Previous seismic study around the Menengai region showed that careful analysis of seismic data within volcanic geothermal system can help identify the origin of the event (Simiyu and Keller, 2001, Simiyu, 2009). For instance, the study showed that events related to the rift tectonic of the hydrothermal fluid movement within the reservoir zone. The tectonic events have classical and clear P and S phase arrival and are deeper occuring along rift faults while the reservoir events lack clear P and S arrival and are shallow within the reservoir zone (Simiyu and Keller, 2001, Simiyu, 2009).

The latest earthquake study (Patlan et al., 2013) was a collaborative effort to characterize the Menengai region. The study was an effort of the Geothermal Development Company (GDC) and the Department of Geological Sciences at the University of Texas at El Paso (UTEP) who deployed a total of fourteen seismometers around the Menengai region from March 2011 to December 2013.

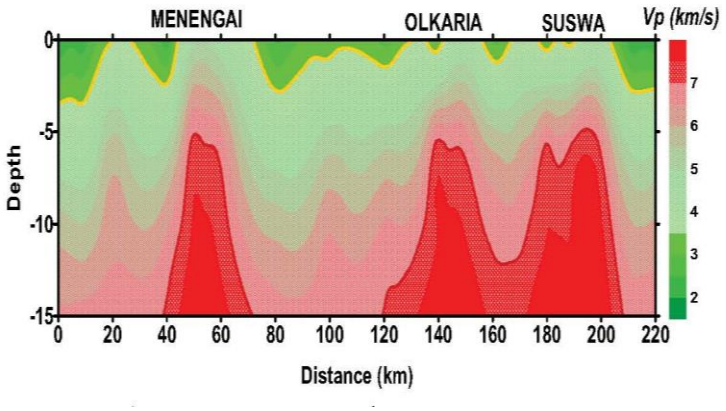

Figure 2-6: Seismic velocity models along the rift axis showing high Velocity zones beneath Menengai Olkaria and Suswa Volcanic centers (Simiyu and Keller, 2000).

An integrated study that combined seismic and gravity data for the southern section of the rift (Simiyu and Keller, 2001) modeled a high-density body 20 km wide and at about 6 km deep in the Menengai region, which was interpreted as an intrusion of mantle related material. In addition, recent resistivity study (Wamalwa et al., 2013) have imaged a conductive zone at about 6 km deep below the surface, which was interpreted as magmatic material which is the source of heat for the geothermal system. This interpretation is consistent with the

interpretation from seismic survey by Simiyu and Keller (2001). The seismic results showed high velocity magmatic intrusions underlying the Menengai, Olkaria and Suswa volcanoes.

The regions of extensional tectonics and magmatic volcanism are often characterized by low level seismic strain release and frequent earthquakes of relatively small magnitudes (Simiyu and Keller 2001, Simiyu 2009). This characteristic can be associated by suppressed faulting by stress equalization due to a built up of magma pressure countering tectonic stress. In the East African rift the difference in the seismicity between the active (magmatic) and inactive (non-magmatic) have been observed (Maguire et al., 1992). In particular the Kenya rift is characterized by basaltic and rhyolitic volcanism (MacDonald et al., 1994). In this rift thermal overprint by up-warped asthenosphere lowers the crustal tensile strength that leads to the decrease in the level of seismically released strain along the rift. The Kenya rift is also characterized by the thinning of the crust that also reduces the potential of down dip rapture width and hence reducing the seismogenic potential of any faults.

Geotechnical studies over geothermal fields can provide fundamental information about the subsurface structures and processes that are key to siting high producing wells as well as an overview of the distribution of active faults within the surveyed region for infrastructural work (e.g. Simiyu, 2000, 2009; Simiyu and Keller, 2001). Previous resistivity and potential field (gravity and magnetic) surveys in the Menengai region have indicated faults and fractures that have been targeted for drilling for steam and intrusions (e.g. Árnason et al., 2010; Wamalwa et al., 2011).

Interpretation of previously collected micro-earthquake data (Simiyu, 2009) also showed that that most of the small earthquake events around Menengai caldera were restricted to the upper 2 to 6 km depth zone indicating a brittle-ductile transition zones at about 6 km depth that is used to infer the presence of a hot magma material.

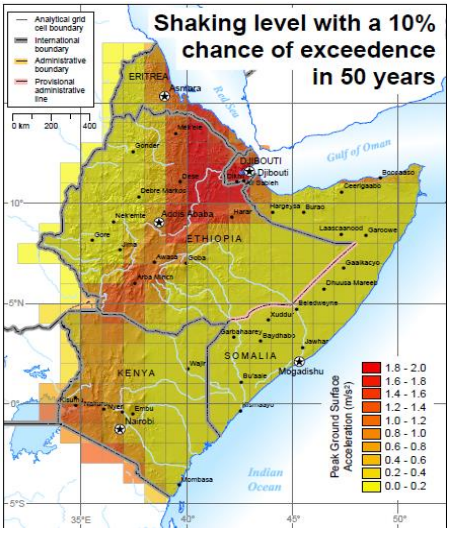

Figure 2-7: Ground shaking levels shown as peak ground acceleration for the Rift system. Results obtained from the Global Seismic Hazard Assessment Program (GSHAP)

Most events cannot be felt on the surface because they are very small in magnate and can only be identified by very sensitive equipment in contact with the bedrocks in the region. Menengai has been having small by the number of events per Julian day. The intensity of the events are micro magnitude that our cause by hydrothermal pockets within Menengai. For earthquakes of this magnitude, the ground shaking levels are extremely low and most of these events are normally never felt at the surface.

A map of the shaking levels expressed as peak ground surface acceleration was developed for the Horn of Africa region by the Global Seismic Hazard Assessment Program, shows that the region around Menengai that peak ground acceleration is about 0.6 to 0.8 m per second squared. This means that the shaking levels (Figure 2-7) in this region are very low. The Figure 2-8 above shows that the preferential orientation of the fractures and faults in the Menengai region is generally north south.

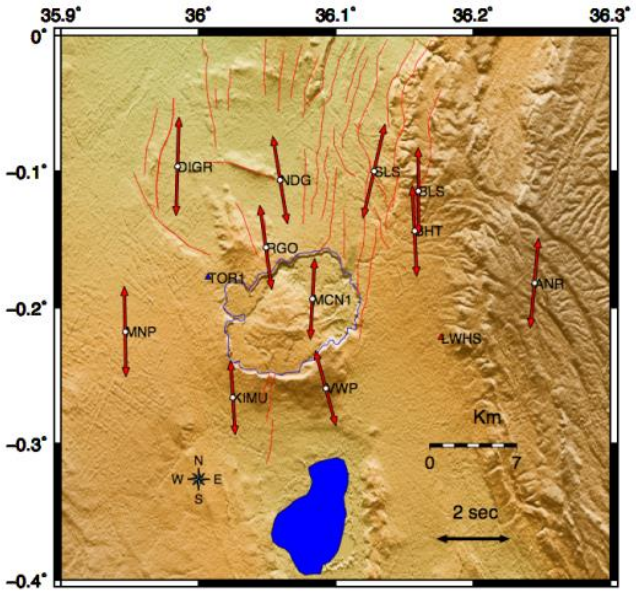

Figure 2-8: A map showing SKS shear wave splitting (GSHA Program)

2.4 Petrology and Petrogenesis of Menengai rock formation.

Menengai is composed almost entirely of strongly quartz-normative, silica-oversaturated, peralkaline trachytes, with subordinate volumes of metaluminous trachytes and pantelleritic rhyolites (Macdonald et al., 1970; 1994; 2011; Macdonald and Bailey, 1973; Macdonald, 1974; Leat et al., 1984; Macdonald and Scaillet, 2006; Macdonald and Baginski, 2009). Macdonald (1974) classified the Menengai rocks to range from comenditic trachyte through pantelleritic trachyte to pantellerite based on Al_2O_3 and FeO contents. A recent TAS plot of cuttings from geothermal wells MW-02, MW-04, MW-06, MW-07 and MW-08 show a chemical variation ranging from basalt through to trachyte and rhyolite in composition. (Mbia, 2014).

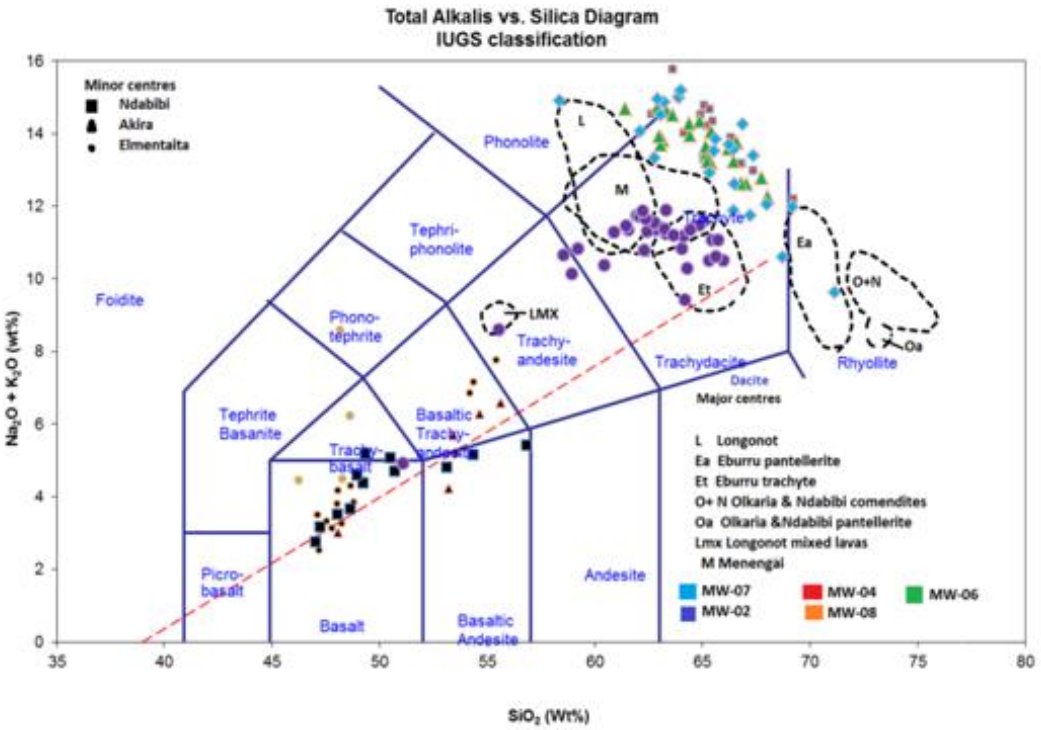

Figure 2-9: Alkali-silica plot showing the compositional range of Menengai subsurface rocks from wells MW-02, MW-04, MW-06, MW-07 and MW-08 and the neighboring volcanic centres.(modified from Clarke et al., 1990; Macdonald, 2006; Mitchell, 1986). (Mbia,2014)

Al_2O_3 versus FeO diagram show subsurface samples displaying two unique distinct trends, with well MW-02 showing similar chemical clustering with surrounding surface samples

from Menengai while the other wells, MW-04, MW-06 and MW-07 cluster between pantellerites and comendite (Mbia, 2014). Selected samples from well MW-08 plots in the pantelleritic trachyte field. The two plots clearly show the importance of fractional crystallization even though other processes like magma mixing, assimilation and hydrothermal activities may possibly be involved. Geochemical trends for volcanic rocks represent a 'liquid line of descent'. This is the path taken by residual liquids as they evolve through the differential withdrawal of minerals from the magma (e.g. Cox et al., 1979).

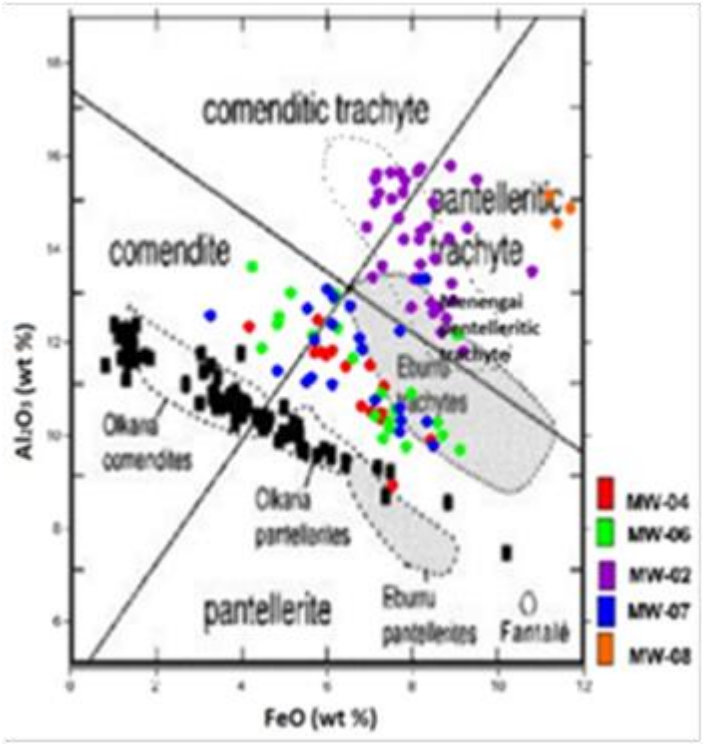

Figure 2-10: Al_2O_3 versus FeO classification of the Menengai rocks and the neighboring volcanic centres (modified from Macdonald, 1974) (Mbia, 2014).

Menengai therefore, shows a complex geochemical evolution, resulting from the interplay of magma mixing, crystal fractionation and liquid state differentiation as noticed by Leat et al., (1984). The controlling mechanism at any time was related to the growth stage of the

complex, the presence of volatile gradients in the chamber, and the distribution of magma densities in the chamber (Leat et al., 1984).

Prior to major ash flow eruptions, the magma reservoir would grow by the addition and mixing of two or more trachytic melts, only slightly different in composition. A volatile-rich cap eventually separated from the lava-forming zone and became compositionally zoned by liquid state processes (Leat et al., 1984). In late pre-caldera times, trachyte magma was able to penetrate into the cap zone, resulting in the eruption of mixed magma (Leat et al., 1984). The first Menengai ash flow tuff was erupted from a compositionally zoned magma chamber which showed strong roof-ward enrichment in Fe, Mn, Cs, Hf, Nb, Pb, Rb, Ta, Th, U, Y, Zn, Zr, and the REE (including Eu) and probably also Na, Cl, and F, and roof-ward depletion in Al, Mg, Ca, K, Ti, P, Ba, and Sc (Leat et al., 1984).

Zoning of the magma chamber was achieved by liquid state differentiation, probably involving volatile transfer and thermodiffusion, and minor crystal fractionation (Leat and Macdonald, 1984). After a period of homogenization of magma remaining in the upper parts of the chamber, the second Menengai ash flow tuff was erupted, with the formation of the present caldera. This unit is also compositionally zoned, although with less observed enrichment factors than the first ash flow. Caldera collapse was followed by convective overturn within the magma chamber and the rise to the roof-zone of a Ba-rich magma from a level not tapped by the ash flow (Leat et al., 1984). Enrichment of volatiles in this zone resulted in the establishment of a stable density interface between an upper, tuff-producing zone, and the lower, lava forming zone.

2.5 Structural and Tectonic Setting of Menengai Caldera

Structurally, Menengai is a pre-caldera low-angle volcanic shield, which has almost vertical embayed caldera walls upto 300 m high (Leat, 1983). The floor of the area depicts

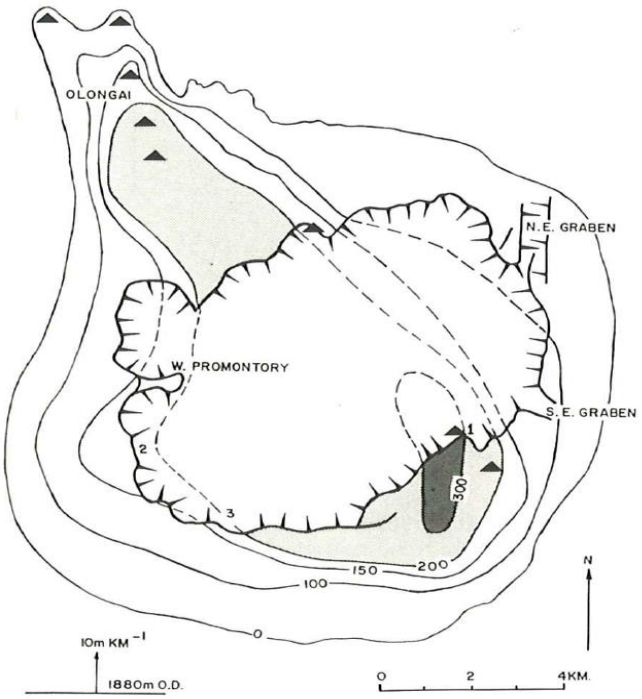

Figure 2-11: Isopach map for the pre-caldera volcanics of Menengai. Solid triangles indicate probable or possible pre-caldera vents. Point 1(the Lion´s head Cliff), point 2(the W cliff) and point 3 (the SW cliff). (Leat, 1984)

extensional tectonics with spatial variation in the stress field, indicated by two main orientations of fault systems. Leat (1984) found that the structures associated with Ol'rongai Tectono-volcanic axis are oriented to the NNW-SSE and are related to the NW-SE pre-caldera orientation. However faults associated with the Solai TVA system have NNE-SSW orientation, which corresponds to the orientation of the Menengai caldera. The Menengai caldera is an elliptical depression with major and minor axes measuring about 11.5 km and 7.5 km respectively (GDC, 2010; Leat, 1983). The circular rim of the caldera ring fault is well preserved with vertical cliff. The ring structure has only been disturbed by the Solai graben faults at the northeastern end of the caldera and at the SSW end.

Isopachs map for the pre-caldera volcanics (Figure 2-11) illustrate that the volcano was shield-like, with flanks dipping away from the summit and had a broadly oval plan, with a major axis of 22 km, trending NW-SE, and a minor axis of 15 km trending NE-SW (Leat 1984). It had a maximum thickness of just over 300m, covered an area of approx. 210 km^2 and probably had a central ridge lying along the major axis, with a line of vents along the crest. This central ridge would have intersected the regional fault trend of about 450 (Leat 1984). It is at this intersection that the caldera collapse occurred (Figure 2-11).

CHAPTER THREE

3.0 METHODOLOGY

3.1 Materials and Methods

The method and approach to this study is a holistically desktop study through correlations of geotechnical findings, seismic and tectonics aimed to identify and characterize the geohazard expected upon development of geothermal resource in Menengai. Insitu structural orientations may dictate the seismic and landmass movements thus directions triggered by tensional and compressive forces from numerous discharging wells within the caldera thereby affecting the developments on the surface.

3.2 Desktop studies

- Study of previous geotechnical survey data from Sosian Energy power plant site, regional and local geological seismicity, structural geology, geology and geothermal study in Menengai prospect.
- Analysis of temperature profiles of drilled geothermal wells to understand tectono-volcanic make-up leading to the current caldera structure general structural geology with the caldera.
- Undertake surficial slope risk matrix using 2-m contour map.
- Characterize possible geohazard events both on the surface and underlying reservoir likely to occur during and upon development of geothermal resource.

3.3 Analytical Assessments of Geohazards attributes

3.3.1 Geotechnical Surveys and Seismic Engineering parameters

Assessment of geotechnical findings at proposed Sosian power plant site during fieldworks and laboratory results are correlated with seismic engineering parameters deduced from Seismic Refraction Tomography (SRT) and Multi-Channel Analysis of Surface Wave (MASW) Seismic Survey. The study aims to observe the homogeneity of the near surface strata geotechnical properties of which shall hold the foundations of the surface constructions at power plant site. Similar geotechnical properties to 30 m depth could pose negative geohazard if the strata are not stable.

Comparison of earthquake events in project area is studied in respect to the Seismic Refraction Tomography (SRT) and Multi-Channel Analysis of Surface Wave (MASW) Seismic parameters. Geothermal production stage is expected to increase seismicity due to increased vibrations at depths following discharging wells all at the same time. Geohazards are expected to be enhanced if seismic engineering properties of underlying geological strata are susceptible to slight trigger of deep landmass movement.

3.3.2 Temperature profiles of geothermal wells and Structural Geology

The structural geology within the caldera is assessed if they indeed control trends of temperature profile curves in respect to locations of geothermal wells. The study aims to check whether geohazard that affect wells' productivity depends on the prevailing geological structure at their locality.

Temperature profile curves can be clustered according to similar shapes and trends in respect to the wells' localities to help deduce and infer geological structures that the wells might have encountered or cut through during drilling process. The comparative study temperature profiles which indicate well's productivity would postulate probable geohazards dictated by

encountered geological structure. The study aims to further evaluate tectonic processes that may have led to the present day caldera floor structure and physiography. The analysis aims to as well identify geohazards controlled by tectono-volcanic processes in relation to geological structures and wells' productivity.

3.3.3 Topographic Slope Risk Analysis

Analysis of surface physiography approach aims to identify risky slopes that are susceptible to fail upon subjected to heavy constructions or influenced by agents of surface weathering. The higher the degree of investment on a particular sloppy surface the higher the risk to the development. The assessment aims to establish risk matrix on different sections of caldera floor.

CHAPTER FOUR

4.0 RESULTS AND DISCUSSION

4.1 Results

4.1.1 Geotechnical Insitu Field Tests and Laboratory Results

Caldera floor is dominantly curved by moderate to extremely weathered trachytic lavas at the surface though appear little bit competent to hold foundations of construction structures below depths of 2 m. The fact that no groundwater was encountered in cored boreholes to 30 m and almost complete circulation losses of drilling water imply a highly fractured and permeable near-surface strata thus high chances of stratigraphic failures when subjected to heavy weights.

Surface lavas weathers to chips of pumiceous medium to large irregular greyish granules with patches of brownish decomposed/altered zones due to leaching of iron. Loose soil could therefore not be attained for Atterberg Limit, Triaxial Tests (i.e. Unconsolidated Undrained Triaxial and Quick Test), Consolidation Test and Unconfined Compression (UCS), Standard proctor/compaction, California Bearing Ratio (CBR) and Bulk density testing. CBR and Proctor tests had to be estimated in the laboratory and pumiceous soils indicated little or no possibility of swelling upon moistening as well as low specific gravity. Near surface rocks observed to be highly fractured and weak on Point load and Uniaxial Compression (UCS) tests with less degree of cohesion thus higher angles of shear. Since no soil was tenable during site investigation, Standard Penetration Test (SPT) could not be performed to assist in determining allowable Soil Bearing Capacity. However, allowable Load Bearing Capacity values was computed using Meyerhof's theory from values obtained from Direct Shear tests, Uniaxial Compression Shear tests of rock cores, Point Load tests, and SPT's N-value of rock core from borehole BH-9B between 1.50 m to 1.95 m depth.

Concentration range of Sulphates and chlorides are moderate to severe hence the formations may be aggressive to concrete and slight alkalinity.

4.1.2 Seismic Engineering Parameters and Earthquake Analysis

Seismic imagery identified three sub-layers (Table 4-1) with first Layer characterized by low Concentration Index (Ci) and high Stress Ratio (Si) which reflects weak incompetent soil /rock, Second layer characterized by relative low Concentration Index (Ci) and less Stress Ratio (Si) which reflected fairly competent soil and Third layer characterized by relative high Concentration Index (Ci) and low Stress Ratio (Si) which reflected moderate competent soil. Material Index (v) values for 1st layer reflected incompetent to slightly competent soil, 2nd layer reflected fairly to moderate competent soil while for the 3rd layer reflects moderate competent to competent soil/rock. Calculated Density Gradient (Di) for the 1st layer is characterized by relative high Density Gradient whereas 3rd layer reveals values characterized by relative low Density Gradient. Correlation of Seismic Refraction Tomography (SRT) and Multi-Channel Analysis of Surface Waves (MASW) where seismic velocities are measured seamed to marry and three layers also noticeable. The upper layer having low seismic velocities (V_P range from 541 to 685 m/sec) and a thickness ranges between 0.0 to 8 m indicative of loose highly weathered layer. The middle layer had higher seismic velocity than the upper layer (V_P range between 1817 to 1554 m/sec, and a thickness range between 2 m to 25 m which could be the upper section of the bedrock and highly fractured and weathered. The lower layer had also high seismic velocity (V_P ranges between 2337 to 5467 m/sec, and a depth ranges between 2m to 28m (Table 4-2).

Table 4-1: Summary of Ranges of the calculated engineering parameters of the bedrock layers (Gibbs, 2015)

Vp m/s	Vs m/s	ρ gm/cc	Poisson's Ratio (σ)	Concentration Index (Ci)	Stress Ratio (Si)	Index Material (v)	Density Gradient (Di)	Young's Modulus (E) Mpa	Shear Modulus (μ) or Rigidity (Mpa)
LAYER 1									
607	305	1.54	0.33	4.02	0.49	-0.33	-0.50	380	143
640	328	1.56	0.40	3.34	0.54	-0.51	-0.43	774	81
LAYER 2									
1609	941	1.96	0.25	5.17	0.32	0.04	-0.60	4338	1735
1546	920	1.94	0.21	5.43	0.30	0.10	-0.65	1642	244.7
LAYER 3									
3400	2017	2.37	0.23	5.38	0.30	0.09	-0.63	23717	9641
2814	1712	2.26	0.24	5.85	0.26	-0.85	-0.67	15898	6624

Table 4-2: Summary of Geo-Velocity values and layer thickness (Gibbs, 2015).

Layer	Average Vp (m/s)	Av. Layer Thickness	Depth Range	Inferred Lithology
1	607	4	0 - 8	Gravelly Silty Sand (Pyroclastic sediments)
2	1609	15	2 - 25	Marginally fractured and partially weathered rocks (pumitic trachyte)
3	3400	Over 12	2 - 28	Intact/Sound bedrock (trachyte)

4.1.3 Analysis of Structural Geology and volcano-tectonic processes through Categorization of Temperature discharge profiles

Studies of temperature discharge profile curves of particular geothermal wells currently drilled show some reversal in temperature along specific trends implying cold water infiltration through deep-seated structures encountered by the wells. Five sets of trends of temperature profiles can evidently be identified and could imply distinctive underlying geological structures that define behavioral changes of geotechnical and geothermal reservoir within the caldera.

1. **Cluster I** – Geothermal wells MW-01, MW-13, MW-19A, MW-23.

2. **Cluster II** – Geothermal wells MW-03, MW-04, MW-04A, MW-08, MW-11, MW-12, MW-15, MW-16, MW-19, MW-21, MW-22.
3. **Cluster III** – Geothermal wells MW-01A, MW-5A, MW-09, MW-10A, MW-17A MW-10ST, MW-17, MW-20A, MW-30.
4. **Cluster IV** – Geothermal wells MW-06, MW-09A, MW-09B, MW-20.
5. **Cluster V** – Geothermal wells MW-07

Cluster I.

This set of wells show gradual steady increase of temperatures from the surface with a slight increase at 600 m to 800 m and 1300 m and 1800 m below ground level. Temperature increase implies hot feed-zones or aquifers. These wells show normal geothermal gradient that is temperature increases with depth. Static groundwater levels vary between 300 m to 600 m with largely characterized with pressure pivots mainly around 1300 m below ground levels implying most permeable section of the well. Figure below show examples of Cluster I temperature profiles of MW-01, MW-10A, MW-13 and MW-19A.

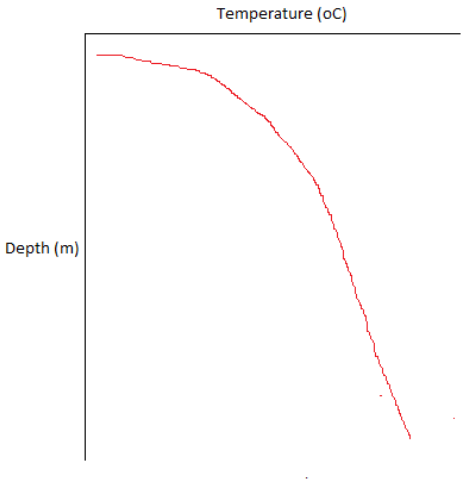

Figure 4-1: Cluster 1 Temperature profiles trend.

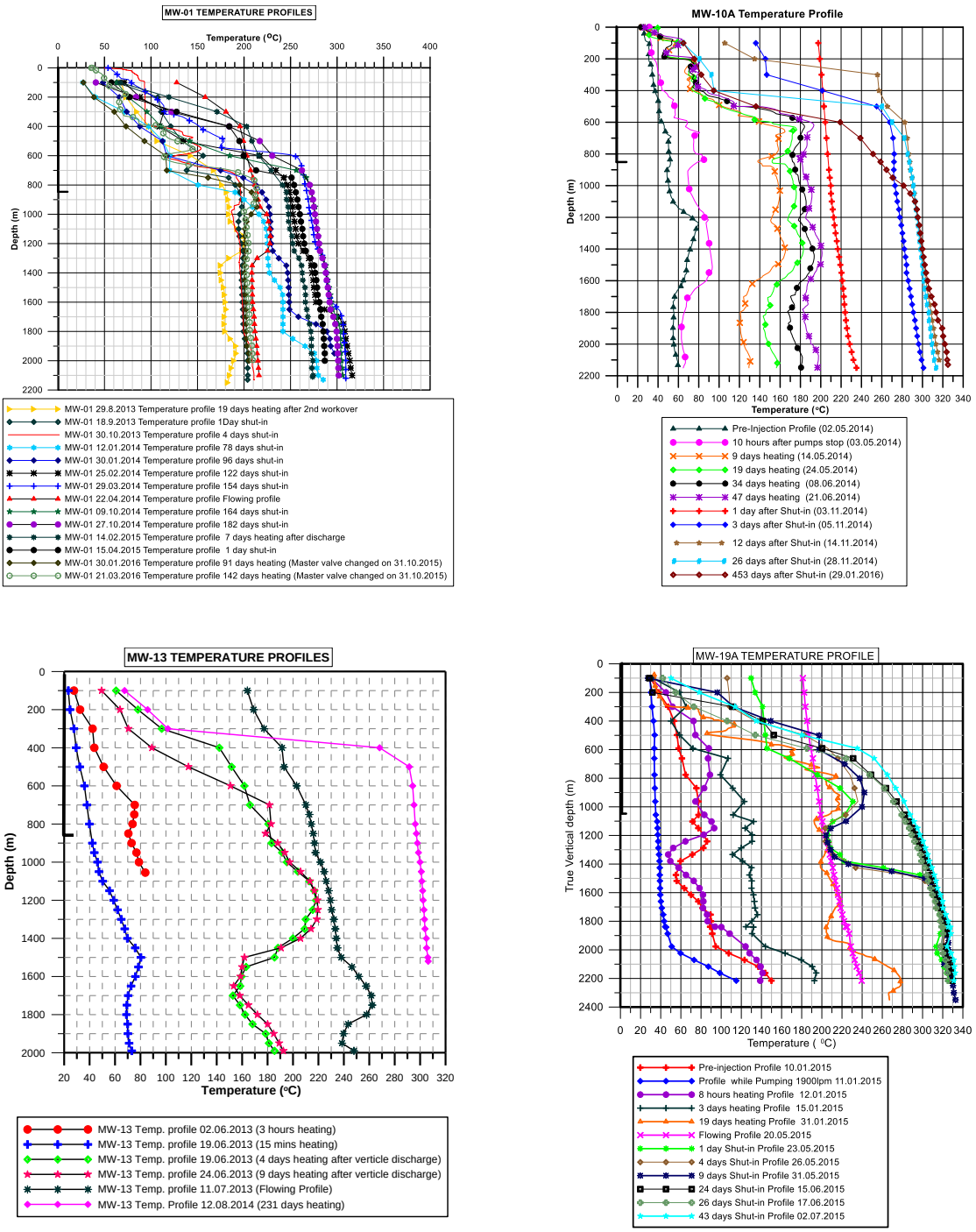

Figure 4-2: Temperature profiles of MW-01, MW-10A, MW-13 and MW-19A.

The wells are located at the central section of the caldera and don't appear to have intersected through a lateral fractures that could be transport cold fluids to the wells.

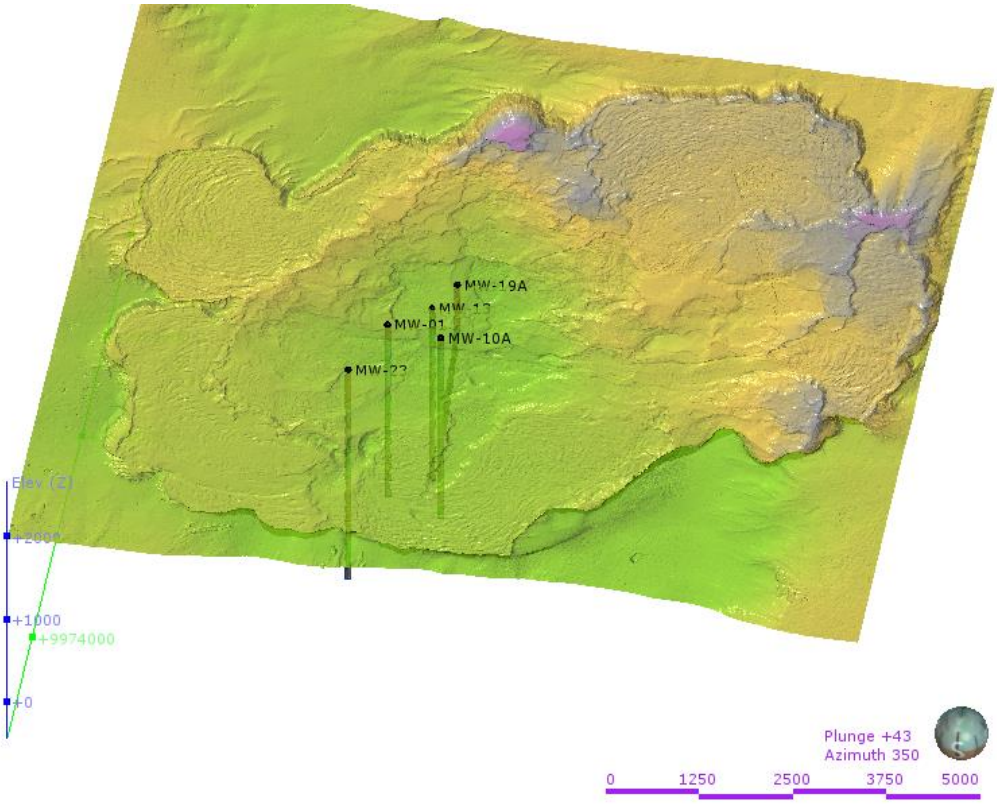

Figure 4-3: 3-D Leapfrog imagery view of Cluster I wells' location on the caldera floor.

***Cluster II*.**

This set of wells has characteristically low temperatures from surface and slightly and gradually increases temperatures between 1200 m to 1300 m with a steady temperature increase below 2000 m and 2200 m downwards. The wells seem to have been drilled through an impermeable hot intrusive body from 2000 m depth.

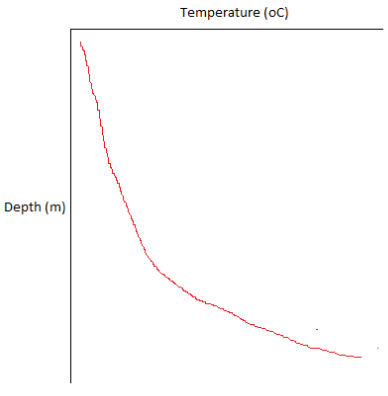

Figure 4-4: Cluster 2 Temperature profiles trend

Figure below show examples of Cluster II temperature profiles of MW-03, MW-04, MW-04A, MW-11, MW-12, MW-15, MW-16, and MW-21.

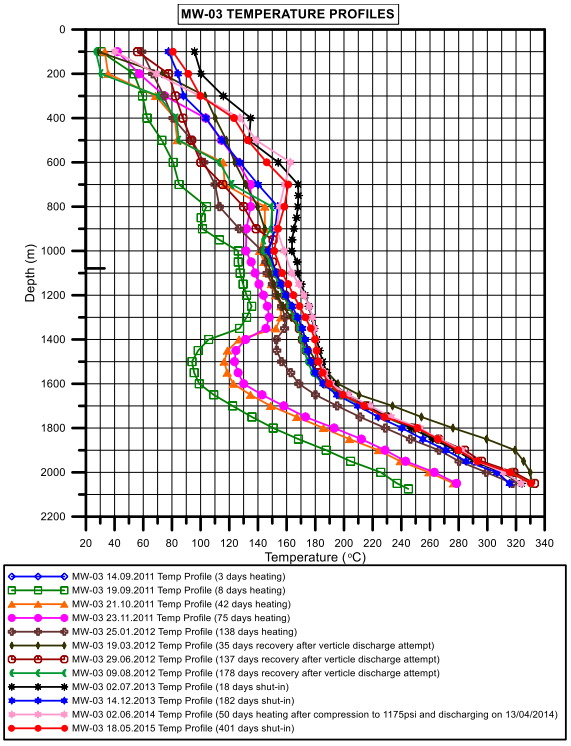
MW-03 TEMPERATURE PROFILES
Depth (m)
Temperature (°C)
MW-03 14.09.2011 Temp Profile (3 days heating)
MW-03 19.09.2011 Temp Profile (8 days heating)
MW-03 21.10.2011 Temp Profile (42 days heating)
MW-03 23.11.2011 Temp Profile (75 days heating)
MW-03 25.01.2012 Temp Profile (138 days heating)
MW-03 19.03.2012 Temp Profile (35 days recovery after verticle discharge attempt)
MW-03 29.06.2012 Temp Profile (137 days recovery after verticle discharge attempt)
MW-03 09.08.2012 Temp Profile (178 days recovery after verticle discharge attempt)
MW-03 02.07.2013 Temp Profile (18 days shut-in)
MW-03 14.12.2013 Temp Profile (182 days shut-in)
MW-03 02.06.2014 Temp Profile (50 days heating after compression to 1175psi and discharging on 13/04/2014)
MW-03 18.05.2015 Temp Profile (401 days shut-in)

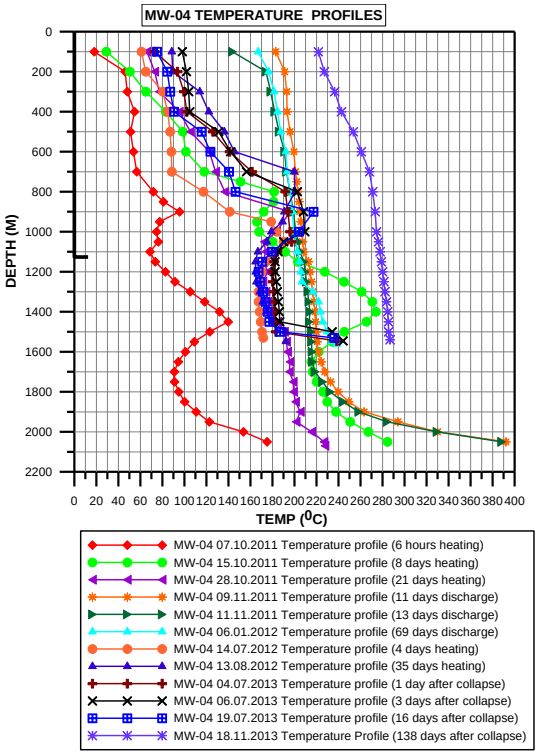
MW-04 TEMPERATURE PROFILES
DEPTH (M)
TEMP (0C)
MW-04 07.10.2011 Temperature profile (6 hours heating)
MW-04 15.10.2011 Temperature profile (8 days heating)
MW-04 28.10.2011 Temperature profile (21 days heating)
MW-04 09.11.2011 Temperature profile (11 days discharge)
MW-04 11.11.2011 Temperature profile (13 days discharge)
MW-04 06.01.2012 Temperature profile (69 days discharge)
MW-04 14.07.2012 Temperature profile (4 days heating)
MW-04 13.08.2012 Temperature profile (35 days heating)
MW-04 04.07.2013 Temperature profile (1 day after collapse)
MW-04 06.07.2013 Temperature profile (3 days after collapse)
MW-04 19.07.2013 Temperature profile (16 days after collapse)
MW-04 18.11.2013 Temperature Profile (138 days after collapse)

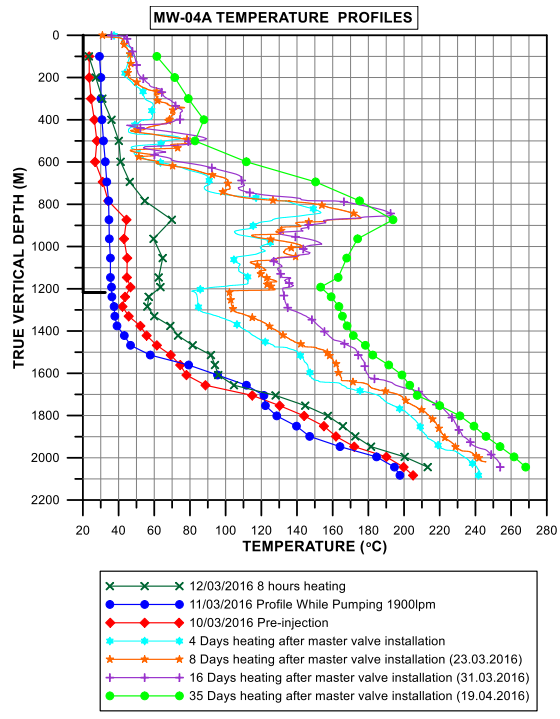
MW-04A TEMPERATURE PROFILES
TRUE VERTICAL DEPTH (M)
TEMPERATURE (°C)
12/03/2016 8 hours heating
11/03/2016 Profile While Pumping 1900lpm
10/03/2016 Pre-injection
4 Days heating after master valve installation
8 Days heating after master valve installation (23.03.2016)
16 Days heating after master valve installation (31.03.2016)
35 Days heating after master valve installation (19.04.2016)

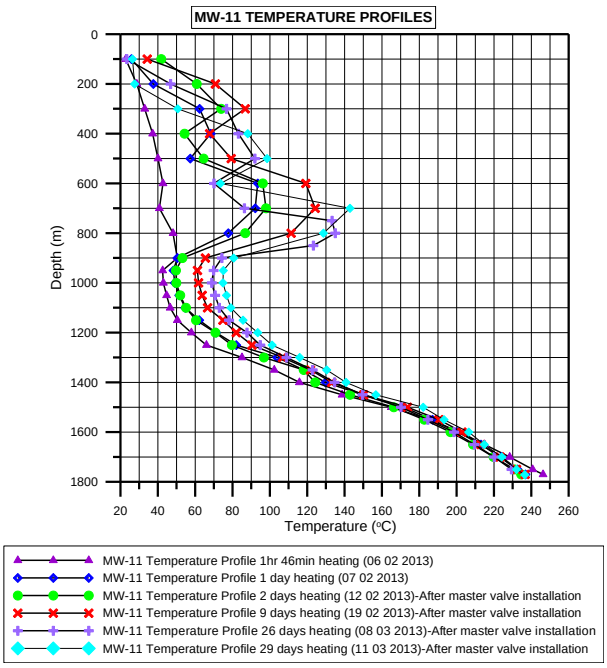
MW-11 TEMPERATURE PROFILES
Depth (m)
Temperature (°C)
MW-11 Temperature Profile 1hr 46min heating (06 02 2013)
MW-11 Temperature Profile 1 day heating (07 02 2013)
MW-11 Temperature Profile 2 days heating (12 02 2013)-After master valve installation
MW-11 Temperature Profile 9 days heating (19 02 2013)-After master valve installation
MW-11 Temperature Profile 26 days heating (08 03 2013)-After master valve installation
MW-11 Temperature Profile 29 days heating (11 03 2013)-After master valve installation

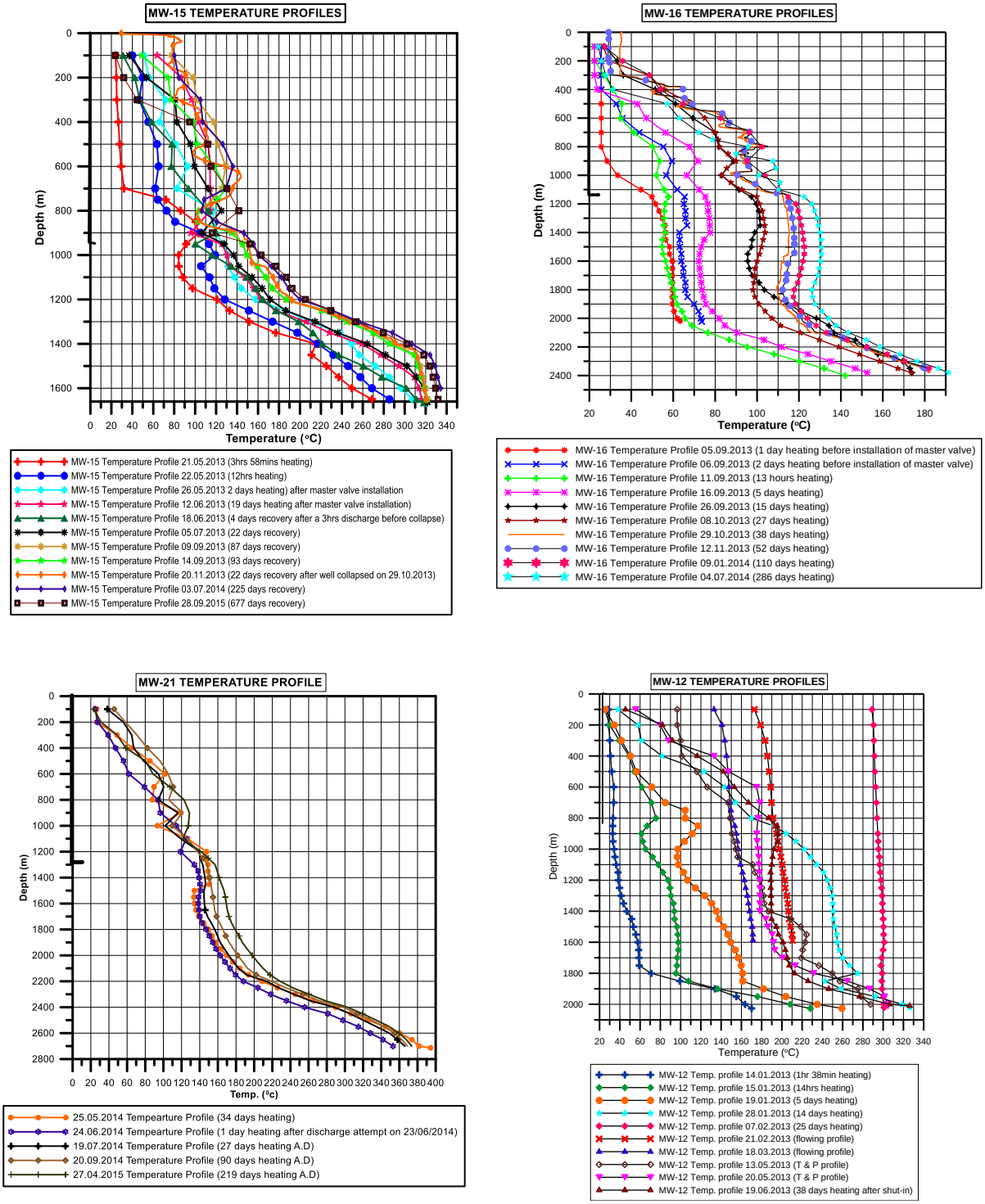

Figure 4-5: Temperature profiles of MW-03, MW-04, MW-04A, MW-11, MW-12, MW-15, MW-16, and MW-21.

Most wells seem to fall within cluster II trends. This indicates existence of an expansive hot intrusive body at the central area of the caldera.

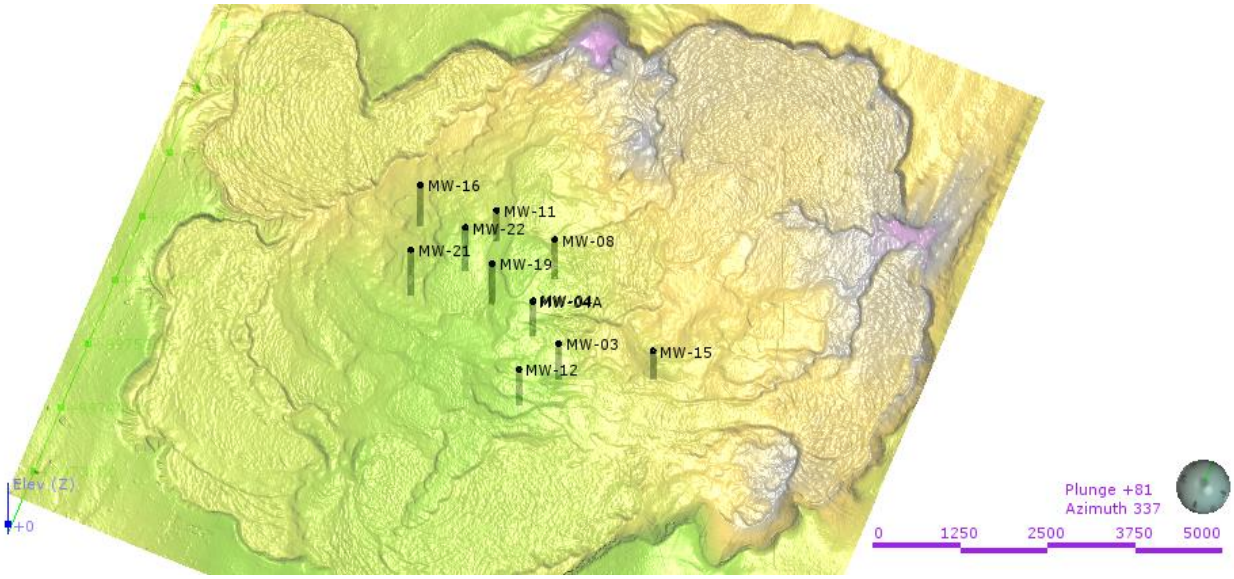

Figure 4-6: 3-D Leapfrog imagery view of Cluster II wells' location on the caldera floor.

Cluster III.

These wells show acute temperature reversal from 1100 m below ground level to deep depths of 1800 m to 2200 m where there is observed slight temperature increase. The reversals imply major cold in-flow through major fracture which can be presumed to be fault-scarps of underlying mini-calderas.

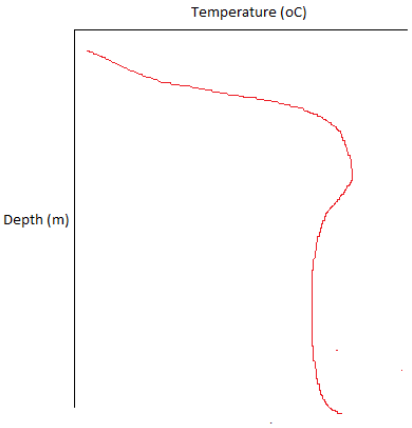

Figure 4-7: Cluster 3 Temperature profiles trend

Sudden cooling of geothermal wells must have been due to a shallow cold in-flow into the wells thus cooling the whole well-bore column to the bottom. The wells might either been drilled through lateral fault-scarps within the caldera.

Below temperature profiles of wells MW-02, MW-06A, MW-09, MW-10, MW-17, MW-17A, MW-20A, MW-23, and MW-30A show similar temperature reversals.

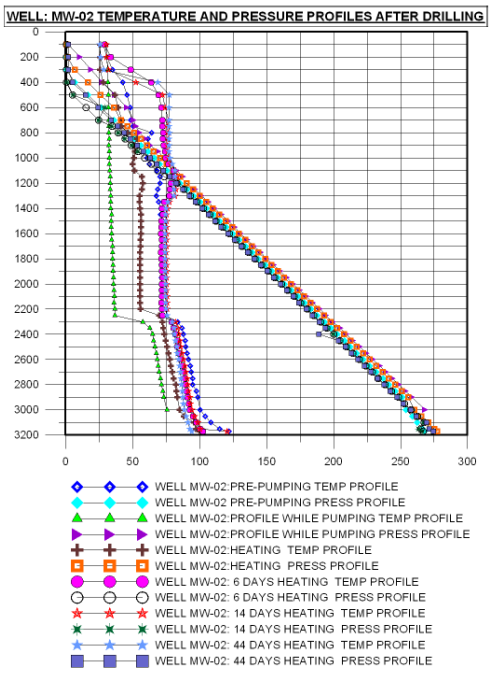
WELL: MW-02 TEMPERATURE AND PRESSURE PROFILES AFTER DRILLING
WELL MW-02:PRE-PUMPING TEMP PROFILE
WELL MW-02 PRE-PUMPING PRESS PROFILE
WELL MW-02:PROFILE WHILE PUMPING TEMP PROFILE
WELL MW-02:PROFILE WHILE PUMPING PRESS PROFILE
WELL MW-02:HEATING TEMP PROFILE
WELL MW-02:HEATING PRESS PROFILE
WELL MW-02: 6 DAYS HEATING TEMP PROFILE
WELL MW-02: 6 DAYS HEATING PRESS PROFILE
WELL MW-02: 14 DAYS HEATING TEMP PROFILE
WELL MW-02: 14 DAYS HEATING PRESS PROFILE
WELL MW-02: 44 DAYS HEATING TEMP PROFILE
WELL MW-02: 44 DAYS HEATING PRESS PROFILE

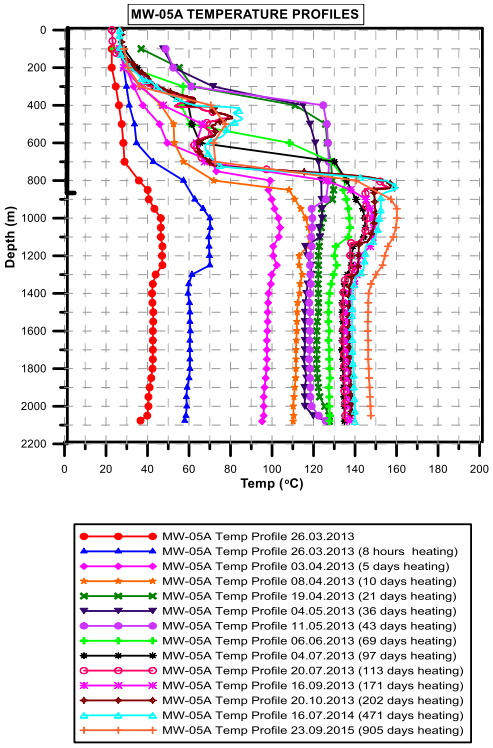
MW-05A TEMPERATURE PROFILES
Depth (m)
Temp (°C)
MW-05A Temp Profile 26.03.2013
MW-05A Temp Profile 26.03.2013 (8 hours heating)
MW-05A Temp Profile 03.04.2013 (5 days heating)
MW-05A Temp Profile 08.04.2013 (10 days heating)
MW-05A Temp Profile 19.04.2013 (21 days heating)
MW-05A Temp Profile 04.05.2013 (36 days heating)
MW-05A Temp Profile 11.05.2013 (43 days heating)
MW-05A Temp Profile 06.06.2013 (69 days heating)
MW-05A Temp Profile 04.07.2013 (97 days heating)
MW-05A Temp Profile 20.07.2013 (113 days heating)
MW-05A Temp Profile 16.09.2013 (171 days heating)
MW-05A Temp Profile 20.10.2013 (202 days heating)
MW-05A Temp Profile 16.07.2014 (471 days heating)
MW-05A Temp Profile 23.09.2015 (905 days heating)

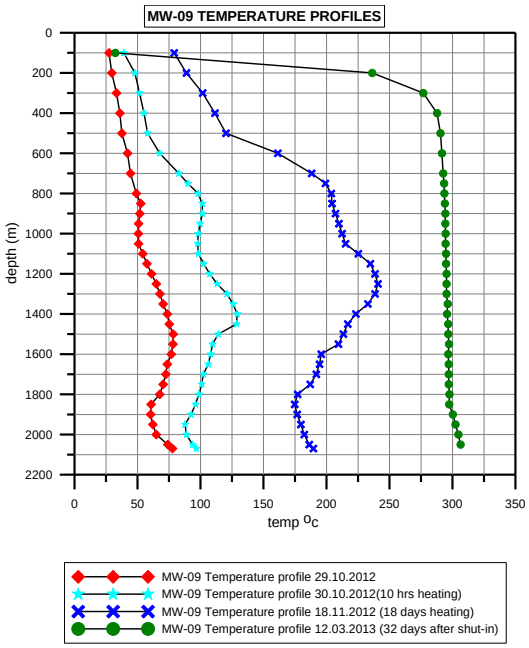
MW-09 TEMPERATURE PROFILES
depth (m)
temp °c
MW-09 Temperature profile 29.10.2012
MW-09 Temperature profile 30.10.2012(10 hrs heating)
MW-09 Temperature profile 18.11.2012 (18 days heating)
MW-09 Temperature profile 12.03.2013 (32 days after shut-in)

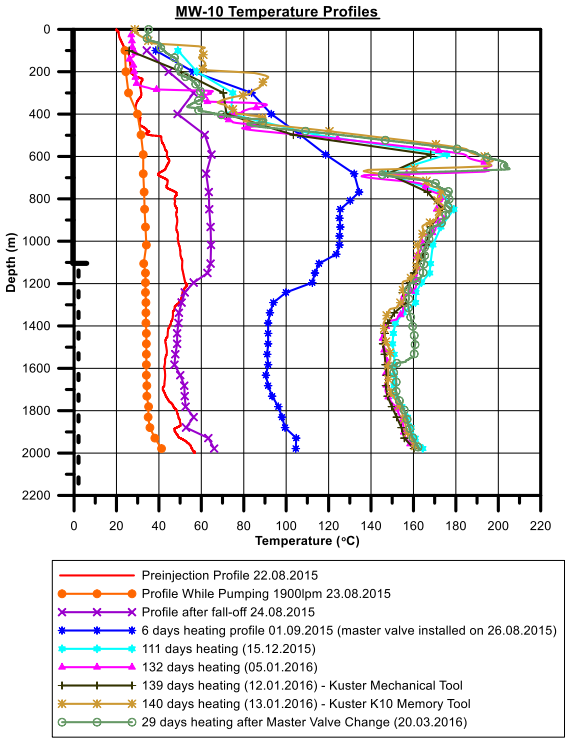
MW-10 Temperature Profiles
Depth (m)
Temperature (°C)
Preinjection Profile 22.08.2015
Profile While Pumping 1900lpm 23.08.2015
Profile after fall-off 24.08.2015
6 days heating profile 01.09.2015 (master valve installed on 26.08.2015)
111 days heating (15.12.2015)
132 days heating (05.01.2016)
139 days heating (12.01.2016) - Kuster Mechanical Tool
140 days heating (13.01.2016) - Kuster K10 Memory Tool
29 days heating after Master Valve Change (20.03.2016)

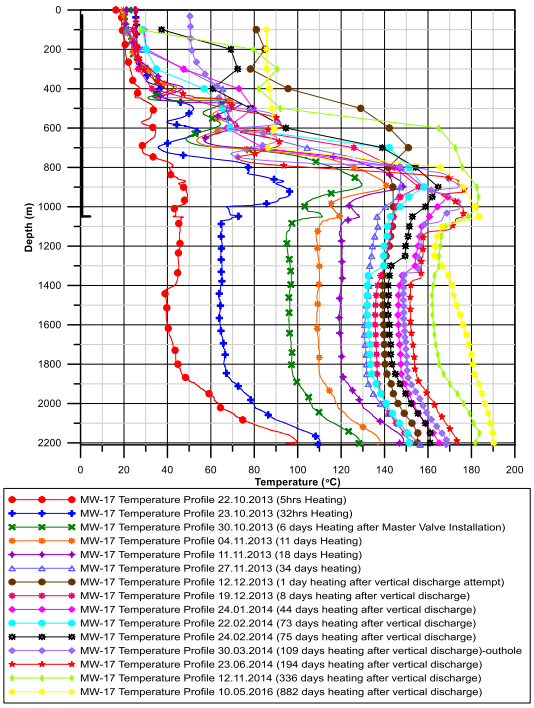
Depth (m)
Temperature (°C)
MW-17 Temperature Profile 22.10.2013 (5hrs Heating)
MW-17 Temperature Profile 23.10.2013 (32hrs Heating)
MW-17 Temperature Profile 30.10.2013 (6 days Heating after Master Valve Installation)
MW-17 Temperature Profile 04.11.2013 (11 days Heating)
MW-17 Temperature Profile 11.11.2013 (18 days Heating)
MW-17 Temperature Profile 27.11.2013 (34 days heating)
MW-17 Temperature Profile 12.12.2013 (1 day heating after vertical discharge attempt)
MW-17 Temperature Profile 19.12.2013 (8 days heating after vertical discharge)
MW-17 Temperature Profile 24.01.2014 (44 days heating after vertical discharge)
MW-17 Temperature Profile 22.02.2014 (73 days heating after vertical discharge)
MW-17 Temperature Profile 24.02.2014 (75 days heating after vertical discharge)
MW-17 Temperature Profile 30.03.2014 (109 days heating after vertical discharge)-outhole
MW-17 Temperature Profile 23.06.2014 (194 days heating after vertical discharge)
MW-17 Temperature Profile 12.11.2014 (336 days heating after vertical discharge)
MW-17 Temperature Profile 10.05.2016 (882 days heating after vertical discharge)

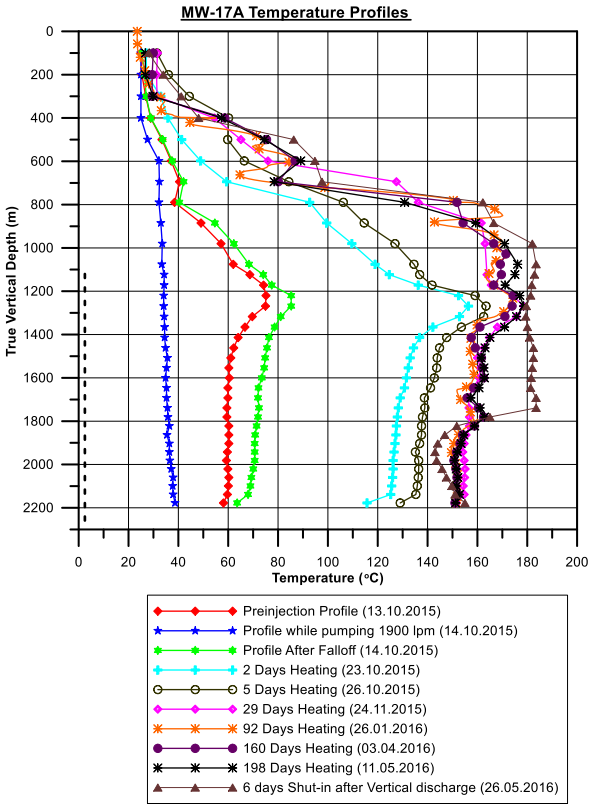
MW-17A Temperature Profiles
True Vertical Depth (m)
Temperature (°C)
Preinjection Profile (13.10.2015)
Profile while pumping 1900 lpm (14.10.2015)
Profile After Falloff (14.10.2015)
2 Days Heating (23.10.2015)
5 Days Heating (26.10.2015)
29 Days Heating (24.11.2015)
92 Days Heating (26.01.2016)
160 Days Heating (03.04.2016)
198 Days Heating (11.05.2016)
6 days Shut-in after Vertical discharge (26.05.2016)

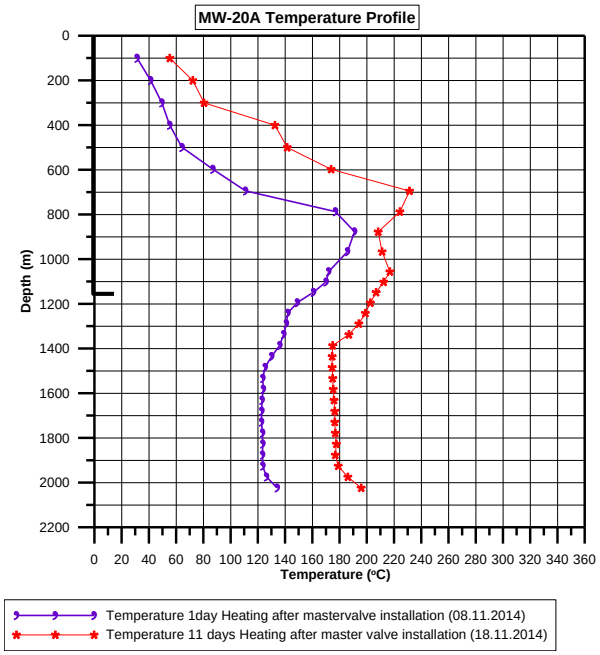
MW-20A Temperature Profile
Depth (m)
Temperature (°C)
Temperature 1day Heating after mastervalve installation (08.11.2014)
Temperature 11 days Heating after master valve installation (18.11.2014)

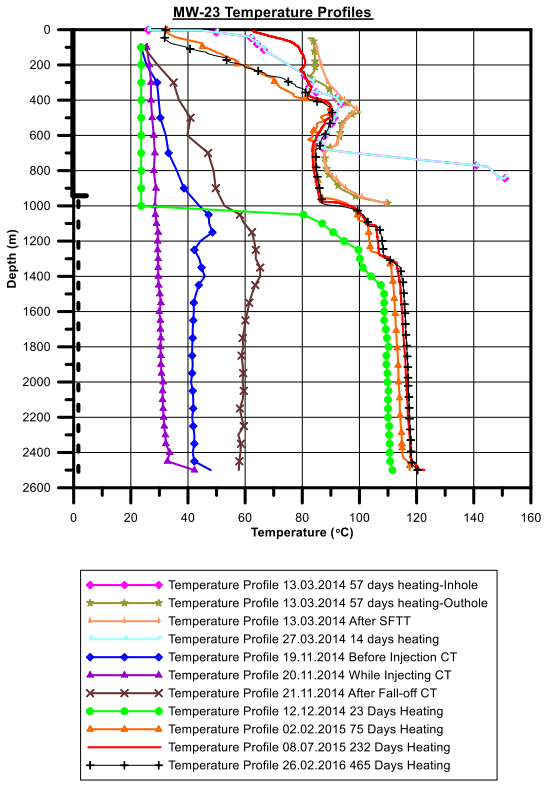
MW-23 Temperature Profiles
Depth (m)
Temperature (°C)
Temperature Profile 13.03.2014 57 days heating-Inhole
Temperature Profile 13.03.2014 57 days heating-Outhole
Temperature Profile 13.03.2014 After SFTT
Temperature Profile 27.03.2014 14 days heating
Temperature Profile 19.11.2014 Before Injection CT
Temperature Profile 20.11.2014 While Injecting CT
Temperature Profile 21.11.2014 After Fall-off CT
Temperature Profile 12.12.2014 23 Days Heating
Temperature Profile 02.02.2015 75 Days Heating
Temperature Profile 08.07.2015 232 Days Heating
Temperature Profile 26.02.2016 465 Days Heating

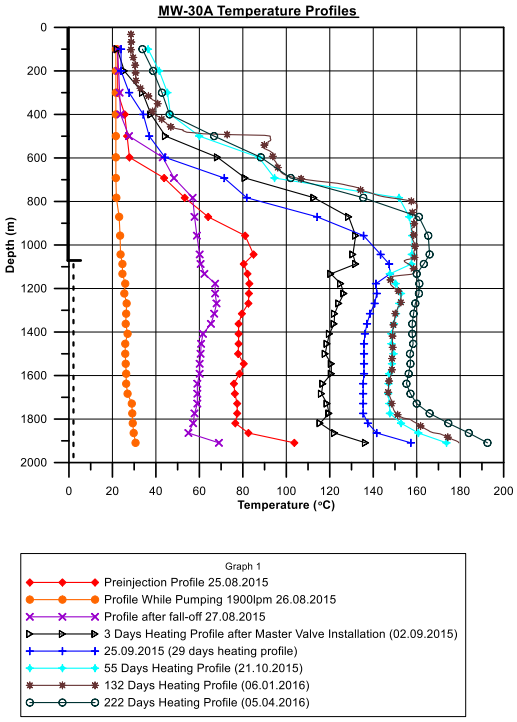

Figure 4-8: Temperature profiles of MW-02, MW-05, MW-09, MW-10, MW-17, MW-17A, MW-20A, MW-23 and MW-30A.

On plotting Cluster III wells, they are observed to lie on zones presumed to be faults-like structures and conduits of huge cold water flows on shallow depths

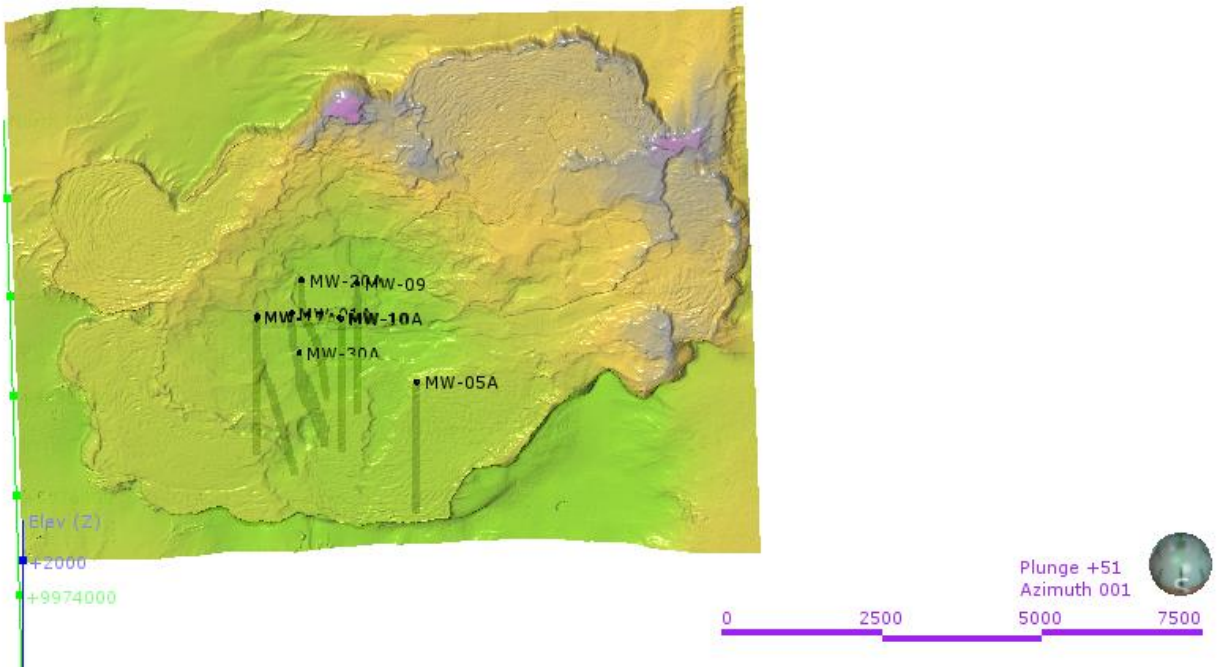

Figure 4-9: 3-D Leapfrog imagery view of Cluster III wells' location on the caldera floor.

Cluster IV.

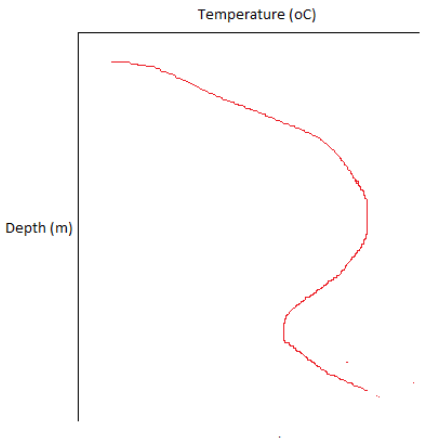

These wells show sharp temperature increase and reverses between 1600 m and 2000 m with slight increase at well bottom of 2200 m. They seem to have intersected a cold permeable zone between 1500 m and 1700 m where temperature reversal is mostly observed.

Figure 4-10: Cluster 4 Temperature profiles trend

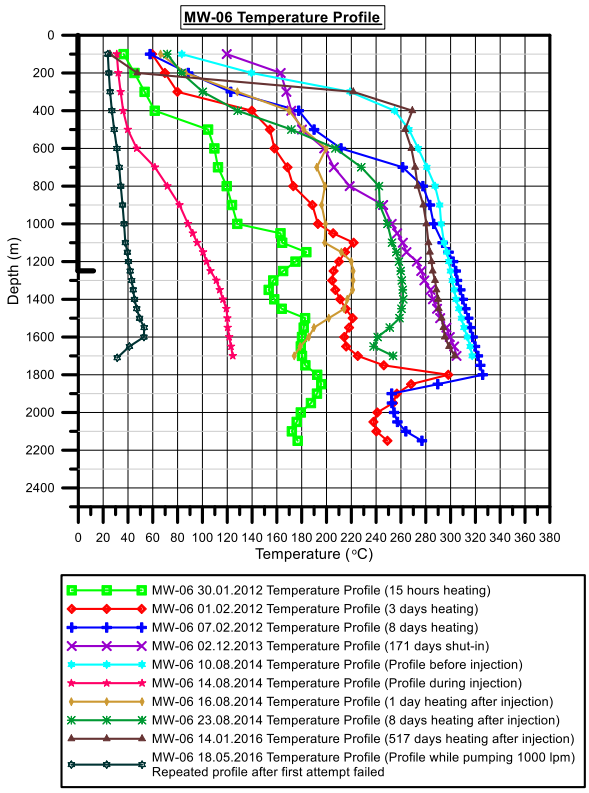

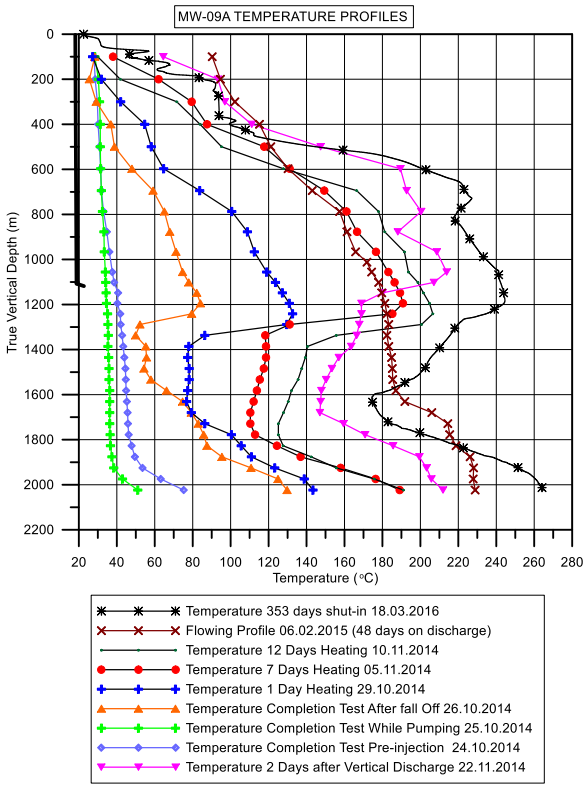

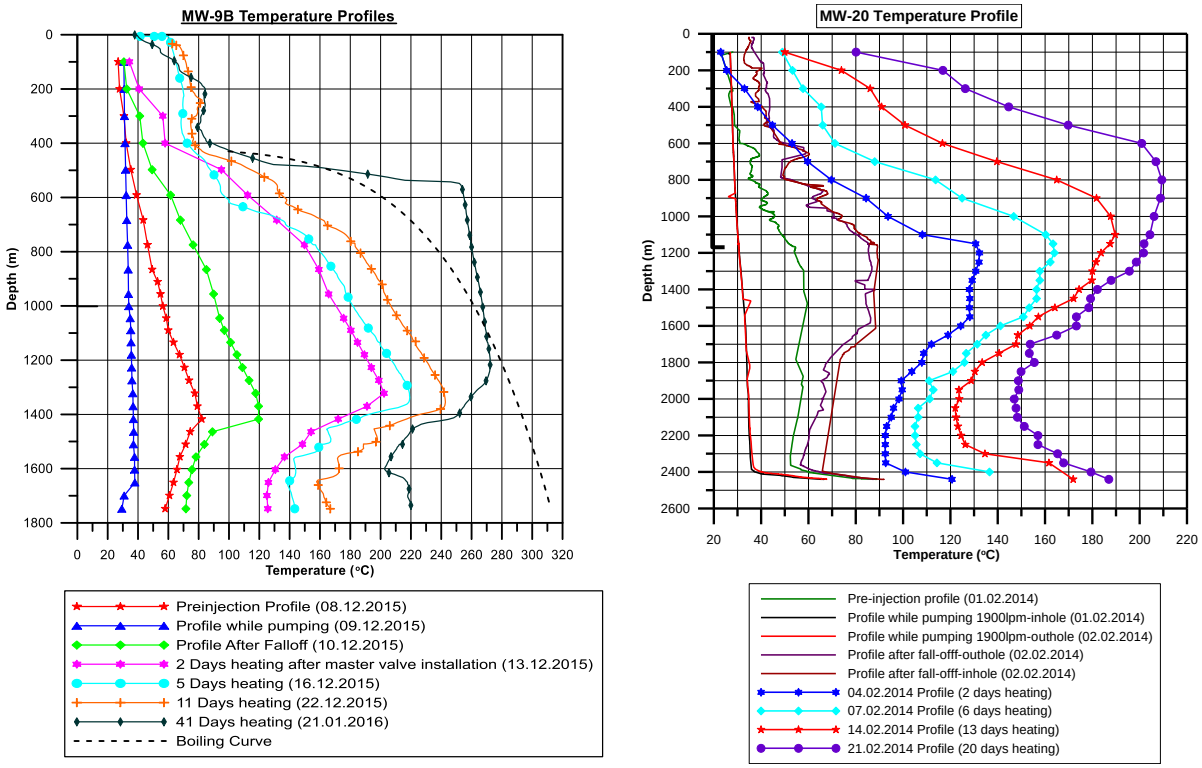

Figure 4-11: Temperature profiles of MW-06, MW-07, MW-09A, MW-9B and MW-20.

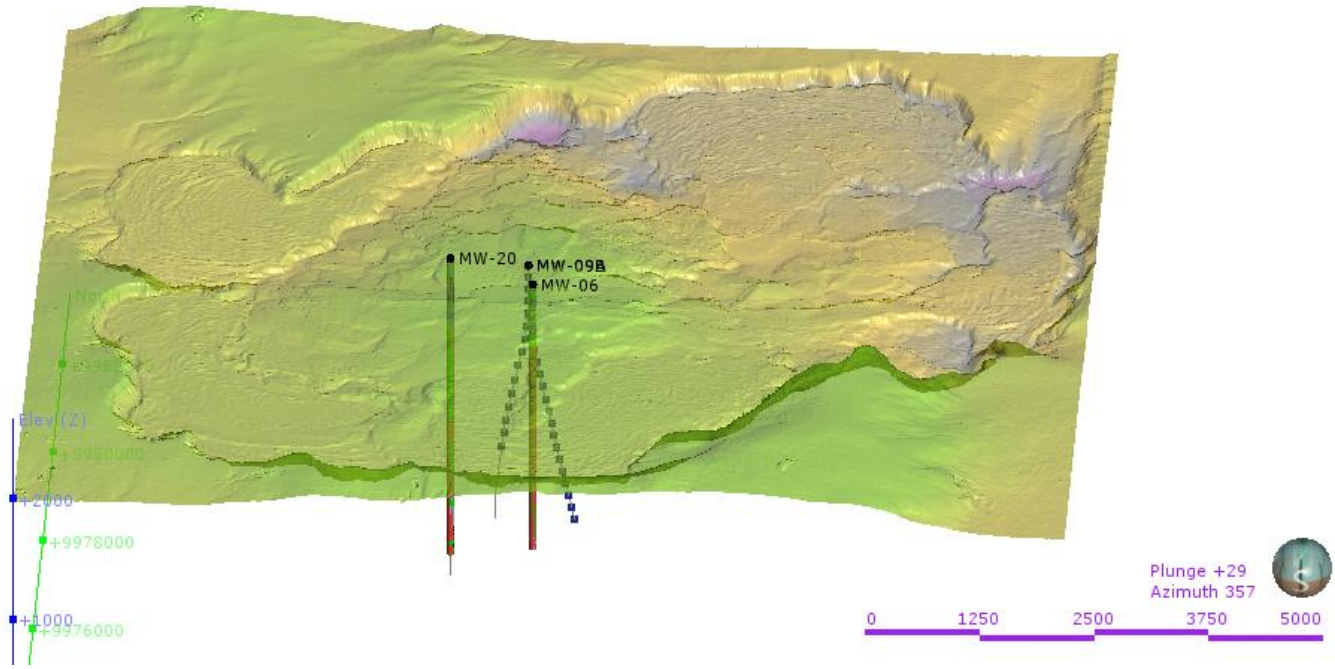

Figure 4-12: 3-D Leapfrog imagery view of Cluster IV wells' location on the caldera floor.

Cluster V.

Wells MW-07 and MW-21A can be categorized in this cluster. They seem to have encountered a hot feed zone between 500 m to 600 m and temperature reversal from 700 m and 1000 m and remain slightly constant all the way to bottom hole. These wells appear to be driven to a fracture at 700 m or 1000 m that passes relatively cooler fluids.

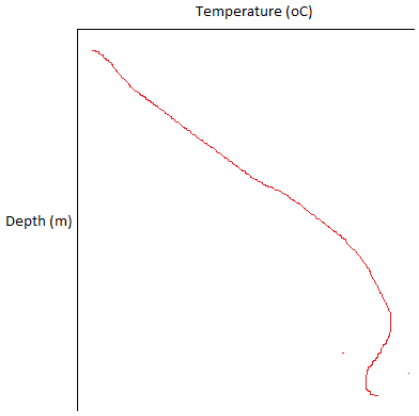

Figure 4-13: Cluster 5 Temperature profiles trend

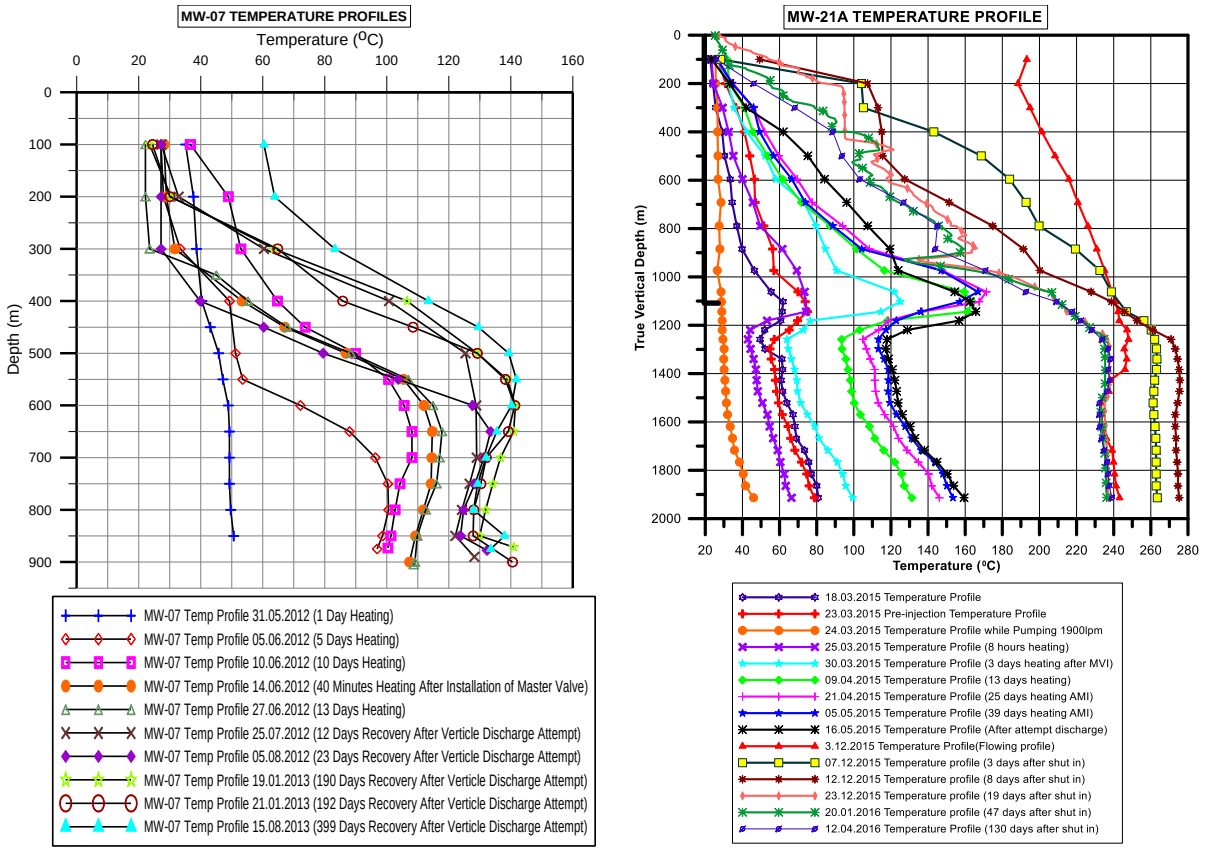

Figure 4-14: Temperature profiles of MW-07 and MW-21A.

Well MW-07 plot on the caldera is seen to have intersected a Solai TVA extensional fault west of caldera.

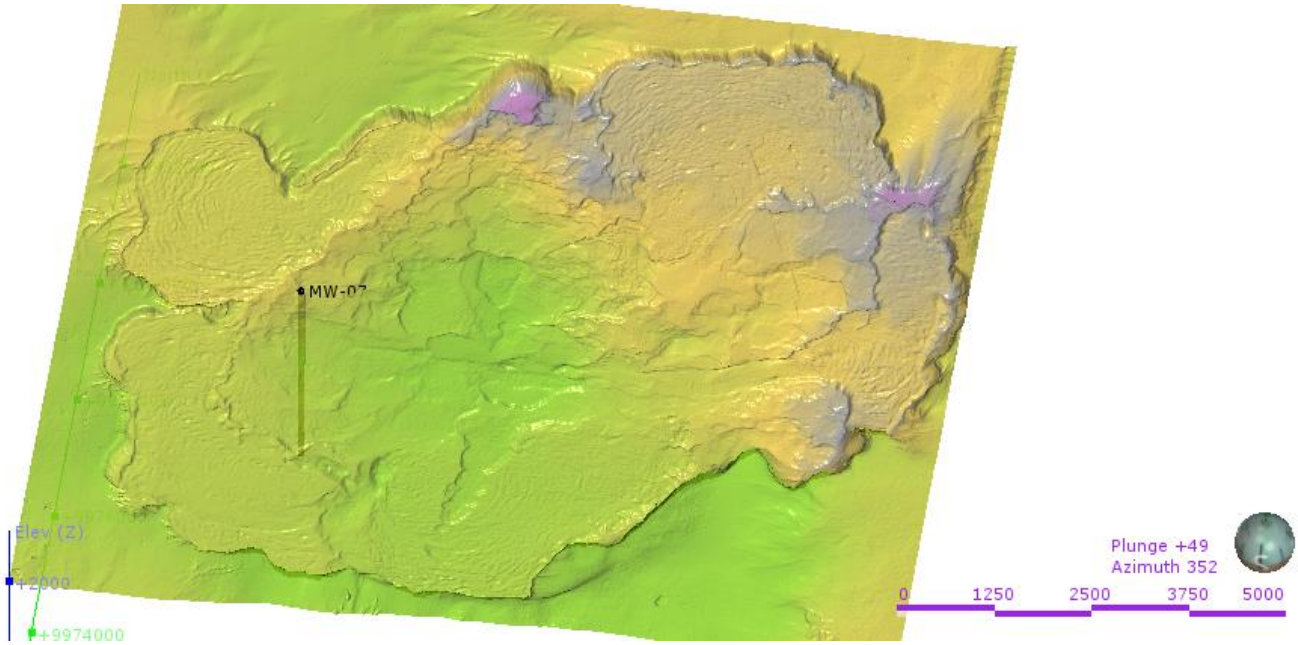

Figure 4-15: 3-D Leapfrog imagery view of MW-07 location on the caldera floor characteristic of Cluster V.

Well clusters were all plotted on caldera floor to check wells' distribution and if can give some specific in trend in their locations. Figure 4-16 below show well clusters distribution.

Closer study of wells' clusters gave an idea of specific defining intra-caldera fractures and inferred faults that could be contributing to temperature variations in geothermal wells.

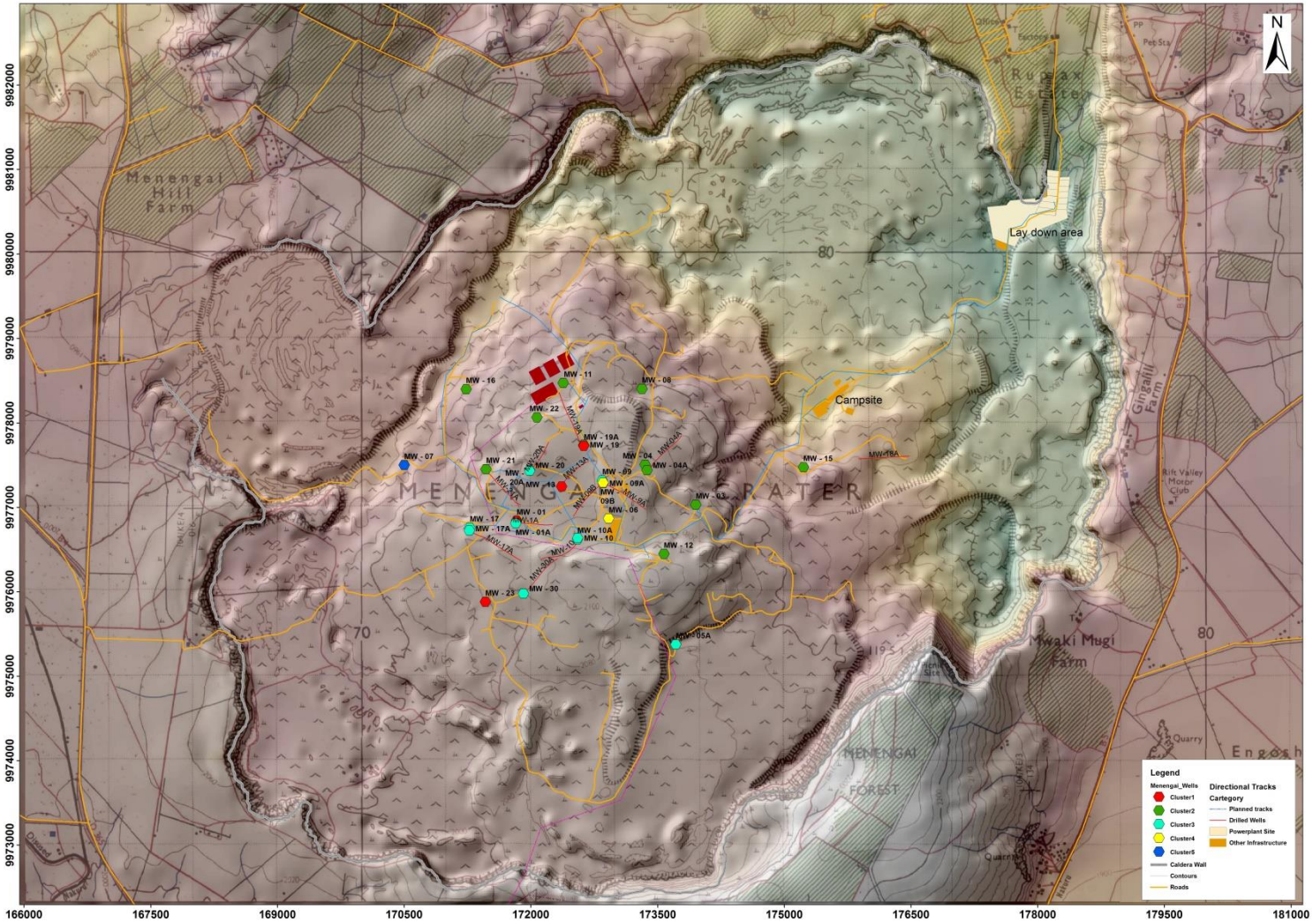

Figure 4-16: Distribution of clusters of wells having similar temperature profile trends

4.1.4 Topographic Slope Risk Analysis

In planning process of a large scale development project, risk evaluation of natural disaster is an important issue for a purpose of maintenance of facilities. The occurrence of natural disaster that bring about fatal damage to the planned plant, such as climate change in global scale, eruption of volcano and big earthquakes, may not be rare in any countries. A process of risk evaluation should be described, where natural disasters that may occur in and around the natural environmental characteristics of the planned site are enumerated and then the risk of the natural hazard is evaluated.

This is majorly desktop study of 2-m contour topographic map of the caldera to try identifying and categorizing risky slopes that may be susceptible for failure upon subjection of little external compressive or tensional force that could be triggered by seismicity for numerous discharging wells within the caldera.

Possible risks in study area include but not limited to: rock falling, slope failure, land slide, debri flow, deep seated landslide, earthquake and flooding. The possibility and degree of hazard occurrence are observed to be different within the caldera floor depending on the elevations, steepness and location and closeness to the geothermal wells.

An example of general idea of risk evaluation is presumable and anticipated disasters on the planned development on the caldera floor. The possibility of any of the above hazard occurrence is hereby plotted on relation of magnitude of damage depending on the prevailing conditions i.e. climatic and argent triggering the hazard i.e. flooding and ground shaking from discharging wells. Probability to occur may be high or low with variable magnitude of damage of the developed structures on caldera floor e.g. power plant, power-lines and steam gathering pipe networks.

Natural disasters and evaluation risk in the planned site and anticipation of possible disasters is required. It is important to grasp the characteristics of planned site and to collect the information as concrete as possible. Correlation of topographic/surface geological information, geotechnical investigation and seismic study is done to try anticipating possible geohazard and developing risk map. Interpretation of aerial photographs to identifying unstable slants was as well performed. The potential area of disaster is identified concretely by the process to further evaluate degree of the danger.

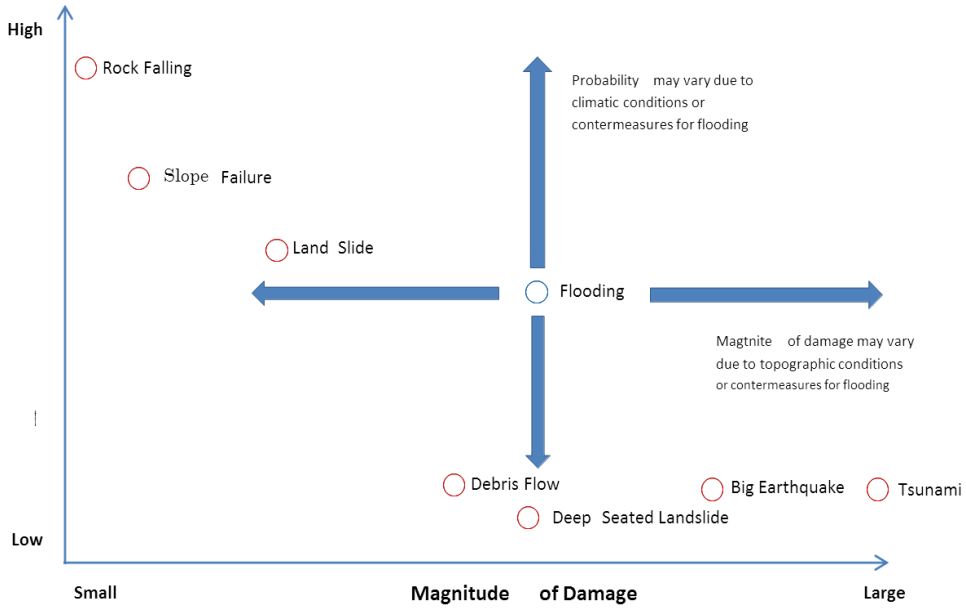

Figure 4-17: Concept of Risk Evaluation for Natural Disasters**.**

4.1.4 Hazardous Topographic Slopes

The Physiographic map below (Figure 4-19) show high degree of undulating land surfaces that is characterized by underlying crisscrossing geological structures that may ease any landmass movement.

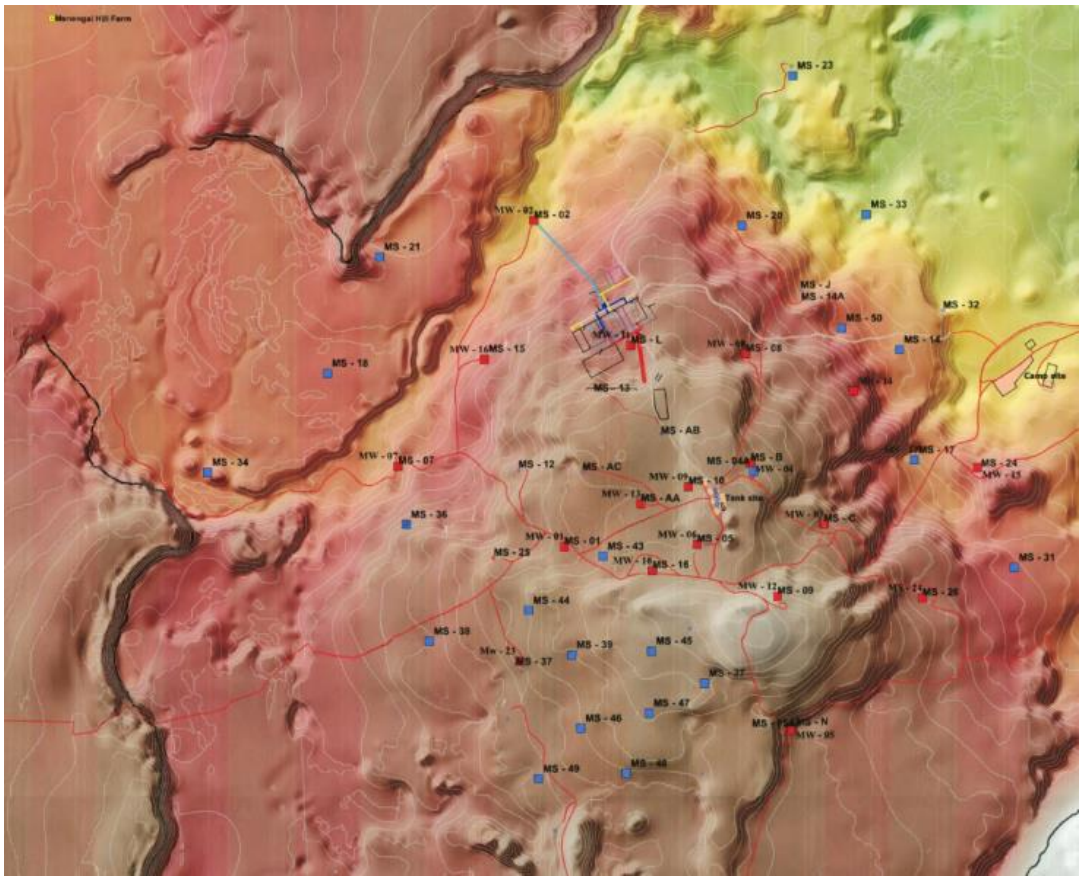

Figure 4-18: Physiographic map of Menengai caldera floor

The potential area of disaster is identified concretely by the process to further evaluate degree of the danger. Hazard map constructed highlight potential areas of natural hazard and plotted on a on 2-m contour map. The planned project site is then superimposed on the map and the map is utilized as the base information for devising the degree of impact map (damage map). Geological risks include sediment related disaster and slope disaster. Debris flow, land slide (surface and deep seated), volcanic disasters involving ash flow, lava flows, pyroclastic flow, volcanic block/bombs.

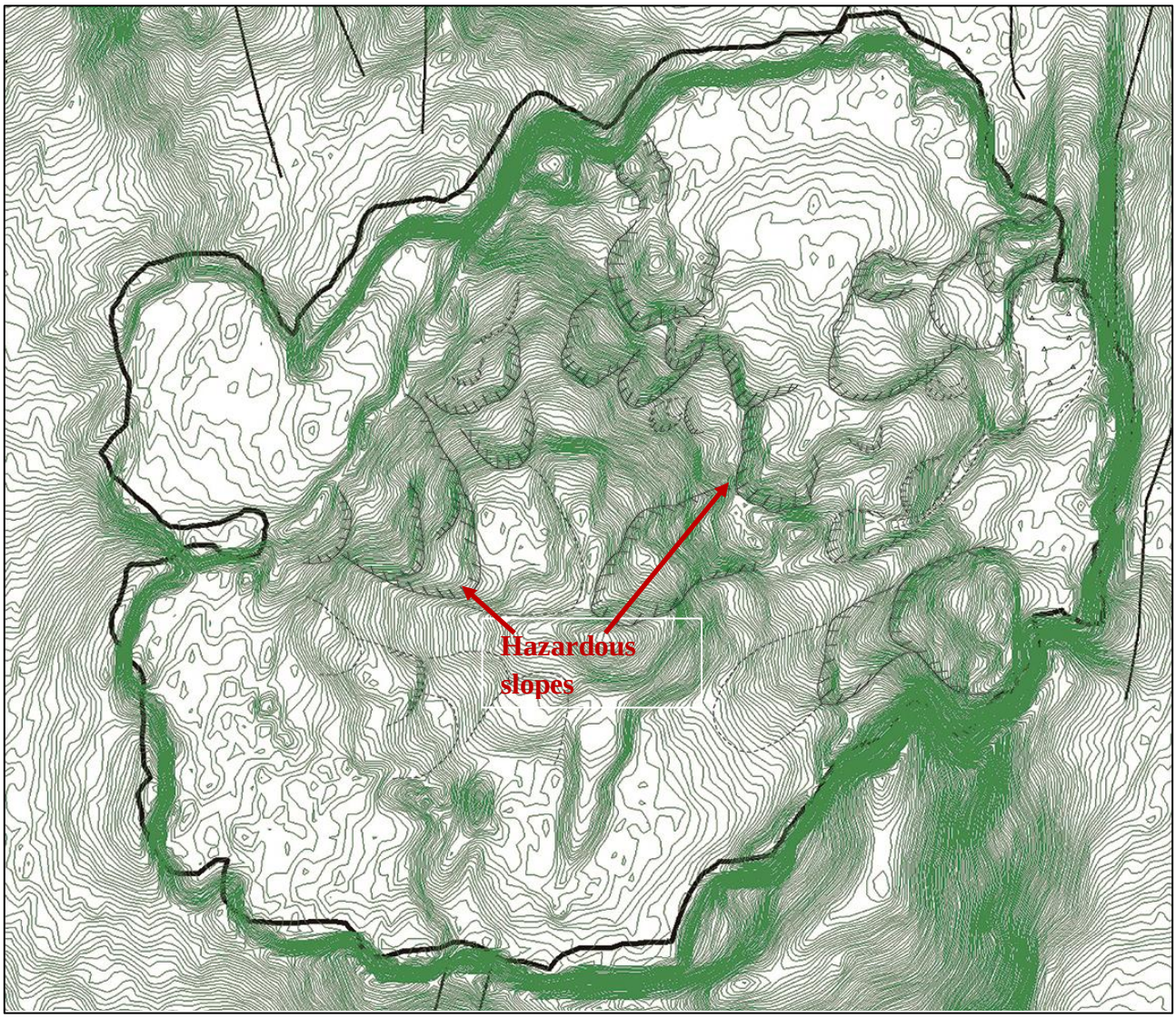

Figure 4-19: Construction of hazardous slopes from 2-m contour map

4.2 Discussion

4.2.1 Geotechnical Interpretation of Results

Foundation Analysis

Analysis of geotechnical field insitu and laboratory observations show incompetent foundation strata of upto 30 m depth associated with intense fractures and permeability. This may pose geohazard to the constructions on the surface.

The top soil layer has a thickness that ranges between 0.5 m and 2.0 m. This layer is composed of silty sandy gravels of extremely weathered volcanic soil with rock fragments as well as roots. In the case of employing any platforms, it's important to note that these will be constructed on a surface free from the above mentioned top layer.

In terms of BS5930 the moderately weathered trachyte classifies as weak to moderately strong, this slightly weathered trachyte is likely to require hard ripping or blasting depending on jointing of the rocks for removal should the foundations be taken at lower depths. Areas with silty sandy gravels matrix of extremely weathered volcanic ash encountered below foundation depth of 2.5m may have to be removed and replaced with mass concrete or the foundations need to be taken to a lower depth to avoid them.

Shallow Foundation Analysis

The ultimate load bearing capacity analysis for shallow foundations was determined according to Meyerhof's theory, by employing the following expression.

1 - Cohesion and angle of shear

$$Qu = c\,Nc\,Sc\,Dc + \gamma D\,Nq\,Sq\,Dq + 0.5\,\gamma B\,N\gamma\,S\gamma\,D\gamma \quad \text{.....(Eqs-I)}$$

Where:

$Nc = \cot\phi\,(Nq - 1)$

$Nq = e^{\pi \tan\phi} \tan^2(45+\phi/2)]$

$N\gamma$ = (Nq-1) tan(1.4ϕ)
Kpr = $\tan^2(45+\phi/2)$, passive pressure coefficient. / TAN(PI/4+PHI/2)^2
Dc=1+0.2$\sqrt{}$(kp)(B/L) - Depth Factor*
Sc=1+0.2kp(B/L) - Shape factor
Dq=Dγ=1 if ϕ=0 otherwise =1+0.1$\sqrt{}$(kp)(D/B) - Depth factors*
Sq=Sγ=1 if ϕ =0, otherwise = 1+0.1kp(B/L) - Depth factors

2 – SPT N-Value

$$q_a = \left(\frac{N}{F_2}\right)\left(\frac{B+F_3}{B}\right)^2 K_d \quad \text{Where } B > F_4 \qquad \text{.....(Esq.-II)}$$

Where q_a = allowable bearing pressure for $\Delta H0$ = 25mm. settlement, kPa.
K_d = 1 + 0.33D/B $\leq$ 1.33 [as suggested by Meyerhof (1965)]

F factors are as follows: -

Meyerhof's f-Factors

	N55		**N70**	**N60**	
	SI	**Fps**	**SI**		**Fps**
F_1	0.05	2.5	0.04	0.05	2
F_2	0.08	4	0.06	0.07	3.2
F_3	0.3	1	Same	Same	same
F_4	1.2	4			

The choice of parameters is a critical aspect in the designing process. The engineer in charge is tasked with the duty of determine whether the soil or stratum that will receive the foundation system has a cohesion-less or cohesive behavior.

The allowable load capacity (Qa) obtained by dividing the ultimate load capacity by a minimum safety factor of 3.

Rock Specimen

To allow for variations in the rock, the foundation design strength should be taken as the lowest measured strength divided by a factor of 10 due rock fractures. In this way the very weak trachyte layer will have a design strength of 6.877/10 = 0.6877MPa in Sosian site.

The minimum design strength recorded from the unconfined compressive strength was 0.6877MPa in BH 7B at a depth of 5.5m. On a pad footing of 1.5m^2, placed 3m below ground level the allowable bearing pressure rock with this strength is in excess of 1000 kPa on a strip

or pad foundation. This bearing pressure was calculated to be five times the unconfined compressive strength divided by a factor of safety. A factor of safety of three has been used.

Analysis of settlements

According to the type of soil detected; the type of settlements that are expected will take place during the construction period, however, no settlement is expected to take place where foundations are taken to a rock formation.

Substituting the corresponding values and employing security factor of 3, the allowable load bearing capacity values of the soil obtained. Differential settlement is estimated to be less than 25 mm.

4.2.2 Seismic Engineering Interpretation of Results and Regional Seismicity

Seismic Engineering parameters deduced by both SRT and MASW depicted a highly brittle near surface geological strata. Findings of near surface seismic parameters may therefore extend to deeper depths thus increasing chances of geohazards. Earlier studies of earthquake analysis conducted both regional (the whole rift) and local (Menengai) show that large earthquake events are associated with the main rift faults and are usually deeper than 7 km depth, while the earthquakes local to a geothermal site are shallow and of low magnitude not exceeding local magnitude 3. The local magnitude estimates of these events show that they are significantly small most of them being less than 1. In addition the estimates from the Global Seismic hazard Assessment program show that the region has a low peak ground acceleration of less than $0.8 m/s^2$. However earthquake events may be enhanced by geothermal wells that will be discharging at one go during production stage.

4.2.3 Well Clusters, Structural geology and Tectonic processes

Wells' clusters obviously indicate they indeed draw from a major geothermal aquifer but are intersecting multiple geological structures. Numerous deep crisscrossing fractures are a geohazard within the caldera since they may catalyze landmass shifts following seismic forces emanating from discharging wells. Each cluster may drift to different directions and magnitudes hence heterogeneous geotechnical conditions. Figure 4-16 shows wells' distribution on the caldera floor. The clusters indicate particular trends that could explain current topographic and slope layout within the caldera as a whole. Inferred structures from the wells cluster that show different geological settings and episodes that led to the main caldera. Cluster II, indicate that majority of wells have been drilled into an impermeable hot intrusive body which appear to be extensive at the center of caldera. The intrusion appears to have been encountered at different depths in the four main compartments within the caldera. The intrusion formed through solidification of upcoming silicic magma through the intersection of faults NS and WE (Figure 4-21). Solidification of magma seemed to be quite rapid due its acidity before total outpour on the surface. The intrusion occur in X-shaped trend at the intersection of the faults structures and appear to be the main course of doming in the central section of the caldera. This study identifies five main compartments: SE, SW, NE, NW and NNW sequentially arranged in the order of tectonic evolution (Figure 4-21).

Topographic layout and surface slopes' orientations are resultant of the structural geology within the caldera and regional volcano-tectonic settings. Present day Menengai caldera appears to be as a result of subsequent segmental and partial subsidence at the triple junction of Molo and Solai Tectono-Volcanic Axes. The caldera surface is largely covered by post caldera lava flows oozing from the centrally located fissures and cracks. The lava fronts results to gentle to steep slopes that may be hazardous to surface developments (Figure 4-19). Past deformation monitoring studies by GDC has however not noticed ground displacement

along major faults and cracks. There is a characteristic doming at the central part of the caldera, uplifted above other segments of caldera floor.

The present day Menengai caldera structure seemed to be have started by subsidence of the triple junction of Solai and Molo tectono-volcanic axes (TVA) resulting to the caldera whose section currently is SE Compartment. A further tectonic movement lead to formation of NS fault scarp rim triggered by Molo TVA thus subsidence of a mini-caldera in the western segment (SW-NW) of the then caldera whose formation forms part of SW Compartment. A further tectonic got triggered with influence of Solai TVA leading to more subsidence in northern segment resulting to W-E fault scarp rim of NW-NE mini-caldera whose current formation can be seen in NE Compartment. The final tectonic evolution of current topography Menengai caldera floor appear to have been triggered by a less eruptive episode targeting the junctions of the already formed mini-calderas thereby uplifting the central section of the whole caldera and post-caldera magma flows majorly towards the low lying northern segments of NW and NE and a very deep basin at the then furthest corner of NE Compartment bounded by Solai graben structure and earlier formed caldera rim. This can be confirmed by the google map view post caldera lava flow in Figure 4-20 below where the latest lava flow is observed to dominate the NW Compartment.

Geothermal well logging of drilling cuttings done by Omondi, 2011 and petrochemical TAS plot by Mbia, 2014 confirms that MW-02 cuts through a more evolved geological setting different from wells at the center of caldera appear fresher and younger lavas. Well MW-02 seems to have therefore cut through geological units which area older compared to geological units at the center of caldera like MW-01.

Figure 4-20: Post-Caldera Lava flows concentrated in low-lying northern section.

The basin at the furthest NE compartment was as well mapped by Leat, 1964 (Figure 1-4) as intra-caldera paleo-lake believed to be the result of overflow from the 'Gamblian' lake into the caldera through the SE graben and partly through underground channels, along joints and through tephra and soil horizons (Leat, 1984).

NW segments underwent a further down warping due to the weight of surface magma and weak triangular fault-lines surrounding the compartment. More tectonic movements within NW Compartment seemed to have resulted to a small gulley subsidence of NNW segment in which geothermal well MW-16, MW-21 and MW-21A lie. MW-21A and MW-20A intersected the southern (y) and northern (x) inferred faults respectively of NNW gulley (Figure 4-21). The inferred gulley edges appears to be the main conduits of cold groundwater at depth channeled through a very dip Solai TVA induced western fault (A) through the northern caldera rim from the Northern Eastern groundwater logged 'paleo-lake' basin. N-S fault scarp seems a little bit welded and less permeable thus not transporting a lot of cold groundwater southwards to the central part of caldera. Geothermal wells intersecting N-S fault scarp are generally good and fall with Cluster 1 with normal geothermal temperature profiles. N-S can therefore be referred to as constructive to the geothermal system within the caldera. Fault scarp W-E among all other inferred fractures are seen to be causing temperature reversal in geothermal wells thus destructive. NW Compartment therefore seems to be the latest tectonic formation within the entire caldera. It is smaller in surface area compared to other compartments, dominated by inferred fractures and fault scarps. Most discharging wells are within enclosed NW Compartment hence we expect a lot of seismicity within the compartment. Menengai geothermal development, construction and infrastructural layout are seen to dominate and located within NW Compartment. The development should therefore be approached cautiously with maximum geohazard mitigation measures put in place for any imminent geotechnical failure.

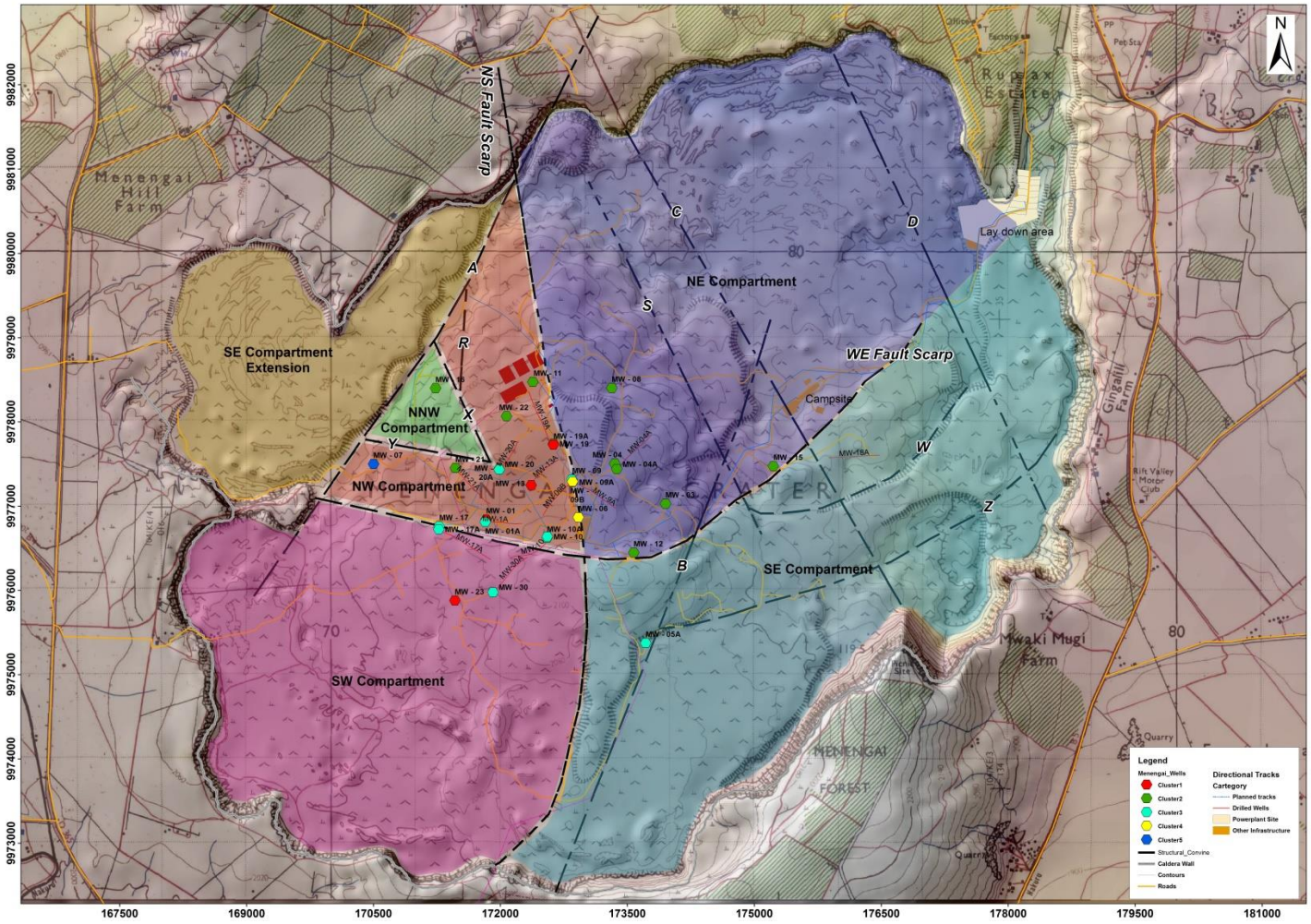

Figure 4-21: Compartments and Inferred Geological fractures within Menengai Caldera floor.

4.2.4 Topographic Slope Analysis and Risk Matrix Extraction

In evaluation of the possibility to destabilize, slope analysis can be checked whether might have already moved or yet to begin moving in future and if factors enabling slope movement and motives to move do exist. Weak geological feature; geological structure that it is easy to destabilize like dip slope structures and fault fracture zone or alternate zones. Motive for a slope to move is checked from the catchment topography indicated surface run-offs which erode in a slope distal end and groundwater levels. Evaluation of phenomenon indicating a slope moving is characterized by cracks on surface and the established structure, outbreaks of the new step topography and vegetation abnormality.

Influence of power station on the ground where the development shall take place is assessed as well as possible disaster that may damage power station and important facilities leading to stoppage of power generation or disasters that may cause human damage at site or damages in the neighboring areas e.g. roads. A flow diagram is here developed for general risk evaluation process. (Figure 4-22).

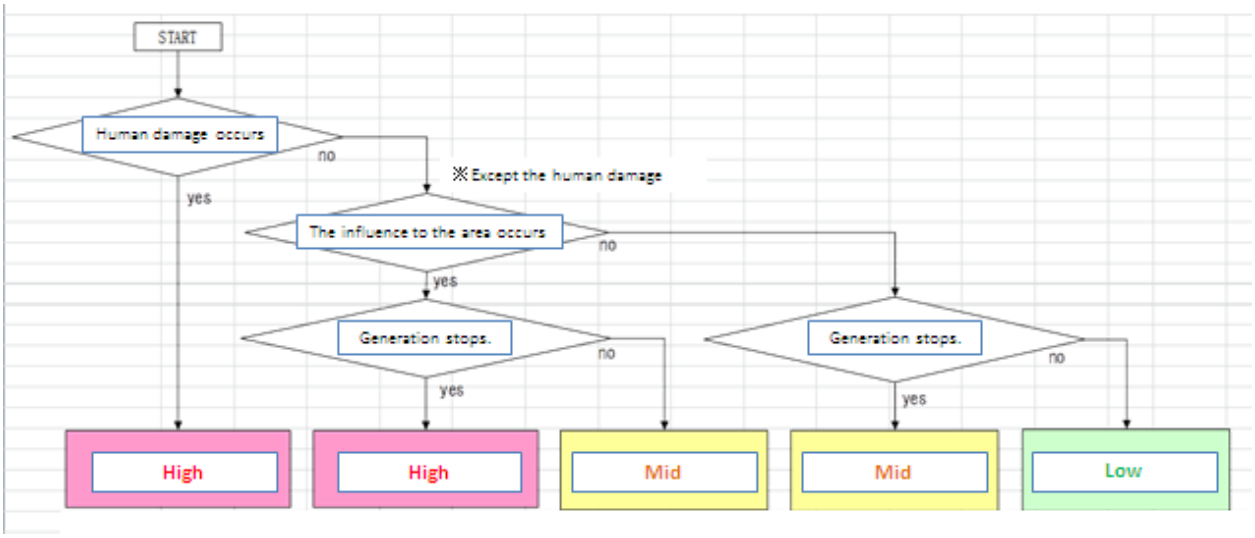

Figure 4-22: Flow diagram showing general risk evaluation process

A risk matrix table to evaluate the degree of influence of power plant or any surface development verses degree of possibility for distability is here developed to help in guiding mitigation measures to put in place during development whether to be considered in construction stage if high risk or not to be considered but to be observed through patrols if regarded as low and unlikely to occur.

Segments of slopes are therefore grouped and categorized in the matrix according to the development that is anticipated in that slope section. Meaning a gentle slope holding development or construction may be grouped as riskier to the highly steep slope having no development or any construction.

Table 4-1 and Table 4-2 subsequently group the categorized slopes in accordance to the degree and influence of upcoming developments program. The slopes are numbered in accordance to the intensity of construction plan and layout of developments on the caldera flow. Slope no. 1 is expected to contain a lot of development i.e. power plant and station hence more development that slope no 18 (Figure 4-24, Figure 4-25 and Figure 4-26). Therefore slope no. 1 is high risk than slope no. 18 (Figure 4-25 and Figure 4-26). Mitigation measures to check possible geohazard therefore need to be put in place slope 1, 2 and 9 more than in slope no. 8 where less or no construction is expected.

Table 4-1: Category of risk matrix influenced development program to possibility to destabilize.

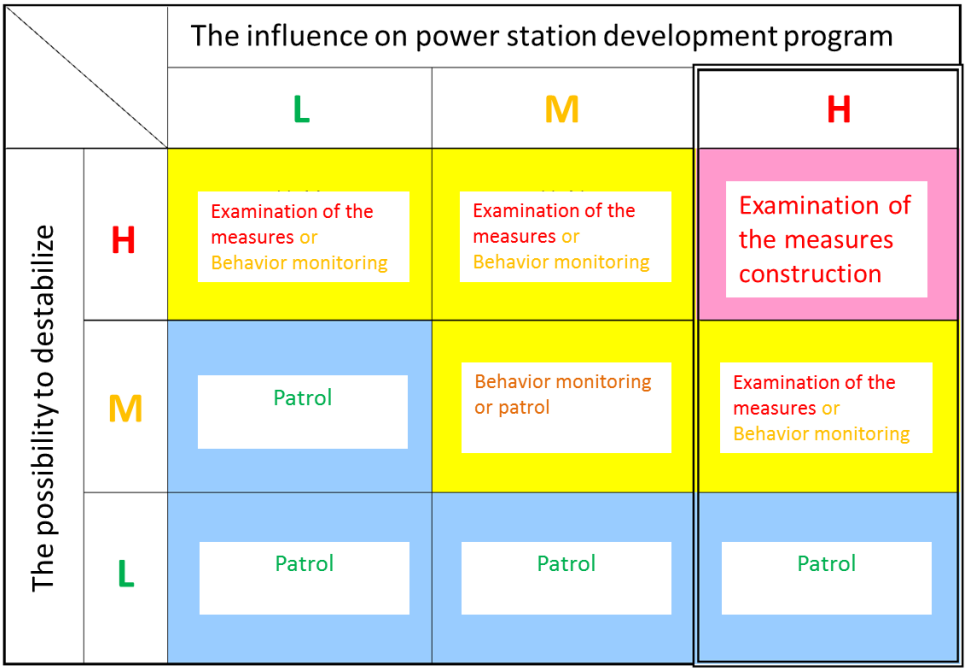

Table 4-2: Slopes categorized in respect of development and level of possibility to destabilize.

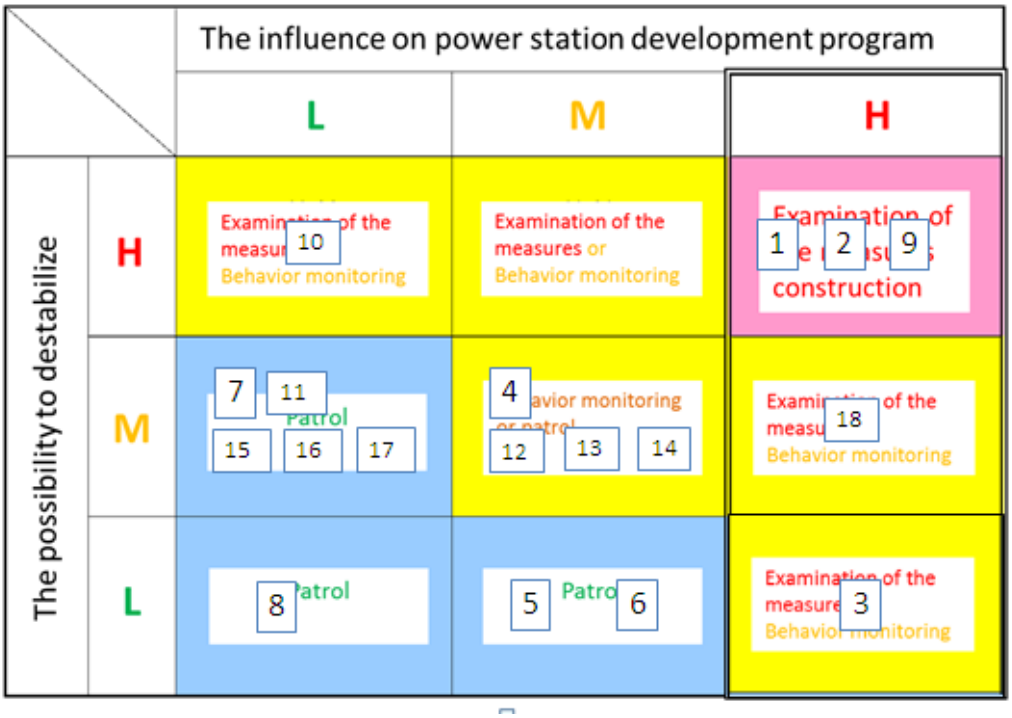

Overlay of marked slopes on the layout of proposed development (Figure 4-23).

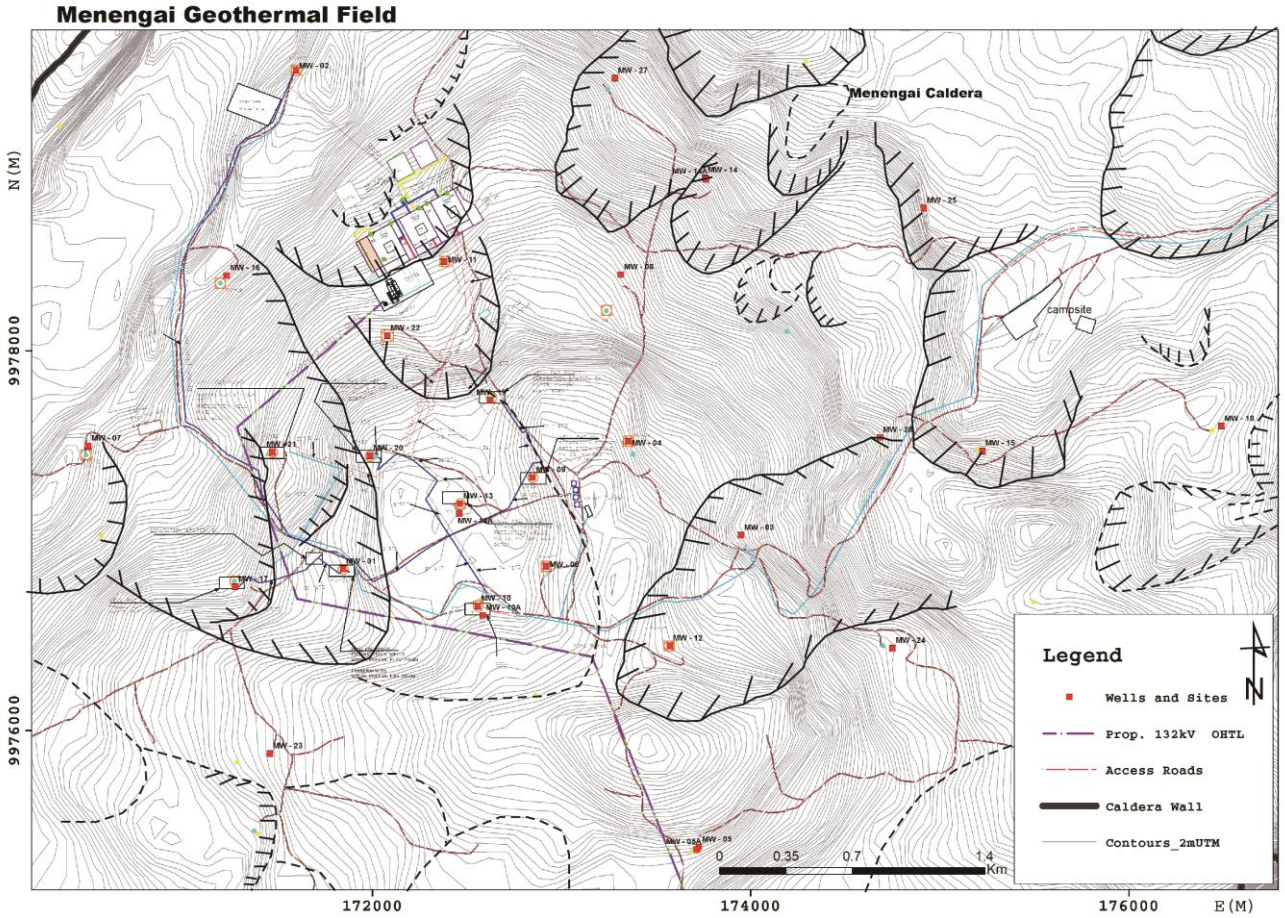

Figure 4-23: Overlay of harzadous slopes on layout of wells and powerplant

Numbering of hazardous slopes within the caldera floor. The study identified 18 slopes within the caldera floor (Figure 4-24 below).

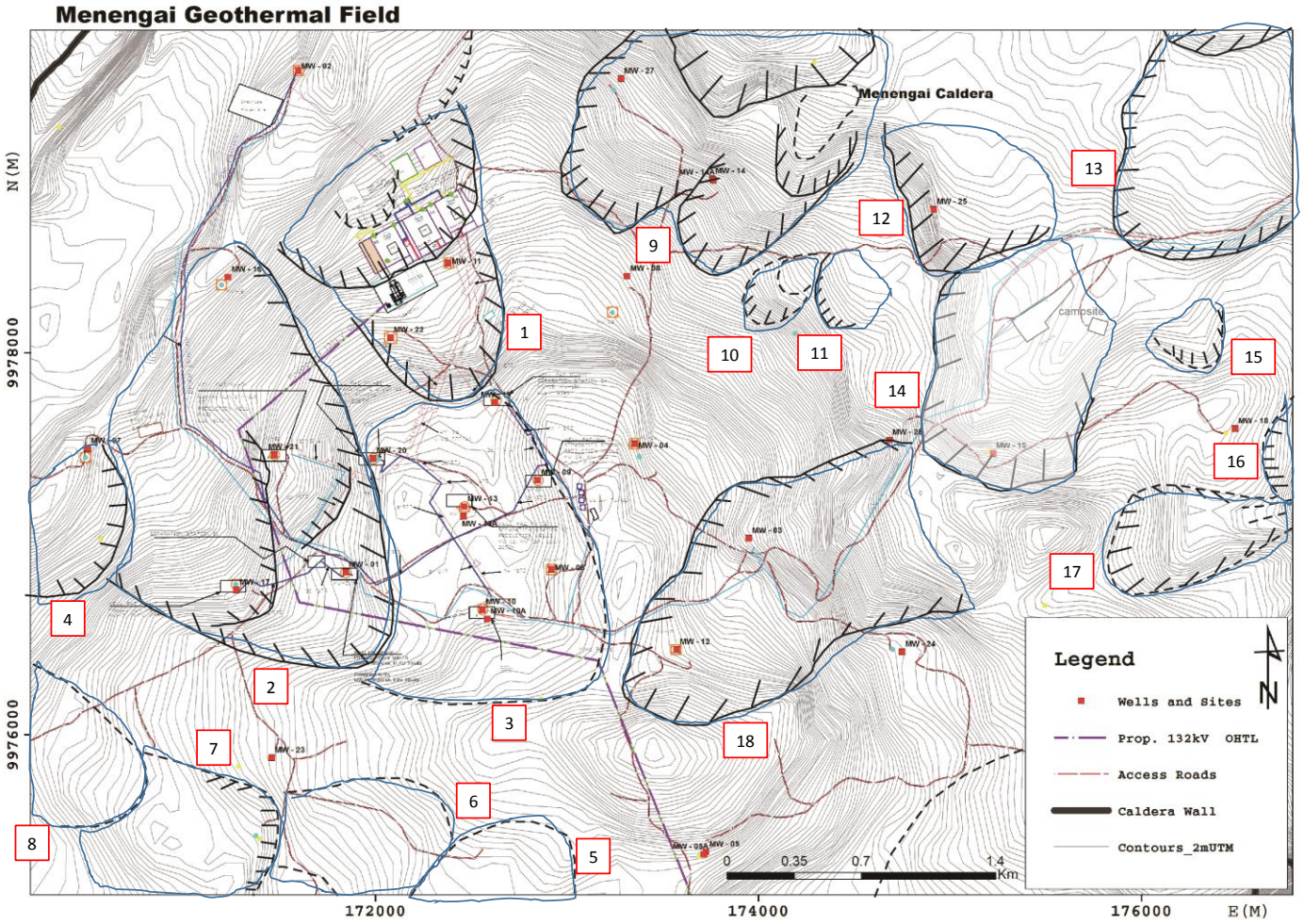

Figure 4-24: Characterization on the risk map (and data base).

Shading of slopes in relation to possibility to destabilize (Table 4-2). Red shade indicate high risk, Green shade indicate medium risk and brown shade indicating very low risky slopes (Figure 4-25).

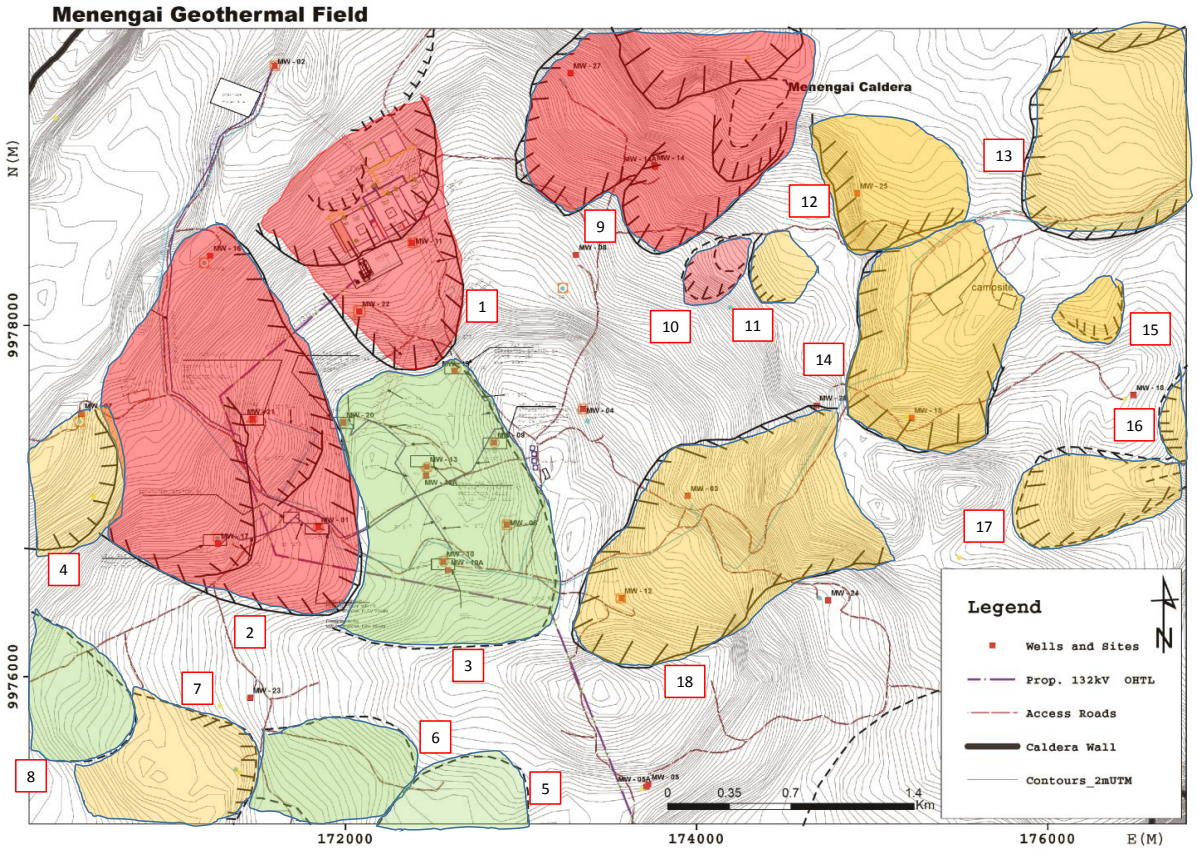

Figure 4-25: Categorization of Slopes according to risk levels

Shading of slope and categorizing the risk Influence degree on power station and proposed surface development (Table 4-2). The green shades at the center of caldera categorized as high risk since most geothermal wells and steam gathering system are located at the central part of caldera thus are more likely to more damages in case of any slope failure (Figure 4-26).

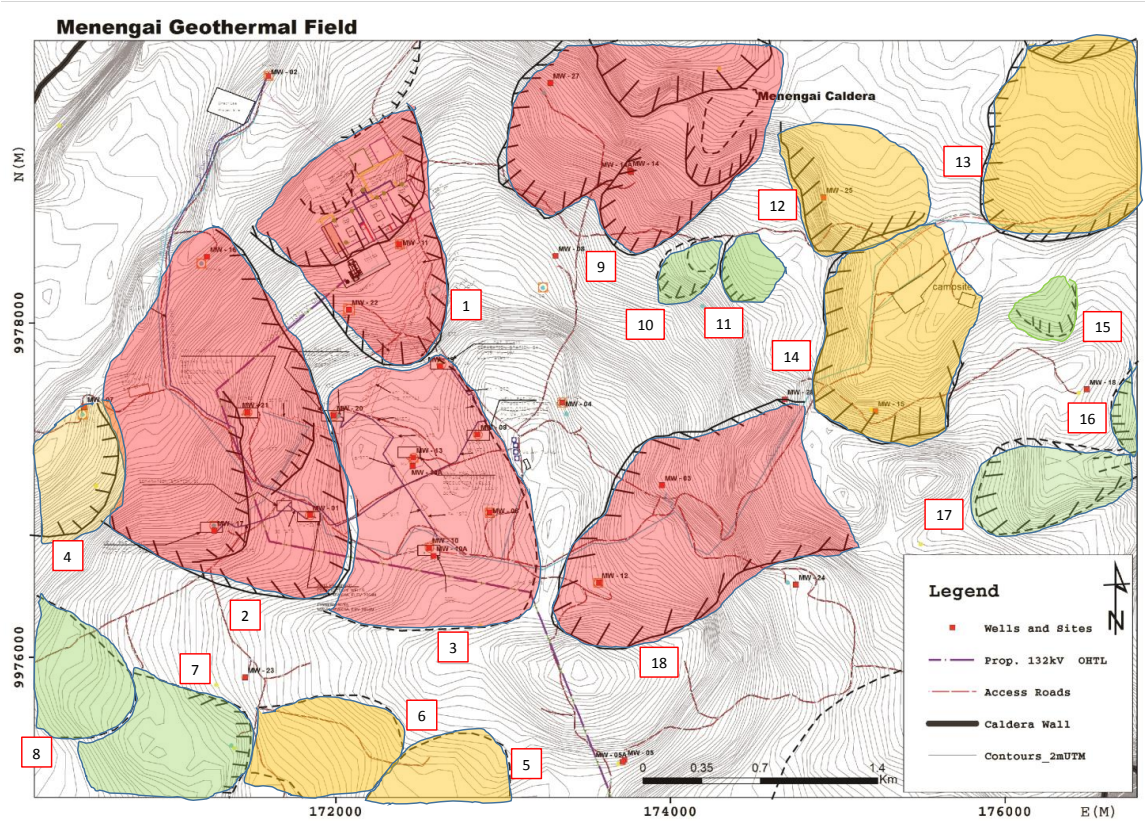

Figure 4-26: Risk levels due to Geothermal Development Program

CHAPTER FIVE

5.0 CONCLUSION AND RECOMMENDATION

5.1 Conclusion

This study aimed to identify possible geohazards that could be triggered by failures in geotechnics, seismic events, geological structures and tectonic processes and topographic slope failures during post geothermal development within Menengai caldera.

Geothermal development involves multiple stages from extraction of resource at depths, transporting the steam to the turbines at the power plant then conversion of the steam energy to electric energy to be consumed by the end user. Geothermal development is at critical stage at Menengai since it is the source of the resource and processing level.

Likely geohazards area thus hereby identified and characterized according to four (4) key areas of my study. Possible geohazards for geothermal development are seen affect geothermal reservoir, productivity geothermal wells, stability of the caldera floor, and stability of buildings, steam gathering system and infrastructure on the caldera floor.

1. Geotechnical geohazards
2. Seismic geohazards
3. Geological structures and tectonic geohazards
4. Topographic slope geohazards

5.1.1 Geotechnical geohazards

Near surface lava surface is generally stable for construction with proper civil designs taken into consideration. Though localized, geotechnical fieldwork and laboratory tests results taken at the proposed power plant location give the general rock and soil properties of lava

surface between 0 – 30 m depth of which comprises the foundation layers. Seismic tomography at proposed power plant site show three thin layers with varied seismic engineering parameters but generally stable for construction. Geotechnical failures shall lead to a large extent, foundation failures thus instability of buildings, steam gathering system and infrastructure on the caldera floor

5.1.2 Seismic geohazards

Past earthquake analysis indicate very low magnitude of seismicity within the caldera however, the studies were taken during a quiet periods of which this may be different following discharging and extraction of geothermal steam from numerous closely located wells within the closed caldera system. Seismic related geohazards are seen to affect productivity of geothermal wells and stability of caldera floor.

Differential frictional forces along the well column that cut through composite layers of different strengths could result to wellbore instability. Menengai caldera formations is observed to comprise lavas of pre-caldera, syn-caldera and post-caldera eruption episodes separated be volcanic ash eruptions resulting to deposition of compositic unconformable almost lateral layers. The ash layers are loose compared to lava layers thus exert different reactional forces to the compressive frictional forces being exerted by up-flowing steam jets from deep feed zones or reservoirs. This differential reactional forces along the well column leads to wobbling of well's liners and casings leading to raptures in sections of geothermal well due to lose of stability. Broken sections of the well draw-in ash or cold water thus cooling off the well. Geotechnical failure may as well be experienced where the well cuts through a fracture or wide void leading to lose of verticality during drilling and no counter reactional forces to steam jet frictional forces.

Seismic shock waves created by frictional forces from steam jets may be so intensive especially when numerous wells are discharging at the same time. The shock wave can be too intensive to the underlying geological formation resulting to insitu landmass movement along weak zones leading to lose of wells verticality or blockage or changing directions of cold dominated fractures to the well thus affecting its productivity all together.

5.1.3 Geological structures and tectonic geohazards

Tectonic evolution of caldera has created underling fault scarps and inferred structures that were not envisaged during the start of drilling program for geothermal wells within caldera. The study has identified the tectonic set-up resulting newly discovered mini-caldera segments /compartments that have been the cause of temperature reversals in the wells and agent of geothermal fluid mixtures at depths resulting calcite scaling within some wells.

Tectonic processes which lead to the present day rugged topography and underlying geological structures appear to be the greatest discovery in thesis study. Assessment of temperature profiles trends of geothermal wells in respect to their location helped to identify major weak zones that could be the main conduits of cold inflows into several wells thereby cooling down the wells. I was as well able to subdivide the caldera into five major compartments bounded by fault scarps believed to be the rims of mini-calderas that resulted to the present main Menengai caldera structure. The compartments seemed to have evolved through partial subsidence influenced by prevailing major weaker fault in this case Molo and Solai TVAs. Subsequently forming compartment was always a down throw.

Underlying geological structures are observed to either constructive or destructive to geothermal reservoir within the caldera. Unpredictive geothermal reservoir is a great challenge to geothermal development. Temperature profiles from several geothermal wells have shown fluctuations; a strong indication that the reservoir is not stable. Structural tectonic

findings and discoveries of mini-caldera rim structures (NS, EW, x, y), inferred faults (z) and Solai TVA extensions (A and B) appear to be the main conduits for feed zones in the reservoir. Presence of large cold shallow groundwater aquifer at the NE Compartment within the caldera has been adversely cooling the reservoir and provide main source of cold inflows to the geothermal wells. The study identified tectonic setting as the main agent to this geohazard.

5.1.4 Topographic slope geohazards

Topographic slopes failure is indicative of unstable caldera floor surface catalyzed weak near sub-surface formation. Ripple effects being falling of debris along on roads, loose foundations of surface constructions, infrastructure and steam pipeline. Drifting of slope could lead to transmission lines being stretched and break off due to shifts of electric poles and transmission towers. Subsidence on some sections of caldera floor may as well lead to dip gulleys thus interfering with transport and movements. Slight shaking of caldera may have ripple effects on stability of buildings, steam pipe network and infrastructure on the caldera floor.

The history and evolution leading to the formation of the caldera compartments is observed to have been influenced by weak and dip crisscrossing tectono-volcanic Molo and Solai axes. This study has as well found out that overhead weight of post caldera lava flows resulted to further subsidence of NW and NNW Compartments. Stability of caldera floor is observed to be affected by all three argents; geotechnical failure, seismicity and tectonic setting. Seismic waves created by discharging geothermal wells at depths may lead to landmass movement that could trigger the already formed caldera compartment to drift or subside further.

5.2 Recommendations

5.2.1 Geotechnical geohazards

Considering the characteristics of the project, the stratigraphic nature and the soil resistance obtained from the field and laboratory studies; it is recommended that the most appropriate foundation system for this project will be through the application of shallow foundations (footings, slabs and concrete blocks).

The top soil layer has a thickness that ranges between 0.5 m and 2.0m, therefore, it's recommended not to lay any foundation system with heavy loading on this layer. This layer is composed of silty sandy gravels of extremely weathered volcanic soil with rock fragments as well as roots, and it will have to be completely removed before commencement of any construction works. In the case of employing any platforms, it's important to note that these will be constructed on a surface free from the above mentioned top layer. For the case of square or rectangular footings, a minimum foundation depth of 2.50 m is recommended.

Moderately weathered trachyte classifies as weak to moderately strong, this slightly weathered trachyte is likely to require hard ripping or blasting depending on jointing of the rocks for removal should the foundations be taken at lower depths. Areas with silty sandy gravels matrix of extremely weathered volcanic ash encountered below foundation depth of 2.5 m should be removed and replaced with mass concrete or the foundations need to be taken to a lower depth to avoid them.

5.2.2 Seismic geohazards

Well spacing should be checked to avoiding crowding that may lead to excessive seismic events that could deep landmass movements and further geotechnical failures.

Deformation monitoring should be established in all fracture zones and compartments to observe any landmass movement. Seismic monitoring should also be put in place to check seismicity within the caldera.

5.2.3 Geological structures and tectonic geohazards

This study notices that NW and NNW Compartments seem to be youngest to evolve within caldera floor. It has further observes that NW and NNW Compartment are bounded by weaker structure that can easily rapture and slip therefore overhead weights should be avoided. Overcrowding of geothermal wells in these compartments should be avoided. NW and NNW Compartments seems the most risky sections going by topographic slope risk analysis and the fact geothermal development constructions and infrastructure plan concentrate.

Agents leading to possible effects to geothermal reservoir are observed to be regional and deeply situated revolving between geological structures and tectonic set-up. Little or no mitigation measures can be humanly implemented to avoid interference of the geothermal reservoir within the caldera due to the fact that it is within a closed volcanic system. Permeable fractures that conduit cold flows to the reservoirs are very deep thus plugging may be challenging. Re-injection of hot geothermal fluids to destructive fracture offers some little solution however this action can also lead the geotechnical failures along the fractures hence more geohazards. Siting of wells should be critically checked not to lead to puncturing some zones that may lead to permeable fracture for may cool the reservoir.

Well siting should avoid destructive permeable fractures that channel cold inflows hence causing temperature reversals in wells. Proper downhole geophysical assessment should be employed to identify underlying geological formation and structures that should be avoided while further siting of wells.

5.2.4 Topographic slope geohazards

All constructions and establishment on the caldera floor should have thorough civil and structural engineering design putting into consideration that any slight landmass movement or slope failure may lead to foundation displacement. Steam and water pipe network should have flexible jointing and expanders ready for any movement of caldera floor. The foundation of the structure should be designed to eliminate unacceptable foundation and structural distress and constructed to maintain or promote constant moisture in the foundation soils. Foundations should always be provided with adequate drainage, and the soil properly prepared to minimize changes in soil moisture and differential movement.

In summary, the study observed Menengai Caldera to be a high risk for geothermal development on account of;

- Weak and highly fractured sub-surface (0 – 30 m) layers thus may not be too competent for heavy constructions.
- Menengai caldera being a closed volcanic system, increased drilling of geothermal wells on the caldera floor could increase seismicity thereby enhancing insitu landmass movements, instability of wellbore columns, increased inferred faults and wells' interferences.
- Productive wells are seen to lie within limited section of NW Compartment which is likely to be tectonically activated with increased drilling operations within the compartment. Instability on this segment of caldera floor would be enhanced thus posing more risk to power plants and infrastructure which are concentrated within the compartment according to development layout plan.
- Topographic slope failures are more likely to occur following susceptibility of landmass movements thus posing risk of instabilities of constructions and infrastructures on the surface.
- Only 20% out of total number of drilled wells (30) are productive implying high degree of deep destructive geological structures which are conduits for cold in-flows reducing most wells' productivity and geothermal reservoir thus uneconomical investment.

CHAPTER SIX

6.0 REFERENCES

Arnórsson, S., Bjarnason, J.Ö., Giroud, N., Gunnarsson, I., and Stefánsson, A., 2006: *Sampling and analysis of geothermal fluids*. Geofluids, 6, 203-216.

Cox, K.G., Bell, J.D. and Pankhurst, R.J., 1979: *The interpretation of Igneous Rocks*.

GDC Strategic plan, 2013

GDC., 2010: Menengai geothermal prospect; An investigation for its geothermal potential. Geothermal Development Company (GDC); Geothermal Resource Assessment project, unpubl. Report.

Geothermica Italiana srl, Navarro, J.M., 1987. *Geothermal Reconnaissance Survey in the Menengai-Bogoria Area of the Kenya Rift Valley*. 2 - Geovolcanology.

Gibbs, 2015: *Geotechnical Report for Proposed Development of 1X30MW Geothermal Plant in Menengai Kenya.*; A Geotechnical and Geophysical Investigation Assessment for the proposed Sosian Power Plant project, unpubl. Report.

Leat, P.T., 1991: *Volcanological development of the Nakuru area of the Kenya rift valley.* J. African Earth Sciences, 13, 483-498.

Leat, P.T., 1984: *Geological evolution of the trachytic caldera volcano Menengai, Kenya Rift Valley*. J. Geol. Soc. London, 141, 1057-1069.

Leat, P.T., Macdonald, R., and Smith, R.L., 1984: *Geochemical evolution of the Menengai caldera volcano, Kenya*. J. Geophys. Res., 89, 8571-8592.

Leat, P.T., 1983: *The structural and geochemical evolution of Menengai caldera volcano, Kenya Rift Valley*. PhD thesis, University of Lancaster U.K.

Macdonald, R., Baginski, B., Leat, P.T., White, J.C., and Dzierzanowski, P., 2011: *Mineral stability in peralkaline silicic rocks: Information from trachytes of the Menengai volcano, Kenya.* Lithos 125 (2011) 553-568.

Macdonald, R., and Baginski, B., 2009: *The central Kenya peralkaline province: a unique assemblage of magmatic systems.* Mineralogical Magazine, 73, 1-16.

Macdonald, R., and Scaillet, B., 2006: *The central Kenya peralkaline province: insights into the evolution of peralkaline salic magmas*. Lithos, 91, 59-73.

Macdonald, R., Navarro, J.M., Upton, B.G.J., and Davies, G.R., 1994: *Strong compositional zonation in peralkaline magma: Menengai, Kenya Rift Valley.* J. Volcanol. and Geothermal Res., 60, 301-325.

Macdonald, R., 1974: *Nomenclature and petrochemistry of the peralkaline oversaturated extrusive rocks.* Bulletin Volcanol., 38, 498-516.

Macdonald, R., and Bailey, D.K., 1973: *The chemistry of the peralkaline oversaturated obsidians*. U.S. Geological Survey Professional Paper 440-N-1, N1-N37.

Macdonald, R., Bailey, D.K., and Sutherland, D., 1970: *Oversaturated peralkaline glassy trachyte from Kenya*. J. Petrology, 11, 507-517.

Maguire, P.K.H., Tongue, J.A., and Young, P.A.V. 1992: *Seismicity distribution from Temporary earthquake recording networks in Kenya.* Tectonophysics Vol. 204, 71-79.

Mbia, 2014: *Sub-surface geology, petrology and hydrothermal alteration of Menengai geothermal field, Kenya*. Msc. Geology Thesis, School of Engineering and Natural Sciences. University of Iceland. Reykjavik.

McCall, G.J.H., 1967. *Geology of the Nakuru-Thompson's Falls - Lake Hannington area*. Geological Survey of Kenya Report No 78, 1-122.

Omondi, C., 2011: *Borehole geology and hydrothermal of wells MW-01 and MW-02, Menengai geothermal field, Central Kenya Rift valley*. Report 30; In: Geothermal training in Iceland 2011. UNU-GTP, Iceland, 737-774.

Patlan E., Wamalwa. A., Kaip G., Velasco A. (2013): *Ambient Noise Cross- Correlation Study of Menengai Caldera: Geothermal Prospect in the Central Kenya Dome*. Geothermal Resource Council Annual Meeting in Las Vegas,NV.

Patlan, E., Wamalwa, M. A., and Velasco, A. A., (2013): *Local Micro-seismic study around the Menengai geothermal prospect in the central Kenya domes*. Kenya Geothermal Conference Proceedings.

Simiyu, S.M., 2009. *Application of micro-seismic methods to geothermal exploration: examples from the Kenya rift,* United Nations University and LaGeo, 1, 1-27.

Simiyu, S.M., and Keller, G.R., 2001: *An integrated analysis of the lithospheric structure across the East African plateau based on gravity analysis and recent seismic studies*. Tectonophysics Vol.278, 327-352.

Simiyu, S.M., 2000: *A volcano-seismic approach to geothermal exploration, 5th World Geothermal Congress 2000*, Morioka, Japan.

Wamalwa, A. M., Mickus, K., and Serpa, L. F. (2013): *Geophysical characterization of the Menengai volcano, central Kenya rift from the analysis of magnetotelluric and gravity data*. Geophysics.78. 4. 187-199.

Wamalwa, A.M., 2011. *Joint geophysical data analysis for geothermal energy exploration*. PhD thesis. University of Texas at El Paso, El Paso, Texas.

APPENDICES

ANNEX I: GEOLOGS

BH No.	Depth	Description of Borehole Log
BH-1B	0.00 to 1.4m	Top layer composed Grey moist silty gravelly sand of extremely weathered volcanic soil with fragments (Pyroclastic material) of rocks
	1.4 to 8.0m	Grey moderately to slightly weathered trachyte moderately fractured clastic materials. This stratum presents a weathering class ranging from grade III to grade II with good to excellent Rock Quality Designation (RQD) of 80% to 100% and an average density of 1686 kg/m^3.
	8.0 to 14.0m	Grey brown moderately weathered trachyte highly fractured and highly vascular and course grained. This stratum presents a variable weathering grade ranging from III to II with a good to excellent Rock Quality Designation (RQD) of 80% to 100
	14.0 to 20.0m	Grey fresh trachyte fine grained and strong, and an excellent Rock Quality Designation (RQD) of 100%.
BH-2B	0.00 to 1.0m	Top layer composed of Dark Grey moist silty sandy gravel of extremely weathered volcanic soil with fragments (Pyroclastic material) of rocks. From 1.0 to 10.6m: Grey slightly to fresh trachyte interacted by black patches. This stratum presents weathering classes of grade I and II and an excellent Rock Quality Designation (RQD) of 100% and an average density of 2196 kg/m^3.
	10.6 to 14.5m	Grayish brown highly fractured highly weathered grade IV volcanic rocks, pyroclastic material and pumice. This stratum presents a very poor Rock Quality Designation (RQD) 0%.
	14.5 to 20.0m	Grey slightly fractured fresh trachyte, slightly vascular and hard. This stratum presents an excellent Rock Quality Designation (RQD) ranging from 95% to 100%.
BH-3B	0.00 to 1.2m	Top layer composed of Dark Grey moist silty sandy gravel of extremely weathered volcanic soil with fragments (Pyroclastic material) of rocks
	1.2 to 2.5m	Grey to green highly fractured highly vascular moderately weathered grade III volcanic rocks intermixed with pyroclastic material. This stratum presents a very poor Rock Quality Designation (RQD) of 10%
	2.5 to 8.0m	Greenish grey to grey volcanic rock, trachyte slightly weathered (grade II) to fresh (grade I), slightly fractured with slight vesicular, very strong with an excellent Rock Quality Designation (RQD) of 90% to 100%. This stratum has an average rock density of 2017kg/m^3.
	8.0 to 12.0m	Greenish grey to grey volcanic rock, trachyte slightly weathered (grad II) to fresh (grade I), highly fractured, slightly vascular with vertical faults, very strong. This stratum presents a varying Rock Quality Designation (RQD) ranging from poor (30%) to excellent (100%).
	12.0 to 20.0m	Greenish grey to grey volcanic rock, trachyte slightly weathered (grade II) to fresh (grade I), slightly fractured, slightly vascular and very strong with a good to excellent Rock Quality Designation (RQD) of 80% to 100% respectfully.
BH-4B	0.00 to 0.7m	Top layer composed of Black moist silty sandy gravel of extremely weathered volcanic soil.
	0.7 to 6.5m	Grayish Trachyte, grey, moderately weathered (grade III) to fresh (grade I) and slightly fractured, slightly vascular and hard. This stratum presents a varying Rock Quality Designation (RQD) with 0% (very poor) between depths of 0.7 to 2.0m, 85% to 100% (good to excellent) at depths of 3.5m to 6.5m respectfully. This stratum has an average rock density of 1855kg/m^3.
	6.5 to 13.9m	Grey moderately to slightly fractured fresh (grade I) trachyte, slightly vascular, fine grained and hard with an excellent Rock Quality Designation (RQD) of 90-100%.
	13.9 to 16.5m	Grayish brown moderately weathered (grade III) vesicular, moderately fractured trachyte. This stratum presents a varying Rock Quality Designation (RQD) dropping from good of 80% to very poor of 15% at depth of 15.2m to 16.5m respectfully.

	16.5 to 20.0m	Grey moderately to slightly fractured fresh (grade I) trachyte, slightly vascular, fine grained and hard, with a varying Rock Quality Designation (RQD) raising from fair to excellent of 73% to 100% respectfully.
BH-5B	0.00 to 0.8m	Top layer composed of Grey moist extremely weathered volcanic soil (Pyroclastic material).
	0.8 to 2.3m	Black volcanic rock -scoria with pyroclastic material presenting a weathering grade of class III and a very poor Rock Quality Designation (RQD) of 0%.
	2.3 to 7.6m	Green to grey volcanic rock, trachyte slightly weathered (grade II) to fresh (grade I), with slight fractures presenting an excellent Rock Quality Designation (RQD) of 100%. This stratum has an average rock density of 1984kg/m^3.
	7.6 to 30.0m	Trachyte, grey fresh, moderately to slightly fractured, vesicular, slightly weathered to fresh (grade II to I) and interacted with volcanic glass at depths of 10.3-12.0m. Rock Quality Designation (RQD) ranges from good to excellent with 85% at 12.0m to 100% to the end of the borehole at a depth of 30.0m respectfully.
BH-6B	0.00 to 1.0m	Top layer composed of Grey moist black silty sandy gravely of extremely weathered volcanic soil (Pyroclastic material)
	1.0 to 2.0m	Dirty sandy gravel (residual sand) with a weathering grade class V and a very poor Rock Quality Designation (RQD) of 0%.
	2.0 to 3.5m	Grey to green slightly weathered volcanic rock with pyroclastic material. This stratum presents a weathering grade class II with a fair Rock Quality Designation (RQD) of 57% and an average density of 1905kg/m^3.
	3.5 to 4.5m	Black moderately weathered volcanic rock (scoria) high vascular and fractured. This stratum presents a weathering grade class III and an excellent Rock Quality Designation (RQD) of 93%.
	4.5 to 10.0m	Greenish grey volcanic rock, trachyte slightly weathered to fresh, slightly fractured and highly vascular. This stratum presents a weathering grade class II and I with an excellent Rock Quality Designation (RQD) of 90% and an average density of 2129kg/m^3.
	10.0 to 15.0m	Brown moderately weathered volcanic rock (scoria) highly fractured and highly vascular. This stratum presents a weathering grade class III and II, Rock Quality Designation (RQD) varies and ranges from very poor to excellent with 0% between depths of 11.0m to 14.0m (highly fractured zone) to 90% respectfully.
	15.0 to 30.0m	Grey fresh trachyte slightly fractured (weathering grade class II to I) slightly to moderate vesicular. Rock Quality Designation (RQD) for these strata is excellent with 90-100%.
BH-7B	0.00 to 1.5m	Top layer composed of Black moist silty sandy gravel (Pyroclastic material)
	1.5 to 7.8m	Greenish grey moderately to slightly weathered volcanic rock -trachyte- highly fractured highly vesicular occasionally interacted by scoria. This stratum presents a weathering grade class III to II with a varying Rock Quality Designation (RQD) ranging from 0% to 67% (very poor to fair) as the depth progressed. This stratum has an average rock density of 1893kg/m^3.
	7.8 to 10.8m	Trachyte, grey fresh, slightly fractured slightly vascular and fine grained. This stratum presents a weathering grade class I with an excellent Rock Quality Designation (RQD) of 100% and an average density of 1746kg/m^3.
	10.8 to 16.3m	Brown to grey trachyte moderately weathered to fresh, highly fractured with a weathering grade class III to I. Rock Quality Designation (RQD) Varies with 50% (fair) to a depth of 12.3m and 10% (very poor) and below to a depth of 16.3m respectfully.
	16.3 to 30.0m	Trachyte, grey fresh, slightly fractured slightly vascular and fine grained. Rock Quality Designation (RQD) for this stratum is excellent with 100%.
BH-8B	0.00 to 1.5m	Top layer composed of Dark Grey moist silty sandy gravel of extremely weathered volcanic soil with fragments (Pyroclastic material) of rocks
	1.5 to 6.0m	Grayish green volcanic rock - trachyte-moderately to slightly weathered, moderately fractured and moderately vesicular. This stratum presents a weathering grade class III and II with good to excellent Rock Quality Designation (RQD) of 75-100% and an average density of 2030kg/m^3.

	6.0 to 9.0m	Grey slightly fractured fresh trachyte, slightly vascular and hard presenting a layer of weathering grade class I and an excellent rock Quality Designation (RQD) of 100% and an average density of 1574kg/m^3.
	9.0 to 17.5m	Brown to grey trachyte, highly fractured polyclastic material and highly weathered at depths of 13.0-14.0m and 16.0-17.5m. This stratum presents a weathering grade class IV to II with Rock Quality Designation (RQD) ranging from very poor (0%-80%) to good due to high fractures and weathering present.
	17.5 to 20.0m	Trachyte Grey slightly fractured fresh trachyte, slightly vascular and hard. Rock Quality Designation (RQD) for this stratum is excellent with 100%.
BH-9B	0.00 to 1.5m	Top layer composed of Dark Grey moist silty sandy gravel of extremely weathered volcanic soil with fragments (Pyroclastic material) of rocks
	1.5 to 2.0m	Dark Grey moist silty sand, residual sand.
	2.0 to 5.0m	Grayish green volcanic rock moderately weathered moderately vesicular (scoria and pyroclastic material) with a weathering grade class III and a fair to excellent Rock Quality Designation (RQD) ranging from 45% to 100%. This stratum has an average rock density of 2098kg/m^3.
	5.0 to 20.0m	Grey volcanic rock, trachyte slightly weathered to fresh , slightly fractured slightly vesicular intermixed with moderately weathered volcanic glass and pyroclastic material at depths of 15.4-18.0m. This stratum presents a weathering grade class II to I with an excellent Rock Quality Designation (RQD) of 100%.
		Note: It is important to note that no ground water was encountered during field work.

TP	DEPTH ACHIEVED (m)	TRIAL PITS SOIL DESCRIPTION
1s	1.0	Black to grey boulders and fragments of volcanic rock (scoria and pumice) highly vascular light weight, irregular shaped with gravels
	2.0	Moist brown silty sandy gravel intermixed with irregular shaped highly vascular medium weight volcanic rock fragments
2s	1.5	Reddish to light grey moist fragment of volcanic rocks intermixed with gravel-pumice and polycaustic material, irregular shaped with vesicles
3s	0.6	Moist grey sandy silt with fragments of volcanic rock gravel (volcanic ash)
4s	1.2	Moist brown silty sandy gravel intermixed with greenish volcanic rock fragments (scoria) irregular shaped and light weight
5s	1.2	Grey to green volcanic rocks(scoria and pumice) highly vascular irregular shaped mixed with sandy gravel
6s	1.0	Black moist caustic material of silty ravel with greenish volcanic irregular shaped rocks
7s	1.5	Greenish grey moist silty sandy gravel with irregular shaped and light weight volcanic rock fragments
8s	1.2	Green moist clastic material of silty sandy gravel intermixed with volcanic rock fragments, irregular shaped and light in weight
9s	1.0	Moist brown silty sandy gravel with irregular shaped light weight volcanic rocks
10s	1.2	Dry grayish brown to black coloration fragments of volcanic rocks (pumice and scoria) with gravels
11s	1.5	Moist brown to grayish green silty sandy gravel (caustic materials)
12s	1.5	Dark grey moist silty sandy gravel with fragments of rocks
13s	1.0	Moist grey silty sandy gravel intermixed with black irregular shaped highly vascular light weight volcanic rocks (scoria and pumice)
	2.0	Greenish grey moist silty sandy gravel (caustic material)
14s	1.2	Reddish grey volcanic rocks (pumice) with sandy gravels
15s	1.0	Reddish grey moist silty sandy gravel with fragments of irregular shaped volcanic rocks (scoria) highly vascular

ANNEX II: SUMMARY OF LABORATORY TEST FOR BOREHOLES & TRIAL PITS

BH	DEPTH	NMC	SG	ATTERBERG LIMITS			COMPACTION AASHTO T99		STRENGTH RESULTS C.B.R %		Coefficient of permeability, k (mm/sec)	DIRECT SHEAR TEST		SOIL GRADING AND CLASSIFICATION SOIL					SOIL CHEMICAL TEST			USCS	SOILDESCRIPTION	
No.	(m)	(%)		LL	PL	PI	MDD (Kg/m^3)	O.M.C (%)	4 DAYS SAOK	Swell (%)		Angle of shear (^{0})	Cohesion (kPa)	CLAY	SILT	SAND	GRAVEL	BOULDERS	PH	SULPHATE	CHLORIDE			
1B	0.0-1.4	5.87	2.10	Non-Plastic			1.055	29.0	24.0	0.0	0.022	20.0	31	7.20	7.10	11.00	35.00		28.00				GP	Poorly graded gravel
2B	0.0-1.0	27.33	2.00	Non-Plastic			1.205	25.2	58.0	0.0	0.023	10.0	37	6.90	5.20	6.90	59.60		21.00				GP	Poorly graded gravel
3B	0.0-1.2	8.70	2.50	Non-Plastic			1.004	28.5	39.0	0.0	0.026	21.0	30	9.60	10.00	8.30	24.20		32.00				GP	Poorly graded gravel
4B	0.0-0.7	3.44	2.50	Non-Plastic			1.006	34.0	41.0	0.0	0.008	21.0	26	11.30	18.30	29.40	35.40		0.00	7.92			GP	Poorly graded sandy gravel
5B	0.0-0.8	12.88	1.90	Non-Plastic			1.030	30.5	31.0	0.0	0.009	12.0	29	0.00	0.00	19.30	33.40		32.00		0.056		GP	Poorly graded sandy gravel
6B	0.0-1.0	13.1	2.4	Non-Plastic			1.018	32.5	88.0	0.0	0.008	18.0	29	6.10	8.20	13.00	45.60		0.00			0.043	GP	Poorly graded gravel
7B	0.0-1.5	9.96	2.1	Non-Plastic			1.085	35.8	41.0	0.0	0.007	13.0	37	7.20	21.30	23.50	48.00		0.00				GP	Poorly graded gravel
8B	0.0-1.5	7.89	2.30	Non-Plastic			1.192	18.2	33.0	0.0	0.028	22.0	32	0.00	0.00	27.30	60.20		0.00		0.043		GP	Poorly graded gravel
9B	0.0-1.0	6.00	2.30	Non-Plastic			1.315	34.5	67.0	0.0	0.006	12.0	28	0.00	0.00	21.20	57.40		0.00			0.021	GP	Poorly graded gravel
	1.0-2.0	11.67	2.30	Non-Plastic										6.00	12.60	25.70	55.70		0.00				GP	Poorly graded gravel

TP	DEPTH	NMC	SG	ATTERBERG LIMITS			SOIL GRADING AND CLASSIFICATION						SOIL
No.	(m)	(%)		LL	PL	PI	CLAY	SILT	SAND	GRAVEL	BOULDERS	USCS	DESCRIPTION
1s	0.0-1.0	0.10	2.50	Non-Plastic			0.00	0.00	2.40	38.80	46.00	GP	Poorly graded gravel with boulders
	1.0-2.0	0.10	1.90	Non-Plastic			0.00	0.00	10.10	61.90	16.00	GW	Well graded sandy gravel with boulders
2s	0.0-1.5	1.00	2.40	Non-Plastic			0.00	0.00	3.90	60.10	36.00	GP	Poorly graded gravel with boulders
3s	0.0-2.0	12.96	2.10	Non-Plastic			1.20	11.10	12.30	43.90	19.00	GP	Poorly graded sandy silty gravel with boulders
4s	0.0-1.2	10.6	1.9	Non-Plastic			2.10	14.40	9.90	51.00	17.00	GP	Poorly graded silty sandy gravel with boulders
5s	0.0-1.2	4.03	1.90	Non-Plastic			0.00	0.00	13.40	60.90	19.00	GP	Poorly graded sandy gravel with boulders
6s	0.0-1.0	19.60	2.10	Non-Plastic			0.00	0.00	16.90	51.60	25.00	GP	Poorly graded sandy gravel with boulders
7s	0.0-1.5	10.01	2.00	Non-Plastic			0.00	0.00	9.90	51.80	29.00	GW	Well graded sandy gravel with boulders
8s	0.0-1.2	6.69	1.90	Non-Plastic			0.00	0.00	6.40	44.80	37.00	GP	Poorly graded gravel with boulders
9s	0.0-1.0	6.00	1.90	Non-Plastic			0.00	0.00	16.50	44.00	24.00	GP	Poorly graded sandy gravel with boulders
10s	0.0-1.2	5.00	2.50	Non-Plastic			0.00	0.00	10.60	47.60	29.00	GP	Poorly graded sandy gravel with boulders
11s	0.0-1.5	8.00	2.70	Non-Plastic			0.00	0.00	17.50	70.50	0.00	GP	Poorly graded sandy gravel
12s	0.0-1.5	5.00	1.90	Non-Plastic			0.00	0.00	9.50	61.20	18.00	GW	Well graded sandy gravel with boulders
13s	0.0-1.0	8.00	1.50	Non-Plastic			0.00	0.00	11.90	74.50	14.00	GP	Poorly graded sandy gravel with boulders
	1.0-2.0	8.00	1.80	Non-Plastic			0.00	0.00	12.20	50.70	25.00	GW	Well graded sandy gravel with boulders
14s	0.0-1.0	9.2	2.3	Non-Plastic			0.00	0.00	18.50	44.10	25.00	GP	Poorly graded sandy gravel with boulders
15s	0.0-1.0	6.00	2.40	Non-Plastic			0.00	0.00	15.10	47.40	26.00	GP	Poorly graded sandy gravel with boulders